Dynamic NMR Spectroscopy in the Presence of Kinetic Hydrogen/Deuterium Isotope Effects

Hans-Heinrich Limbach*

Institut für Physikalische Chemie der Universität Freiburg, Albertstr. 21, D-7800 Freiburg i. Br., FRG

Table of Contents

* Present address: Fachbereich Chemie, Takustr. 3, D-1000 Berlin 33

NMR Basic Principles and Progress, Vol. 23

The determination and interpretation of kinetic hydrogen/deuterium isotope effects of chemical and biochemical reactions constitutes a challenging problem to physicists and chemists. So far, kinetic isotope effects have mainly been measured using conventional kinetic methods. In view of the great potential of dynamic multinuclear NMR spectroscopy—which includes the techniques of lineshape analysis, polarization transfer and relaxation time measurements—the question arises whether this method can also be a useful kinetic tool in the chemistry of hydrogen isotopes. The scope of this review is to show that dynamic NMR spectroscopy can indeed contribute to the development of the field of isotopic reaction kinetics. Certain kinetic isotope effects can even only be observed using this method.

The first sections provide a theoretical background of dynamic NMR spectroscopy in the presence of kinetic isotope effects. Then, vacuum methods for the preparation of sealed NMR samples of high purity with defined reactant concentrations and deuterium fractions in the mobile proton sites are described. In the subsequent sections examples for the determination of multiple kinetic hydrogen/deuterium isotope effects on intramolecular and intermolecular double and triple proton transfer reactions in the liquid and the solid state by NMR are given. Finally, the results obtained so far, as well as possible areas of isotope chemistry where the NMR technique could be applied in the future are briefly discussed.

Explanation of Symbols

c_{A_i}	concentration of A in state i
dC_{rs}/dt	number of molecules per volume leaving from environment r to s during the time dt
g_{κ_r}	statistical weight of the spin function k in the environment r
$\hbar$	Planck's constant devided by 2π
e	± 1
i	$=\sqrt{-1}$
k	exchange rate constant of a degenerate process
k_{rs}	pseudo first order exchange rate between environment r and s
k_{rls}	unimolecular rate constant of the rate limiting step of a reaction
$k_{rs}(A)$	pseudo first order rate constant of exchange of group A in environment r to environment s, same as τ_{rs}^{-1}
k_+, k_-	forward and backward rate constants
k_i	rate constant of reaction i
n_{Ar}	number of spin states in group A of environment r
p_r	population or mole fraction of an environment r
r, s	molecular environments, species, states etc.
t	time, mixing time in polarization transfer experiments
t_1	evolution time in two-dimensional NMR experiments
t_2	detection time in two-dimensional NMR experiments
A^rB^r	molecule or molecular environment r consisting of two parts A and B
B_0, B_1	external magnetic fields in the laboratory and the rotating frame
C^l, C^r	"left" and "right" matrix diagonalizing $\mathscr{M}$
C_r	total concentration of environment r
C_A	total concentration of species AH + AD
C_{AL}	total concentration of species AH or AD
D	overall deuterium fraction
D_A	deuterium fraction in environment A
$\mathscr{H}$	Hamilton operator
I_i, I_{zi}	angular momentum operators of spin i in the subsystem r.
I^-	lowering operator

I^+	raising operator
J_{ij}, $J_{A^rB^r}$	coupling constant in Hz between spins i and j or between A and B in environment r
K_{ij}	reduced coupling constant between spin i and j
K_{rs}	equilibrium constant of the interconversion of environment r and s
K_i	equilibrium constant of reaction i
L	hydrogen isotope
$\mathscr{L}$	Liouville superoperator
$\mathscr{L}_r$	Liouville superoperator of environment r
$\mathscr{L}_{A^r}$, $\mathscr{L}_{B^r}$	Liouville superoperator of group A and B in environment r
$\mathscr{L}_{A^rB^r}$	part of the Liouville superoperator describing the scalar spin–spin interaction between groups A and B in environment r
$M_r(t)$	magnetization of environment r as a function of time
$\mathscr{M}$	superoperator in Liouville space describing the time dependence of the density matrix
N_r	number of spin states in the environment r
O_{rs}	permutation operator which changes a spin function of environment r into the corresponding spin function of environment s
P	primary kinetic isotope effect
P_{rs}	probability of interconversion of environment r to environment s
Q_m	complex intensity of transition m
Q_m^{re}	real part of Q_m
Q_m^{im}	imaginary part of Q_m
$\mathscr{R}$	Redfield relaxation superoperator
$\mathscr{R}^{(1)}$, $\mathscr{R}^{(2)}$	longitudinal and transverse part of the Redfield relaxation superoperator
S	secondary kinetic isotope effect
T_{1r}	longitudinal relaxation time in the environment r
T_{2r}	transverse relaxation time in the environment r
T_{2r}^*	effective transverse relaxation time in the environment r which includes the inhomogeneity of the magnetic field B_0
$T_{1\rho}$	longitudinal relaxation time in the rotating frame
$Y(\nu)$	lineshape function
W_{0r}	effective NMR-line width of environment r in the absence of exchange
α	spin state of a spin 1/2 nucleus
β	spin state of a spin 1/2 nucleus
γ_i	gyromagnetic ratio of spin i
δ_{rs}	Kronecker symbol, $=1$ for $r=s$ and $=0$ for $r \neq s$
μ_r, ν_r	spin functions of environments r
ν	frequency in Hz
ν_i	Larmor frequency of spin i in Hz

π	3.14159
$\rho, \rho(t)$	density matrix at time t
σ_i	the screening constant of the magnetic field of nucleus i
τ_r	average lifetime of environment r
τ_{rs}^{-1}	average inverse lifetime of environment r before the conversion to environment s, same as k_{rs}
$\tau_{rx}^{-1}(A)$	average inverse lifetime of group A in environment r before reaction to environment x, same as $k_{rx}(A)$
τ_{AL}^{-1}	inverse lifetime of group L in A
τ_{AHXH}^{-1}	average lifetime of H on A before the jump to X
$\tau_{AHXD}^{-1}, \tau_{AHXH*}^{-1}$	average inverse lifetime of A before H it is replaced by D or another H and before A rearranges to X
τ_{ALXL}^{-1}	average inverse lifetime of L in AL before it is incorporated into XL
τ_{ALA}^{-1}	inverse lifetime of group A in AL before L leaves A
Φ	inverse equilibrium constant of fractionation of isotopes between two different sites (fractionation factor)
$\Phi^{\ddagger}$	inverse kinetic isotope effect or fractionation factor between ground and transition state
$\Delta\nu$	frequency interval in Hz
$\Delta\Omega$	frequency interval in rad/sec
Λ_m	mth eigenvalue of $\mathscr{M}$
Λ_m^{re}	real part of Λ_m
Λ_m^{im}	imaginary part of Λ_m
ω_1	$=\gamma B_1$
Ω_r	Larmor frequency of environment r in radian/sec
Ξ	exchange superoperator

1 Introduction

In 1931 Urey, Brickwedde, and Murphy discovered the hydrogen isotope deuterium. The isotopic enrichment was found to arise from the fact that the electrolysis of light water is faster than of heavy water [1, 2]. This success showed that although different isotopes of an element behave identically from a chemical standpoint the different isotopic masses nevertheless lead to both isotope effects on equilibrium as well as on rate constants of chemical reactions. Soon, ratios of equilibrium constants of isotopic reactions were called "equilibrium isotope effects" (EIE), ratios of isotopic rate constants "kinetic isotope effects" (KIE). Isotope effects have been found to be especially large for those elements which are directly involved in bond breaking and bond formation during the reaction studied [3]. Such effects are, therefore, referred to as "primary". Isotopic substitution in atomic sites which maintain all chemical bonds with their neighbors during the reaction of interest leads then only to smaller "secondary" isotope effects. Because of the unique mass relation between the different hydrogen isotopes hydrogen/deuterium isotope effects are particularly large and have attracted most attention. The largest contributions to these effects arise from changes in the vibrational frequencies of the reactants. The theory of equilibrium isotope effects has been founded by Urey [4] and Bigeleisen [5, 6] and has widely been accepted [3]. Generally, kinetic isotope effects can be much larger than equilibrium isotope effects; this is because of the particular vibrational structure of transition states of chemical reactions which involve "non bonded" atoms. However, since transition states cannot directly be observed, the interpretation of kinetic isotope effects is not always straightforward. Nevertheless, KIE are often the only source of information on molecular events in a variety of chemical and biochemical reactions. By combining the latter with Eyrings's transition state theory [7] Bigeleisen [8] derived a general theory of kinetic isotope effects for over barrier reactions [3]. This theory was modified by Bell in order to include tunneling in the case of hydrogen transfer reactions, a phenomenon Bell had already discussed in the thirties [9, 10]. In the last decades efforts have been made to develop models of kinetic hydrogen/deuterium isotope effects [11–16] and of proton transfer in general [9, 10, 17–27] based on more rigorous quantum mechanical treatments.

Hydrogen transfer reactions in which either protons, hydrogen atoms or hydride ions are transferred are not only interesting from a theoretical standpoint but play a major role in different areas of chemistry as a quick look in textbooks of organic, inorganic or biological chemistry will show. One finds complicated nucleophilic substitution and reduction/oxidation reactions as well as simple proton transfer processes [27]. Multiple proton transfer reactions are related to bifunctional and enzymatic catalysis [28–54]. When hydrogen transfer systems are incorporated in dyes they can also be induced by light, even at cryogenic temperatures if certain requirements are met [55–60].

In the past decades kinetic isotope effects in chemical reactions have mainly been studied using conventional kinetic [3, 27] or fast reaction methods [27, 61–63] where concentrations of reactants or products are monitored as a function of time. Although various spectroscopic techniques have been used for this purpose such as UV/VIS-, IR- and mass spectroscopy etc., dynamic Nuclear Magnetic Resonance (DNMR) techniques [64–81] have been employed only very recently in this research area. In view of the great potential of multinuclear pulse Fourier Transform NMR spectroscopy [72, 73] to selectively monitor different isotopes of a given nucleus as spin probes for molecular structure and dynamics, this situation is surprising. The main purpose of this article is, therefore, to show that and how the so far separate fields of isotope chemistry and dynamic NMR spectroscopy can be linked together.

NMR can be used in different ways to study kinetic isotope effects. First, as in conventional techniques the concentrations of reacting isotopic species can be measured as a function of time if the reactions studied are slow enough and if non-equilibrium initial states can be prepared. Secondly, when the reactions become too fast it is sometimes still possible to obtain kinetic isotope effects from an NMR isotope analysis of the products. Especially ^2H NMR spectroscopy has been applied for this purpose [82–84]. The third use of NMR spectroscopy in isotope chemistry, the topic of this article takes full advantage of NMR as a fast reaction method, which includes the techniques of line shape analysis [64–72], and polarization transfer [73–81], in one or two dimensions.

NMR is a special method covering reactions which are not easily studied by other techniques. Therefore, one has to discuss for which kind of reactions kinetic isotope effects can be obtained by this approach. In principle, any reversible reaction can be studied. In practice, however, NMR performs best when the concentrations of reactants and products are of equal magnitude, i.e. when the equilibrium constant of the reaction studied is unity. This is just the type of reaction which cannot easily be followed by other techniques, which require that $K \neq 1$. It is, therefore, understandable, that the literature on kinetic isotope effects mainly refers to asymmetric reactions. From a theoretical standpoint, however, the knowledge of kinetic isotope effects on symmetric or quasisymmetric reactions is especially important. Therefore, NMR constitutes a valuable complement to conventional kinetic methods.

Since the largest kinetic isotope effects are found in reactions where hydrogen isotopes are transferred, NMR will be applied in the near future mostly to this type of reactions. Proton transfer reactions have been studied by dynamic NMR spectroscopy since its early days [85–88]. Mostly proton exchange in water and other protic solvents were studied where H_3O^+, OH^- or other acids and bases act as catalysts of the exchange. These reactions are, generally, very complex and it is, therefore, not surprising that only very few proton and deuteron exchange rates have been studied by NMR [88–90]. Kinetic hydrogen/deuterium isotope effects of reactions in protic media have, therefore, mainly been measured using other kinetic methods [9, 10, 27, 43].

Because of the high complexity of proton exchange in protic media there has been a trend in the past decade to study proton exchange reactions in aprotic solvents [3, 27, 39, 91–129]. However, in these media the problem of hydrogen/deuterium exchange with residual mobile protons on glass walls and traces of water arises. This problem is smaller in the case of hydrogen transfers to strong bases. Therefore, mostly the latter reactions were studied using conventional kinetic techniques. In early dynamic NMR studies of kinetic isotope effects residual mobile protons in the NMR samples were removed by adding deuterated alcohols to the NMR samples [109, 111], a procedure which is not practical. The problem of preparing pure NMR samples of proton donors in organic solvents with defined deuterium fractions in the proton sites was, however, solved [87, 104–106]. Thus, it has been possible to measure KIE of symmetric proton transfer reactions between nitrogen atoms and oxygen atoms by DNMR. Both intermolecular [86, 87, 100–108] and intramolecular proton exchange reactions [105, 109, 111, 115, 120, 122, 124–129] in aprotic solvents were studied. These reactions have attracted considerable theoretical interest [15, 16, 130–144].

One problem in the study of proton transfer reactions is the determination of the number of protons which are transferred in the rate limiting step. E.g., when proton donors like H_2O or more complicated bifunctional catalysts are present in is often difficult to distinguish between the processes

$$AL\cdots B \rightleftharpoons A\cdots LB, \quad L = H, D \tag{1.1}$$

and

$$AL\cdots XL\cdots B \rightleftharpoons A\cdots LX\cdots LB, \quad L = H, D \tag{1.2}$$

etc. and to measure their kinetic hydrogen/deuterium isotope effects. Whereas the process described by Eq. (1.1) depends only on the two isotopic rate constants k^H and k^D the process described by Eq. (1.2) is characterized by four different forward rate constants k^{HH}, k^{HD}, k^{DH}, and k^{DD} which are difficult to determine but which are interesting to know from a theoretical standpoint. In order to determine the number of protons transferred, generally, kinetic measurements have to be performed as a function of the deuterium fraction in the mobile proton sites [42–48]. This method has been called "proton inventory technique" [43]. However, the extraction of reliable numbers requires knowledge of the multiple kinetic isotope effects which is difficult to obtain when the exact reaction mechanism is unknown. Therefore, most workers have assumed the validity of the so called "rule of the geometric mean (RGM)", which states for a double proton transfer that [43]

$$k^{HD} = (k^{HH}\cdot k^{DD})^{1/2}, \quad \text{i.e.} \quad k^{HH}/k^{HD} = k^{HD}/k^{DD}. \tag{1.3}$$

This rule was originally derived by combination of equilibrium isotope effect [5] and transition state theory [7] for concerted double proton transfers.

Since NMR has the advantage of being able to perform experiments selectively on different nuclei it can be helpful in the study of multiple kinetic

hydrogen/deuterium isotope effects of proton transfer reactions. Thus, it has become possible to determine such effects in the case of some double proton transfer reactions without using the RGM. E.g., full kinetic HD/HD/DD isotope effects were reported in 1982 for proton exchange between methanol and acetic acid in tetrahydrofuran [105, 106] and for the porphyrin tautomerism [105]. Subsequently, such effects have been determined by NMR for several other inter- and intramolecular double proton transfer systems [107, 108, 120, 124–129]. In these studies major unexpected deviations from the RGM have been found, from which interesting insights into the reaction mechanisms could be obtained. Thus, questions such as whether tunneling plays a role and whether the double proton motion is concerted or stepwise were studied. Note that kinetic H/D isotope effects of intramolecular proton transfer reactions have also been obtained by dynamic EPR spectroscopy [145–151] which is, however, restricted to radicals. Recently, the development of high resolution solid state NMR techniques [152–165] has paved the way for studies of fast reactions in the solid state [162, 166–191]. Especially variable temperature NMR studies [162] under the conditions of cross polarization (CP) [152–154], magic angle spinning (MAS) [155–157], and proton decoupling [154] have been used in the past in order to determine some kinetic hydrogen/deuterium isotope effects [164, 167, 179]. The whole potential of this technique for the study of KIE has, however, not yet been fully exploited.

The purpose of this review is to present a framework for the study of kinetic hydrogen/deuterium isotope effects by dynamic NMR spectroscopy and to discuss stratagems, possibilities and drawbacks of this method. For the reasons stated above experimental examples will be presented from the area of multiple hydrogen transfer reactions, although strategies arising from these studies are general and could equally well be applied to other atom transfer processes.

The article is organized as follows: Section 2 contains a short description of general techniques of dynamic NMR spectroscopy based on the quantum mechanical density matrix formalism. Since exchange reactions can be followed only if they are associated to a change in the nuclear spin hamiltonian, we discuss in Sect. 3 the aptitude of the different nuclear magnetic interactions for use in the study of kinetic isotope effects. So far, NMR techniques have mostly be applied to single reactions systems. Therefore, the concept of group exchange is introduced in Sect. 4, which allows us to give a description of dynamic NMR lineshapes in the presence of different superposed complex bond breaking/bond formation processes. In Sect. 5 a theoretical background of the theory of the NMR proton inventory technique is provided where kinetic measurements are performed as a function of the deuterium fraction in the mobile proton sites. Especially, relations between the kinetic parameters obtained by NMR and rate constants of isotopic reactions are derived. These relations depend on the type of processes studied and can be quite complex especially in intermolecular multiple proton transfer reactions. In Sect. 6 typical NMR lineshape equations encountered in the study of intra- and intermolecular proton exchange reactions

are presented. In Sects. 7 and 8 computational aspects of NMR lineshape analysis and NMR sample preparation techniques are described, adapted for the study of kinetic hydrogen/deuterium isotope effects in aprotic solvents.

The following sections are then devoted to practical examples of the determination of kinetic isotope effects in intramolecular (Sect. 9) and intermolecular (Sect. 10) multiple proton transfer reactions in liquids as well as in solids (Sect. 11). The review ends with a short discussion (Sect. 12) and a summary (Sect. 13).

2 General Dynamic NMR Spectroscopy

In this section we briefly review the theory of dynamic pulse Fourier transform NMR spectroscopy [64–73, 159, 160]. First, we will treat the theory of lineshapes in the presence of chemical exchange; for this purpose, the notation of Binsch [71] will be employed. Then, polarization transfer techniques in the slow exchange range, and, finally, relaxation methods will be discussed. For all techniques introductory examples will be given.

2.1 NMR Lineshape Theory

We consider ensembles of nuclear spins in different environments r, s,... which are subject to chemical exchange. Such superposed spin systems can be characterized in Hilbert space by the density matrix ρ with the elements $\rho_{\mu_r \nu_r}$, where μ_r and ν_r are the spin states of the spin system in the environment r. The diagonal elements $\rho_{\mu_r \mu_r}$ correspond to polarizations, the off-diagonal elements $\rho_{\mu_r \nu_r}$ to quantum coherencies whose order is given by the difference in magnetic quantum numbers of the associated spin states. In Liouville space ρ corresponds to a vector whose time dependence is governed by the master equation in the rotating frame [71, 73]

$$\frac{d\rho}{dt} = \mathcal{M}(\rho - \rho(\infty)), \tag{2.1}$$

where $\rho(\infty)$ is the density matrix for $t \to \infty$. The matrix $\mathcal{M}$ is given by [71]

$$\mathcal{M} = i\mathcal{L} + \mathcal{R} + \Xi, \tag{2.2}$$

where $i = \sqrt{-1}$, $\mathcal{L}$ the Liouville operator, $\mathcal{R}$ the Redfield relaxation operator and Ξ the operator describing the chemical exchange. The elements of $\mathcal{L}$ are given by

$$\mathcal{L}_{\mu_r \nu_r \kappa_s \lambda_s} = -2\pi(\mathcal{H}_{\mu_r \kappa_s} \delta_{\lambda_s \nu_r} - \mathcal{H}_{\lambda_s \nu_r} \delta_{\mu_r \kappa_s}), \tag{2.3}$$

where δ is the Kronecker symbol. $\mathcal{H}$ is the nuclear spin Hamiltonian whose

elements will be discussed in the following section. In the absence of radio frequency pulses as typical for free induction decays the above master Eq. (2.1) splits up in a longitudinal and a transverse part:

$$\frac{d}{dt}\begin{vmatrix} \rho_{\mu_r\mu_r} \\ \rho_{\mu_s\mu_s} \\ \rho_{\mu_r\mu_r} \\ \rho_{\mu_s\mu_s} \end{vmatrix} = \begin{vmatrix} \mathscr{R}_r^{(1)}, \Xi & \Xi & & \\ \Xi & \mathscr{R}_s^{(1)}, \Xi & & \\ & & i\mathscr{L}_r, \mathscr{R}_r^{(2)}, \Xi & \Xi \\ & & \Xi & i\mathscr{L}_s, \mathscr{R}_s^{(2)}, \Xi \end{vmatrix} \begin{vmatrix} \rho_{\mu_r\mu_r} - \rho_{\mu_r\mu_r}(\infty) \\ \rho_{\mu_s\mu_s} - \rho_{\mu_s\mu_s}(\infty) \\ \rho_{\mu_r\nu_r} - \rho_{\mu_r\nu_r}(\infty) \\ \rho_{\mu_s\nu_s} - \rho_{\mu_s\nu_s}(\infty) \end{vmatrix} \tag{2.4}$$

$\mathscr{R}_r^{(1)}$ describes the longitudinal relaxation of the spin system in r, $\mathscr{R}_r^{(2)}$ the transverse relaxation. In the absence of spin–spin coupling $\mathscr{R}_r^{(1)}$ and $\mathscr{R}_r^{(2)}$ are diagonal with the elements given by

$$\mathscr{R}^{(1)}_{\mu_r\mu_r\mu_r\mu_r} = -1/T_{1r} \quad \text{and} \quad \mathscr{R}^{(2)}_{\mu_r\nu_r\mu_r\nu_r} = -1/T_{2r}, \tag{2.5}$$

where T_{1r} and T_{2r} are the longitudinal and transverse relaxation times in the environment r. In high resolutions studies of liquids, generally, artificial and apparative line broadening is included in $\mathscr{R}^{(2)}$, i.e.

$$\mathscr{R}^{(2)}_{\mu_r\nu_r\mu_r\nu_r} = -1/T^*_{2r} = -\pi W_{0r}, \tag{2.6}$$

where W_{0r} is the effective NMR line width of environment r in the absence of exchange. The approximation Eq. (2.5) holds also in the presence of spin–spin coupling as long as $|\Xi| \gg |\mathscr{R}|$.

The exchange operator Ξ depends on the particular exchange problem studied. The simplest exchange problem can be written as

$$r \underset{k_{sr}}{\overset{k_{rs}}{\rightleftharpoons}} s. \tag{2.7}$$

k_{rs} is the pseudo-first order reaction rate constant of the forward reaction defined by

$$k_{rs} = -\frac{1}{C_r}\frac{dC_{rs}}{dt}. \tag{2.8}$$

C_r is the concentration of environment r and dC_{rs} the number of moles per volume leaving from environment r to s during the time dt. k_{rs} is equal to the average inverse lifetime τ_{rs}^{-1} of environment r before the conversion to environment s occurs. Defining τ_r as total lifetime of r and P_{rs} as probability of interconversion to environment s it follows that

$$\tau_{rs}^{-1} = k_{rs} = P_{rs}\tau_r^{-1}. \tag{2.9}$$

The equilibrium constant of the above reaction is given by

$$K_{rs} = k_{rs}/k_{sr} = C_s/C_r = p_s/p_r, \tag{2.10}$$

where p_r is the mole fraction of environment r. If K_{rs} is known, only one pseudo first order rate constant, either k_{rs} or k_{sr} needs to be determined in order to characterize the kinetics of the reversible reaction in Eq. (2.8). In other words, the backward reaction step does not need to be treated explicitly.

In the simple case of intramolecular exchange or in the case of intermolecular exchange in the absence of spin–spin coupling the effect of the exchange $r \rightarrow s$ on the spin functions can be described by the operator equation

$$O_{rs}\mu_r = \kappa_s \quad \text{and} \quad O_{rs}\nu_r = \lambda_s \tag{2.11}$$

where O_{rs} is a permutation operator. The elements of the exchange operator are then given by [71]

$$\Xi_{\mu_r \nu_r \kappa_s \lambda_s} = -\delta_{rs}\delta_{\mu_r \kappa_s}\delta_{\nu_r \lambda_s}\left(\sum_{r \neq t} k_{rt}\right) + (1-\delta_{rs})\delta_{\mu_r \kappa_s}\delta_{\nu_r \lambda_s}k_{rs}. \tag{2.12}$$

As indicated in Eq. (2.4) the master equation splits up in two separate sets of equations for the polarizations and the coherences. The first describes polarization transfer due to chemical exchange which can be detected in the slow exchange regime by appropriate pulse experiments (see Sect. 2.3). Thus, from such experiments rate constants of the exchange can be obtained. In order to extract kinetic data from exchange broadened NMR lineshapes only the second set of equations describing the time evolution of the coherences—for which $\rho(\infty) = 0$—has to be solved. Since only single quantum coherences are observable density matrix elements corresponding to multiple quantum coherences are omitted in conventional lineshape calculations of spectra obtained by Fourier transformation of simple free induction decay signals. The dimension of the complex matrix $\mathcal{M}$ is equal to the number of observable transitions in the NMR spectrum of interest. Each transition m is characterized by the width Λ_m^{re} and the position Λ_m^{im}, where $\Lambda_m = \Lambda_m^{re} + i\Lambda_m^{im}$ is the mth complex eigenvalue of the matrix $\mathcal{M}$, calculated by diagonalization of $\mathcal{M}$ according to the transformation

$$\Lambda = C^{l}\mathcal{M}C^{r}. \tag{2.13}$$

The lineshape function is then conveniently written in the form

$$Y(\nu) \sim \sum_m \{[Q_m^{re}\Lambda_m^{re} - Q_m^{re}(\Lambda_m^{im} - 2\pi\nu)]/[(\Lambda_m^{re})^2 + (\Lambda_m^{im} - 2\pi\nu)^2]\}, \tag{2.14}$$

where each transition m is further characterized by the complex intensity

$$Q_m = Q_m^{re} + iQ_m^{im} = Q_m = \left(\sum_k I_k^- C_{km}^r\right)\left(\sum_l \rho_l(0)C_{lm}^l\right). \tag{2.15}$$

In Eq. (2.15) I_k^- are the elements of the lowering operator

$$I_k^- = I_{\mu_r \nu_r}^- = N_r^{-1}\langle \mu_r / I_r^- / \nu_r \rangle, \tag{2.16}$$

and N_r the number of spin states in the environment r. $\rho_l(0)$ represents the elements of the density matrix at the beginning of the acquisition at $t = 0$. For

one-pulse experiments these elements are given by

$$\rho_l(0) = \rho_{\mu_r \nu_r}(0) = p_r \langle \mu_r / I_r^- / \nu_r \rangle. \tag{2.17}$$

p_r is the mole fraction of the environment r to which the spin states μ_r and ν_r are associated. In actual calculations it is only necessary to set up the matrix $\mathcal{M}$ and the vector $\rho(0)$. $\rho(0)$ is equal to the population vector p in the absence of scalar coupling.

2.2 *Example of a Simple NMR Lineshape Analysis*

As an example let us consider the simplest lineshape problem, i.e. exchange between two states r = 1 and s = 2, each containing only one spin. We assume that the Hamiltonian is such that both environments can be characterized by the absorption frequencies $\Omega_1 = 2\pi\nu_1$ and $\Omega_2 = 2\pi\nu_2$ in the rotating frame. The matrix $\mathcal{M}$ and the vector $\rho(0)$ are then given by

$$\mathcal{M} = \begin{bmatrix} -k_{12} - \pi W_{01} + i\Omega_1 & k_{21} \\ k_{12} & -k_{21} - \pi W_{02} + i\Omega_2 \end{bmatrix}, \quad \rho(0) = p = \begin{bmatrix} p_1 \\ p_2 \end{bmatrix}, \tag{2.18}$$

because the elements of the vector I^- are equal to 1. The lineshape can now easily be calculated using the equations of Sect. 2.1. An example is shown in Fig. 2.1. In the slow exchange region two lines of unequal intensity appear at

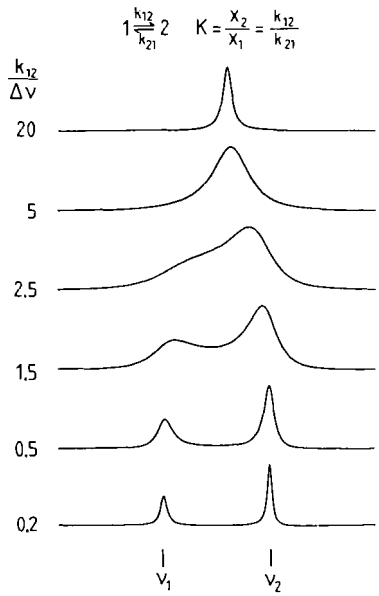

Fig. 2.1. NMR line shapes in the presence of exchange between two states, each containing one uncoupled spin, calculated according to Eq. (2.18)

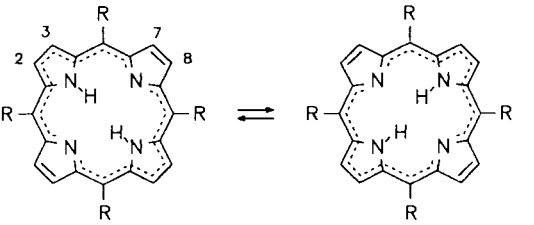

Fig. 2.2. The tautomerism of porphyrin (R = H) and of *meso*-tetraphenylporphyrin (TPP, R = phenyl)

positions given by the chemical shifts of the two states, i.e. ν_1 and ν_2. The line intensity ratios correspond to the equilibrium constant K_{12}. As k_{12} is increased the lines broaden and coalesce when $k_{12} > |2\pi\Delta\nu|$, where $\Delta\nu = \nu_1 - \nu_2$. The positions of the averaged line is given by

$$\nu = p_1\nu_1 + (1 - p_1)\nu_2 = (\nu_1 + K_{12}\nu_2)/(1 + K_{12}). \tag{2.19}$$

Thus, the equilibrium constant K_{12} can be obtained from the line position in the fast exchange regime if the chemical shifts are known.

As an application of Eq. (2.18) let us consider the tautomerism of meso-tetraphenylporphyrin (TPP, Fig. 2.2). This reaction was discovered by Storm et al. [109] and has been studied by several authors [109–116, 119, 125, 167, 168]. As shown in Fig. 2.3 two separate signals of equal intensity are observed in the low temperature ^{1}H NMR spectra of TPP dissolved in toluene-d_8. The low field line was assigned to the 2,3 protons and the high field line to the 7,8 protons [109]. As the proton transfer in TPP becomes fast both types of protons interconvert, leading to line broadening and line coalescence. In the fast exchange regime only one single line survives. Therefore, $K_{12} = 1$ in Eq. (2.19) and $k_{12} = k_{21} = k$. The spectra in Fig. 2.3 were simulated using Eq. (2.18) varying mainly the rate constant k. In the fast exchange regime the chemical shifts ν_1 and ν_2 had to be extrapolated from the slow exchange range. Examples of more complicated lineshape changes involving more complex spin systems will be discussed in later sections.

2.3 *Polarization Transfer Methods*

A problem with the low temperature experiments of Fig. 2.3 is that the residual line widths W_{01} and W_{02} strongly increase as the temperature is lowered, due to slow rotational diffusion and shortening of T_2 [116, 119]. Therefore, the value of $k = 5.5\,s^{-1}$ at 200 K obtained by lineshape analysis is affected by a large systematic error. Such uncertainties of rate constants in the slow exchange regime are encountered in all dynamic NMR experiments. As a remedy to this problem, polarization transfer experiments in the laboratory frame [75–77, 79] and in the rotating frame [80, 81, 164], in one and two dimensions, have been proposed. Whereas the first method is limited by the longitudinal relaxation time T_1 the latter is limited by $T_{1\rho}$, the longitudinal relaxation time in the rotating

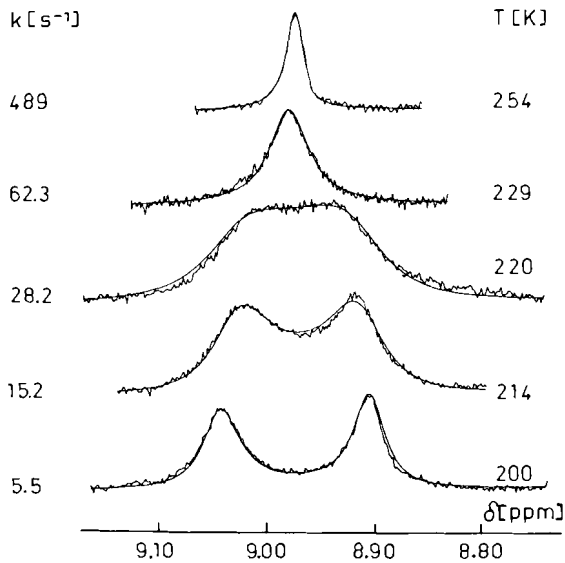

Fig. 2.3. Superposed experimental and calculated CW-100 MHz ^{1}H NMR line shapes of the β-pyrrole protons 2,3 and 7,8 of TPP dissolved in toluene-d_8. At low temperatures, the low field line (protons 2,3) shows an extra broadening due to an unresolved scalar long range coupling to the inner protons [109]. k is the calculated rate constant of the tautomerism in Figure 2.2. Reproduced with permission from Ref. [115]. See also Sect. 9.1.3 and 11.1.1

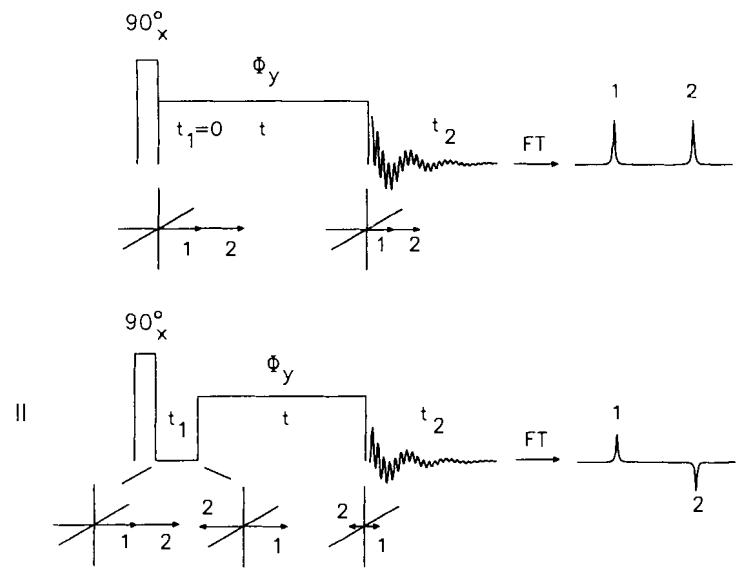

Fig. 2.4 Top: Pulse sequence for the measurement of the longitudinal relaxation time $T_{1\rho}$ in the rotating frame under the influence of a spin-locking pulse ("parallel experiment I"). **Bottom**: Pulse sequence for the detection of polarization transfer in the rotating frame according to Ref. [80] with $t_1 = 1/(2\Delta\nu)$ ("antiparallel experiment II"). The *arrows* indicate the exchanging polarizations

frame. Let us discuss here briefly the rotating frame exchange method for which experimental examples in DNMR of isotope effects will be given in Sects. 8 and 9.

The pulse sequence used is briefly discussed in Fig. 2.4. During the preparation period transverse magnetization is created by a 90^0_x pulse. After an evolution period t_1 a spin locking pulse of the strength $\omega_1 = \gamma B_1$ is applied in the y-direction of the rotating frame for the time t. The magnetizations become then polarizations in the spin locking field. After this mixing period follows the detection period t_2. This method is especially simple if neither scalar nor dipolar coupled spins are involved, and if only two exchanging polarizations M_1 and M_2 of equal probability are present, i.e. if $k_{12} = k_{21} = k$. In a typical one-dimensional experiment two sets of experiments with variable time t are performed. In experiment I, $t_1 = 0$; the exchanging polarizations M_r are parallel and decay exponentially with $T_{1\rho}$

$$M_r = M_r(0)\exp(-t/T_{1\rho}), \quad r = 1,2. \tag{2.20}$$

This decay is monitored choosing several values for the mixing time t. In Eq. (2.20) it is assumed that $T_{1\rho}$ is equal for both polarizations or that the difference has been averaged out by the exchange. In experiment II the polarizations are prepared in an antiparallel way using a delay $t_1 = 1/(2\Delta\nu)$, where $\Delta\nu = \nu_1 - \nu_2$, between the two pulses. The carrier frequency is set to one of the exchanging lines. The exchange between the polarizations is given by [80]

$$M_r = M_r(0)\exp(-(1/T_{1\rho} + 2k)t), \quad r = 1,2, \quad M_1(0) = -M_2(0). \tag{2.21}$$

Since $k_{12} = k_{21} = k$, both polarizations have the same decay constant $1/T_{1\rho} + 2k$. Thus, k can easily be obtained from the difference of the polarization decay in

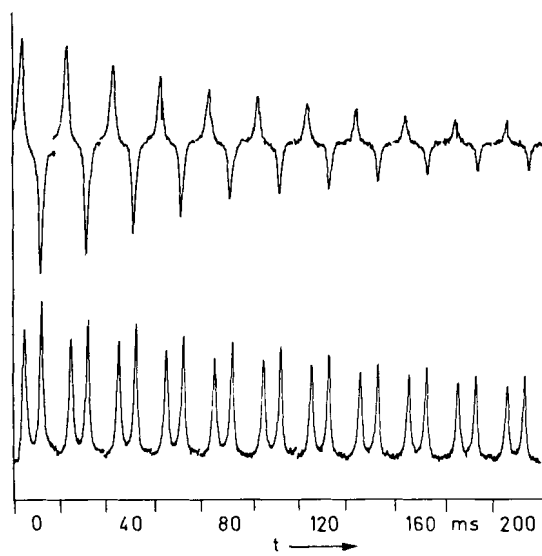

Fig. 2.5. Polarization transfer experiment performed on TPP dissolved in tetrahydrofuran-d_8 at 203 K and 90 MHz. **Bottom**: $T_{1\rho}$-experiment, **top** (i): polarization transfer in the rotating frame, with $t_1 = 1/(2\Delta\nu)$, $\Delta\nu = 25$ Hz. For further description of the experiment see text. Reproduced with permission from Ref. [80]

experiments I and II. The generalization to asymmetric reaction systems is straightforward [164].

As an example we consider again the case of TPP (Fig. 2.2) whose exchange broadened ^{1}H NMR signals were already shown in Fig. 2.3. The results of a ^{1}H NMR polarization transfer experiment in the rotating frame, performed on TPP in tetrahydrofuran at 203 K [80] are shown in Fig. 2.5. In both experiments exponential decays of the polarizations were observed. According to Eq. (2.20) the decay is governed in the "parallel" experiment by the longitudinal relaxation rate $T_{1\rho}^{-1} = 2.6 \pm 0.4\,s^{-1}$. By contrast, the decay in the "antiparallel" experiment is much faster, i.e. given according to Eq. (2.21) by $T_{1\rho}^{-1} + 2k = 8.4 \pm 0.4\,s^{-1}$. Thus, a value of $k = 2.9\,s^{-1}$ was obtained at 203 K which is substantially smaller but also much more precise than the low temperature value obtained by ^{1}H NMR lineshape analysis in Fig. 2.3.

In the presence of many exchanging polarizations a two-dimensional version of the experiment is to be preferred, where, in addition, t_1 is systematically incremented and where Fourier transformation is employed along t_1 [81].

Note that polarization transfer due to nuclear Overhauser effects (NOE) in the rotating frame must be taken into account [80] when the exchanging magnetizations are dipolar coupled. This phenomenon has been employed also to study cross-relaxation dynamics (Camelspin [192], Roesy [193]) in slow tumbling biomolecules. Note also that in the presence of scalar coupling coherent polarization transfer in the rotating frame occurs which can also be used for analytical purposes (Tocsy [194] and Hohaha [195]).

2.4 Relaxation Time Measurements

Kinetic information cannot only be obtained from magnetization transfer and lineshape experiments but also from the measurement of longitudinal relaxation times T_1, longitudinal relaxation times in the rotating frame, $T_{1\rho}$, and transverse relaxation times T_2. Since T_1 is sensitive only to motions in the MHz-range where—in the liquid phase—molecular motions dominate, it can rarely be used for the determination of rate constants of chemical reactions, including their kinetic isotope effects. Exceptions are longitudinal relaxation time measurements in the solid state where T_1 is solely governed by the proton and deuteron transfers of interest [180–187]. By contrast, the measurement of T_2 and $T_{1\rho}$ of coalesced lines provides similar information as lineshape analysis in the fast exchange regime [72], with the difference that the relaxation measurements are more precise and that the difference of chemical shifts, $\Delta\nu$, can be obtained even in the fast exchange regime.

The $T_{1\rho}$ method is especially simple in the case of symmetric exchange processes, the absence of scalar spin–spin coupling, and the case of extreme line narrowing. In this case it has been shown that [67, 73]

$$T_{1\rho}^{-1} - T_1^{-1} = \frac{\pi^2 \Delta\nu^2}{2k}\left(\frac{1}{1 + \omega_1^2/4k^2}\right), \qquad \omega_1 = \gamma B_1. \tag{2.22}$$

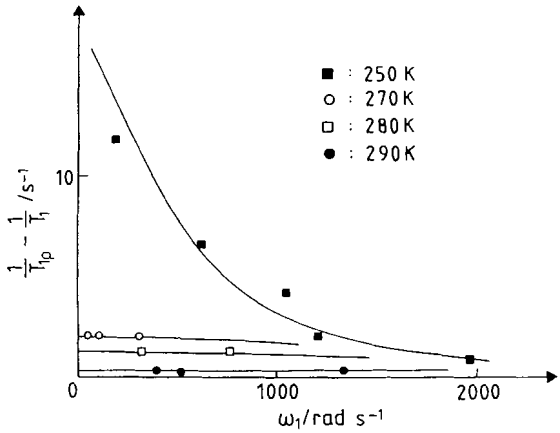

Fig. 2.6. Analysis of a ^1H–$T_{1\rho}$-experiment in the fast exchange region on the β-pyrrole protons of TPP dissolved in toluene-d_8. Values of $T_{1\rho}^{-1} - T_1^{-1}$ as a function of the strength of the rotating magnetic field $\omega_1 = \gamma B_1$. The data were adapted to Eq. (2.22) by non-linear least squares fit. ■: 250 K, ○: 270 K; □: 280 K; ●: 290 K. Reproduced with permission from Ref. [115]

By measuring $T_{1\rho}^{-1}$ as a function of ω_1 the rate constant k as well as the chemical shift difference $\Delta\nu$ can be obtained. As an example, consider the experimental $T_{1\rho}^{-1} - T_1^{-1}$ values of the coalesced line of Fig. 2.3 shown in Fig. 2.6 as a function of temperature. At 250 K the $T_{1\rho}^{-1}$ vs. ω_1 dispersion is well pronounced. At higher temperatures the term $\omega_1^2/4k^2$ becomes much smaller than 1, and

$$T_{1\rho}^{-1} - T_1^{-1} \cong \frac{\pi^2 \Delta\nu^2}{2k} \tag{2.23}$$

becomes independent on ω_1. Still, k can be obtained if $\Delta\nu$ is known. At very large k—values the difference $T_{1\rho}^{-1} - T_1^{-1}$ will, however, become so small that rate constants can no more be determined using this method.

Note that when performing ^{13}C $T_{1\rho}$ experiments proton decoupling has to be suppressed during the spin lock period [74]. Note also that the measurement of T_2 in a Carr–Purcell sequence as a function of the pulse distance leads to similar results as the $T_{1\rho}$ method [67, 72].

3 The Modulation of Nuclear Spin Hamiltonians in the Presence of Isotopic Bond Breaking/Bond Formation Processes

One condition for the study of dynamic processes by NMR is that a modulation of the nuclear spin Hamiltonian $\mathscr{H}$ occurs during the process to be studied, i.e. that $\mathscr{H}_r \neq \mathscr{H}_s$ during an interconversion between the environments r and s. This requirement is not always easy to fulfill when studying symmetric exchange reactions, the main domain of dynamic NMR spectroscopy. In this section we discuss the sensitivity of different magnetic interactions with respect to bond breaking and bond formation processes of isotopically labeled molecules of the

type r ≡ AL, where L represents the hydrogen isotopes H and D. In the following we will call the L spins also the "mobile" spins since they are transferred during the reactions studied. Spins in the remaining group A will be called "remote" spins.

For most NMR studies of condensed matter it is sufficient to include the following terms in the Hamiltonian $\mathscr{H}_r$ of a nuclear spin system in a given environment r [67]:

$$\mathscr{H}_r = \mathscr{H}_r^{CS} + \mathscr{H}_r^{CSA} + \mathscr{H}_r^{S} + \mathscr{H}_r^{SA} + \mathscr{H}_r^{DD} + \mathscr{H}_r^{Q}. \tag{3.1}$$

$\mathscr{H}_r^{CS}$ is the Hamiltonian of the isotropic chemical shift interaction, $\mathscr{H}_r^{CSA}$ of the chemical shift anisotropy, $\mathscr{H}_r^{S}$ of the isotropic scalar spin–spin interaction. $\mathscr{H}_r^{SA}$ represents the anisotropy of the latter, $\mathscr{H}_r^{DD}$ the Hamiltonian of the dipole–dipole interaction, $\mathscr{H}_r^{Q}$ the Hamiltonian of the quadrupole interaction. Expressions of all spin Hamiltonians can be found in the literature. Since $\mathscr{H}_r^{CSA}$, $\mathscr{H}_r^{SA}$, $\mathscr{H}_r^{DD}$, and $\mathscr{H}_r^{Q}$ are averaged out in the liquid state where most kinetic studies of isotope effects are performed only $\mathscr{H}_r^{CS}$ and $\mathscr{H}_r^{S}$ [67] need to be discussed here:

$$\mathscr{H}_r^{CS} = \sum_i (\nu_i - \nu)\mathbf{I}_{zi}, \quad \nu_i = \gamma_i \hbar \mathbf{B}_0 (1 - \sigma_i), \tag{3.2}$$

$$\mathscr{H}_r^{S} = \sum_{i<j}\sum \mathbf{J}_{ij}\mathbf{I}_i\mathbf{I}_j, \mathbf{J}_{ij} = \gamma_i\gamma_j\mathbf{K}_{ij}. \tag{3.3}$$

The sums have to be carried out over all spins, remote and mobile, of the environment r. ν_i is the Larmor frequency of spin i in environment r, γ the gyromagnetic ratio, $\mathbf{B}_0$ the external magnetic field, $\hbar$ Planck's constant, σ_i the screening constant of the magnetic field of nucleus i in the environment r, $\mathbf{J}_{ij}$ the coupling constant between i and j in Hz, $\mathbf{J}'_{ij}$ the reduced coupling constant, and $\mathbf{I}_i, \mathbf{I}_{zi}$ the usual angular momentum operators of spin i in the subsystem r.

In the following, the use of the different Hamiltonians in the study of kinetic isotope effects by dynamic NMR spectroscopy will be discussed. Such studies depend on whether one looks at the exchanging hydrogen isotopes L or on the remote spins A.

3.1 The Determination of Kinetic Isotope Effects via a Modulation of the Isotropic Chemical Shift Interaction

The magnetic interaction of nuclei that is the most sensitive to different chemical environments is the isotropic chemical shift interaction. Thus, a modulation of this interaction during the course of the reaction of interest makes it possible to obtain rate constants by NMR. As stated above, here bond breaking processes of molecules AL, L = H, D are studied. Depending on the chemical structures involved, these processes may induce chemical shift changes either

of the mobile spins L or of the remote spins located in group A. Thus, the information content depends on whether the spectra of group A or of the isotopes L are analyzed. Examples for both types of spectral analyses will be given in Sects. 9 to 11. It is clear that the use of the isotropic chemical shift interaction necessitates the measurement of high resolution NMR spectra. This does not constitute a problem when liquids are studied. In the case of solids, it is necessary to remove all orientation dependent interactions for this purpose.

We will now discuss which nuclei are the most apt for the study of kinetic hydrogen/deuterium isotope effects, making use of the isotopic chemical shift interaction.

3.1.1 NMR Studies of Mobile Hydrogen Isotopes

3.1.1.1 ^{1}H NMR Spectroscopy

The first experiments which are, generally, performed before entering deeper into an isotopic research project by NMR are ^{1}H NMR experiments. This method is the most sensitive NMR technique and no isotopic enrichment is necessary. Also, concentration dependent studies are most easily performed by ^{1}H NMR spectroscopy. One disadvantage is the presence of additional ^{1}H signals, e.g. solvent signals which might interfere with those carrying the kinetic information. Therefore, during the course of the research it may often be necessary to suppress certain proton signals, e.g. by deuteration. Elimination of unwanted signals is especially necessary if experiments have to be performed as a function of the deuterium fraction D in the mobile proton sites because of the limited dynamic range of the NMR receiver system. The use of signal suppression techniques or selective pulse experiments often leads to base line errors which are awkward if exchange broadened lines are to be monitored.

3.1.1.2 ^{2}H NMR Spectroscopy

The problem of the limited dynamic range of the NMR receiver is less severe in ^{2}H NMR spectroscopy because, generally, the signals of the interesting deuterated compounds are stronger than the signals of the natural abundant (0.2%) solvent deuterons. However, the smaller gyromagnetic ratio $\gamma_{^2H} \approx \gamma_{^1H}/6$ of the deuteron constitutes a severe problem. Since the gyromagnetic ratio enters the chemical shift Hamiltonian in Eq. (3.2) the typical frequency differences $\Delta\nu$ between two chemically different environments are reduced by $\gamma_{^2H}/\gamma_{^1H}$, which limits the dynamic range of ^{2}H NMR spectroscopy as a kinetic tool. This effect can be overcome partly by performing experiments at higher magnetic field and partly by the occurrence of kinetic hydrogen/deuterium isotope effects.

A more serious drawback of ^{2}H NMR spectroscopy is the quadrupole moment of ^{2}H which may lead to short longitudinal and transverse relaxation times T_1 and T_2, i.e. to broad lines. Since relaxation becomes faster when the

molecular correlation times increase, only small molecules can be studied at not too low temperatures.

3.1.1.3 ^{3}H NMR Spectroscopy

From the standpoint of chemical kinetics the measurement of kinetic hydrogen/deuterium/tritium isotope effects is extremely desirable. In view of the progress made in ^{3}H NMR spectroscopy [196, 197] and the favorable gyromagnetic ratio $\gamma_{^3H}/\gamma_{^1H} = 1.1$, it seems surprising that kinetic hydrogen/tritium isotope effects have not yet been reported. The reason is that radioactive tritium is absent in natural samples, which necessitates isotopic enrichment. Unfortunately, because of the radioactivity of this isotope samples of interest can, generally, be tritiated only to a small extent. Such degrees of tritiation are sufficient for structural NMR studies or for kinetic studies of single proton transfer reactions; however, for the elucidation of the kinetics of multiple proton transfer fully tritiated molecules would have to be studied which constitutes a substantial hazard, apart from the fact that high tritium content may lead to sample decomposition as a consequence of radiation.

3.1.2 NMR Spectroscopy of Remote Spins

Let us recall again that remote spins remain bonded to their respective neighbor atom but may experience a modulation of their spin Hamiltonian during the hydrogen transfer process. Remote spins in this sense can be all types of nuclei including non-labile protons such as protons bound to carbon.

3.1.2.1 Liquid State Remote Spin Probes

It is clear that ^{1}H NMR spectroscopy of remote ^{1}H spins, e.g. C–H protons, will always be the first choice because of the sensitivity of this method. The second choice will be naturally abundant ^{13}C NMR spectroscopy. In the presence of exchange broadened lines and low solubilities it might, however, sometimes be necessary to artificially enrich the compounds studied. From the standpoint of NMR sensitivity, an almost ideal alternative is the introduction of a ^{19}F label, which might, however, constitute a major perturbation of the chemical kinetics.

At first sight, the most ideal choice for the study of ^{15}N enriched NH···N proton transfer systems is ^{15}N NMR spectroscopy because of the large chemical shift change between protonated and non-protonated nitrogen atoms. A problem of ^{15}N NMR spectroscopy is, however, the fact that most often ^{15}N atoms relax via dipole–dipole coupling to protons. Therefore, ^{15}N atoms in deuterated ^{15}ND···^{15}N transfer systems can have very long relaxation times which makes it very difficult to record their exchange broadened NMR lineshapes. The situation is improved when working with high magnetic fields

where the anisotropy of the chemical shifts becomes a major mechanism of longitudinal relaxation.

3.1.2.2 Solid State CPMAS Remote Spin Probes

Note that the situation is quite different in solid state ^{15}N NMR studies of ^{15}N enriched molecules under the conditions of cross polarization (CP) and magic angle spinning (MAS) [152–162]. ^{15}N CPMAS NMR spectra of $^{15}ND\cdots{}^{15}N$ units have successfully been measured [167, 179]. This is because in this technique the bottleneck is not the longitudinal relaxation time of the ^{15}N but of the ^{1}H spins. In addition, there are no solubility problems.

Surely, for $HO\cdots O$ protons transfer systems embedded in organic compounds it will, in general, be necessary to use ^{13}C CPMAS NMR.

3.2 The Determination of Kinetic Isotope Effects via a Modulation of the Scalar Spin–Spin Coupling Interaction

By contrast to isotropic chemical shifts coupling constants are much less affected by chemical exchange. This is especially true for coupling constants among remote spins. However, the situation is different when scalar coupling between a mobile hydrogen isotope L and a remote spin A is present. Then, hydrogen exchange will lead to observable changes of the spin–spin splitting pattern of the L signals. As will be shown below, this change will depend on whether the proton is transferred along an intramolecular or an intermolecular pathway. Note that this modulation of the scalar spin–spin interaction is the only way to monitor a proton self exchange reaction between like molecules.

Unfortunately, scalar coupling constants are, generally, not very large and cannot be increased by increasing the magnetic field which limits the dynamic range of this method. Of practical importance is, however, scalar coupling between ^{15}N and ^{1}H spins in $^{15}NH\cdots X$ proton transfer systems because $^{1}J_{^{1}H-^{15}N}$ coupling constants are of the order of 80 to 100 Hz and provide, therefore, a quite large dynamic range.

A problem arises, however, in the study of the related $^{15}ND\cdots X$ deuteron transfer systems. Because of Eq. (3.3) the coupling constant J_{AD} is $\gamma_{^{1}H}/\gamma_{^{2}H}$ times smaller than the corresponding constant J_{AH}. Therefore, the scalar A–D interaction will, generally, be of limited use for the determination of kinetic isotope effects of proton transfer reactions.

There are, however, exceptions to this statement. Thus, as will be shown in Sects. 9 and 10, the scalar spin–spin interaction $J_{^{1}H-^{15}N}$ can be employed to study the partial kinetic HH/HD isotope effects of intra- and intermolecular hydrogen transfer reactions.

3.3 The Determination of Kinetic Isotope Effects via a Modulation of Orientation Dependent Nuclear Spin Interactions in Solids

Since proton and deuteron transfers are proton dislocations in space these processes also lead to a modulation of the orientation dependent nuclear spin interactions in solids, i.e. of the anisotropy of the chemical shift, the dipole–dipole interaction and the quadrupole interaction. The determination of kinetic hydrogen/deuterium isotope effects on solid state hydrogen transfer reactions by taking advantage of these interactions is, however, not easy, because of the different gyromagnetic ratios of ^1H and ^2H, the fact that ^1H has no quadrupole moment, and the problem that, generally, more than one interaction is modulated when the transfer occurs. The latter problem may be circumvented by studying single crystals instead of microcrystalline powders. This is because the spectra of single crystals are much simpler since all molecules have the same orientation with respect to the magnetic field. In the case of ^2H NMR the situation is furthermore simplified because only the quadrupole interaction needs to be taken into account. Using this method partial kinetic HD/DD isotope effects of double hydrogen transfer reactions can be studied. The determination of the corresponding HH reaction is more complicated. In favorable cases it can be achieved when the jumping protons are dipolar coupled among themselves or coupled to a remote spin. This method will generally require deuteration of all immobile protons in the sample. Finally, it seems to be possible also to look at remote spins which are dipolar coupled to the jumping protons. One also could take advantage of the modulation of the chemical shift anisotropy of the remote spins in order to obtain kinetic H/D isotope effects under conditions of ^1H decoupling in order to remove heteronuclear dipolar couplings.

4 Dynamic NMR Spectroscopy in the Presence of Complex Bond Breaking/Bond Formation Processes

4.1 The Concept of Group Exchange

In chemical reactions involving bond breaking and bond formation processes the exchange operator in Eq. (2.12) is valid only in the absence of scalar spin–spin coupling. The exchange broadened NMR spectra of general spin systems can, however, conveniently be described using the concept of "group exchange" [94]. This concept is further developed in the following, with special emphasis on the description of isotopic exchange reactions.

Let r, s, x, y be molecular species subject to the general forward reaction

$$r + s \xrightarrow{k_+} x + y, \tag{4.1}$$

characterized by the second order forward rate constant k_+. Note that this reaction is not one-sided but that, as stated above, the backward reaction

$$x + y \xrightarrow{k_-} r + s \tag{4.2}$$

does not need to be treated explicitly as long as the equilibrium constant of the reaction is known.

In order to trace the pathways of atoms or groups of atoms during the reaction described by Eq. (4.1) we formally rewrite each reactant r as a combination of groups of nuclei A^r, B^r... In the simplest case we have $r \equiv A^rB^r$. A^r and B^r are defined in such a way that the nuclei within each group stay together during the reaction of interest. In the case where all molecules contain two groups Eq. (4.1) becomes

$$A^rB^r + C^sD^s \xrightarrow{k_{+1}} A^xC^x + B^yD^y, \tag{4.3}$$

which is characterized by the rate constant k_{+1}. This notation takes into account that a group of nuclei A^r may rearrange or may change its spin Hamiltonian when it is incorporated as group A^x into the molecule $x \equiv A^xC^x$. This notation also allows to trace reaction pathways of the spins in the different groups.

In order to facilitate the line shape calculations we decompose Eq. (4.3) into the following group exchange reactions:

$$A^r \xrightarrow{\tau_{rx}^{-1}(A)} A^x, \quad B^r \xrightarrow{\tau_{ry}^{-1}(B)} B^y, \quad C^s \xrightarrow{\tau_{sx}^{-1}(C)} C^x, \quad D^s \xrightarrow{\tau_{sy}^{-1}(D)} D^y. \tag{4.4}$$

$\tau_{rx}^{-1}(A)$ is the average inverse lifetime of group A in the reactant r before reaction to x occurs. $\tau_{rx}^{-1}(A)$ is equal to the pseudo first order group exchange rate constant $k_{rx}(A)$ of the exchange process in Eq. (4.3). Since the elements of the exchange operator Ξ depend on these quantities, the latter can be obtained by dynamic NMR spectroscopy. Using formal kinetics the inverse lifetimes can be linked to the rate constants, as will be demonstrated in Sect. 5.

The introduction of group exchange rate constants has not only the advantage that the group exchange pathway can be traced, but also, that possible additional symmetric exchange reactions of the type

$$A^rB^r + A^{x*}C^x \xrightarrow{k_{+2}} A^{r*}B^r + A^xC^x, \tag{4.5}$$

$$A^rB^r + B^{y*}D^y \xrightarrow{k_{+3}} A^rB^{r*} + B^yD^y, \tag{4.6}$$

$$A^rB^r + A^{r*}B^{r*} \xrightarrow{k_{+4}} A^{r*}B^r + A^rB^{r*} \tag{4.7}$$

etc. are "built" into the formalism. Consider, for example, Eq. (4.5) which can be decomposed into the group exchange reaction set

$$A^r \xrightarrow{\tau_{rx}^{-1}(A)} A^x, \quad B^r \xrightarrow{\tau_{rr}^{-1}(B)} B^r, \quad A^{r*} \xrightarrow{\tau_{rx}^{-1}(A)} A^{x*}, \quad C^x \xrightarrow{\tau_{xx}^{-1}(C)} C^x. \tag{4.8}$$

By comparison with Eq. (4.4) it follows that the quantity $\tau_{rx}^{-1}(A)$ does not depend

only on the rate constant k_{+1} in Eq. (4.3) but also on the constant k_{+2} defined in Eq. (4.5). As further seen by inspection of Eq. (4.8) one needs only to include in the set of group exchange rate constants $\tau_{rx}^{-1}(A)$ the possibility that $r = x$, in order to take self exchange reactions of the type described in Eqs. (4.4) to (4.8) into account.

A further advantage of the concept of group exchange rate constants is that one can drop the above restriction to two groups in each molecule. Thus, the presence of additional dissociation and transfer reactions of the type

$$A^rB^r + C^sD^s \xrightarrow{k_{+5}} A^t + B^uC^uD^u, \tag{4.9}$$

$$A^t + C^sD^s \xrightarrow{k_{+6}} A^xC^x + D^v \tag{4.10}$$

etc. is taken into account by considering the additional group exchange reactions

$$A^r \xrightarrow{\tau_{rt}^{-1}(A)} A^t; \quad B^r \xrightarrow{\tau_{ru}^{-1}(B)} B^u; \quad C^s \xrightarrow{\tau_{su}^{-1}(C)} C^u; \quad D^s \xrightarrow{\tau_{su}^{-1}(D)} D^u;$$

$$A^t \xrightarrow{\tau_{tx}^{-1}(A)} A^x; \quad C^s \xrightarrow{\tau_{sx}^{-1}(C)} C^x; \quad S^s \xrightarrow{\tau_{sv}^{-1}(D)} D^v. \tag{4.11}$$

Thus, it is easy to set up the NMR lineshape equations for exchanging systems without assuming a particular reaction network when using pseudo first order group exchange rate constants.

When setting up lineshape equations it is useful to neglect spin–spin interactions between the different groups in a first stage. Then, the whole master equation splits up into separate sets of equations, one set for each reacting group. The matrix $\mathcal{M}_A$ of group A has the structure:

$$\mathcal{M}_A = \begin{array}{|c|c|c|} \hline i\mathcal{L}_{A^r}^{CS} + \Xi_{A^r} + \mathcal{R}_{A^r} & \Xi_{A^sA^r} & \cdots \\ \hline \Xi_{A^rA^s} & i\mathcal{L}_{A^s}^{CS} + \Xi_{A^s} + \mathcal{R}_{A^s} & \cdots \\ \hline & & \cdots \\ \hline \end{array} \tag{4.12}$$

The elements denoted by $\Xi_{A^rA^s}$ and $\Xi_{A^sA^r}$ depend only on single group exchange rate constant $\tau_{rs}^{-1}(A)$, those denoted by Ξ_{A^r} on the sum of all group exchange rate constants. The actual elements can be calculated from Eq. (2.12) and are given by

$$\Xi^{(A)}_{\mu_r\nu_r;\kappa_s\lambda_s} = \tau_{rs}^{-1}(A)\,\delta_{\mu_r\kappa_s}\delta_{\nu_r\lambda_s} - \delta_{\mu_r\kappa_s}\delta_{\nu_r\lambda_s}\sum_t \tau_{rt}^{-1}(A), \quad t = r,s \tag{4.13}$$

The elements of $\mathcal{L}_{A^r}$ are calculated according to Eqs. (2.3), (3.2) and (3.3). In the case where A^r contains more than one interacting spin either a product base of the single spins is used or the eigenbase of the Hamiltonian $\mathcal{H}_{A^r}$. As stated above, $\mathcal{L}_{A^r}$ is diagonal in the latter case and the diagonal elements correspond to the transition frequencies.

In a second stage scalar coupling between different groups A^r and B^r of a molecule r is introduced. Note that because of the group exchange processes present one cannot use an Eigenbase of the total spin Hamiltonian $\mathscr{H}_r$ of the molecule r, but has to use the product base A^rB^r. Thus, the spin functions are written in the form $\mu_{A^r}u_{B^r} \equiv \mu_r u_r$, where a greek letter has been used for the spin functions of group A^r and a latin letter for the spin functions of B^r. Then, the Liouville operator of the molecule $r = A^rB^r$

$$\mathscr{L}_r = \mathscr{L}_{A^r} + \mathscr{L}_{B^r} + \mathscr{L}^S_{A^rB^r}, \quad \mathscr{L}_{A^r} = \mathscr{L}^{CS}_{A^r} + \mathscr{L}^S_{A^r} \tag{4.14}$$

contains non-diagonal elements connecting the two blocks $\mathscr{L}_{A^r}$ and $\mathscr{L}_{B^r}$ because of the interaction term $\mathscr{L}^S_{A^rB^r}$. In constructing the exchange operator one has to take into account that the number of spin states in the spin systems in the different groups are different. The following general exchange operator has been derived to deal with this problem [94]:

$$\begin{aligned}
&\Xi_{\mu_r u_r \nu_r v_r; \kappa_s x_s \lambda_s y_s} \\
&= \tau_{rs}^{-1}(A)\, n_{B^r}^{-1}\, \delta_{u_r v_r}\delta_{x_s y_s}\delta_{\mu_r \kappa_s}\delta_{\nu_r \lambda_s} g_{x_s} - \delta_{u_r v_r}\delta_{\mu_e \kappa_s}\delta_{v_r y_s}\delta_{\nu_r \lambda_s}\sum_t \tau_{rt}^{-1}(A) \\
&\quad + \tau_{rs}^{-1}(B)\, n_{A^r}^{-1}\delta_{\mu_r \nu_r}\delta_{\kappa_s \lambda_s}\delta_{u_r x_s}\delta_{v_r y_s} g_{\kappa_s} - \delta_{\mu_r \nu_r}\delta_{\nu_r y_s}\delta_{u_r x_s}\delta_{\nu_r \lambda_s}\sum_t \tau_{rt}^{-1}(B), \\
&\qquad\qquad\qquad\qquad\qquad\qquad\qquad\qquad\qquad\qquad t = r, s \cdots
\end{aligned} \tag{4.15}$$

n_{A^r} and n_{B^r} represent the number of spin states in A^r and B^r. g_{k_s} and g_{x_s} represent the statistical weights of the spin function k_s and x_s. $g_{k_s}(g_{x_s})$ is different from unity when an Eigenbase of the group spin-Hamiltonian $\mathscr{H}_{A^r}(\mathscr{H}_{B^r})$ is used [94].

4.2 *Dynamic NMR Spectroscopy in the Presence of Isotopic Exchange Reactions*

The above theory of NMR lineshapes in the presence of group exchange can immediately be applied to the problem of superposed isotopic exchange reactions by taking into account that the different environments r, s, ... in the previous section may correspond not only to different chemical species such as AH and XH, but also to isotopically different molecules of the same species, e.g. AH and AD. Since isotopic reactions introduce, however, a higher degree of complexity it is preferable to study reaction mixtures in which only one chemical reaction is present. Before starting a systematic study of kinetic isotope effects it is, therefore, always desirable to find experimental conditions where the dynamic quantities measured are determined only by a single reaction.

Before we can set up typical NMR lineshape equations in order to determine kinetic hydrogen/deuterium isotope effects of proton transfer reactions we first have to relate the inverse lifetimes accessible by dynamic NMR to conventional kinetic quantities, as shown in the following section.

5 The NMR Proton Inventory Technique

In order to obtain information on kinetic hydrogen/deuterium isotope effects by dynamic NMR spectroscopy it is necessary to measure inverse proton and deuteron life times as a function of the deuterium fraction in the mobile proton sites. The function obtained will depend on the actual exchange mechanism and will provide information about the rate constants of the isotopic reactions. Kinetic experiments of this kind are called in the literature "proton inventories" [43]. Therefore, the term "NMR proton inventory technique" is used.

Unfortunately, because of the multitude of different mechanisms and rate laws of hydrogen transfer reactions it is not possible to derive reactions between inverse lifetimes and rate constants of isotopic reactions in a general way. In this section it will be demonstrated—using specific examples of proton and deuteron transfer reactions relevant in the context of this study—how such relations may be obtained. The extension to other reactions and isotopes is then straightforward. Intra- and intermolecular single and multiple H/D transfer reactions are treated in separate sections; some of the equations given in this section were first derived in Refs. [106–108].

5.1 Intramolecular Hydrogen Transfer Reactions

The term "intramolecular reaction" is used here to describe reactions in molecules or molecular systems where all groups of atoms may rearrange but stay together for an infinite time as compared to the NMR-timescale. It is clear that hydrogen transfer reactions within monomeric molecules fall into this definition, but, in principle, also intermolecular hydrogen transfer reactions in molecular aggregates such as dimers, if the lifetime of the latter is large enough, as, for example, in the solid state.

In the case of intramolecular reactions the quantities entering the elements of the exchange operator Ξ are the first order rate constants themselves. In this section, therefore, one does not need to apply the concept of group exchange proposed in Sect. 4.

5.1.1 Single Intramolecular Hydrogen Transfer Reactions

Let us consider first an intramolecular single hydrogen transfer between heavy atoms of a molecular fragment. Denoting the latter as A before and as X after the transfer process one can write

$$\mathrm{AH} \underset{k_-^H}{\overset{k_+^H}{\rightleftharpoons}} \mathrm{XH}, \tag{5.1}$$

$$AD \underset{k_-^D}{\overset{k_+^D}{\rightleftharpoons}} XD. \tag{5.2}$$

More precisely, AL, L = H, D may correspond to A–B–L and XL to L–A–B. The quantities k_+^L and k_-^L represent the first order forward and backward rate constants. At an arbitrary deuterium fraction the H and the D transfer reactions are superposed without mutual interference. Thus, the ^1H NMR signals of the mobile L spins only contain contributions from AH and XH molecules, whereas the ^2H NMR signals exclusively arise from the AD and XD species. Changing the overal deuterium fraction D in the mobile proton sites only changes the ratio of the protonated vs. the deuterated molecules but not their contributions to the NMR line-shape. As a consequence, the ^1H NMR signals contain information about the quantity k_+^H and the ^2H NMR signals about the quantity k_+^D. By contrast, the spectra of the A and the X spins depend on both quantities. One can, therefore, choose the most convenient way to determine the isotopic reaction rate constants. Note, that it might in some cases be difficult to derive both quantities k_+^H and k_+^D from the A/X spectra of a single sample at an intermediate deuterium fraction D because isotope effects on the A/X chemical shifts will be too small to resolve the lineshape contributions of the protonated and the deuterated molecules. These quantities can, however, easily, be derived from the A/X NMR spectra of samples with deuterium fractions of D = 0 and D = 1.

5.1.2 Double Intramolecular Hydrogen Transfer Reactions

An intramolecular double hydrogen transfer system contains two mobile hydrogen atoms. The reaction, can, therefore, be written in the form

$$AHH \underset{k_-^{HH}}{\overset{k_+^{HH}}{\rightleftharpoons}} XHH, \tag{5.3}$$

$$AHH \underset{k_-^{HD}}{\overset{k_+^{HD}}{\rightleftharpoons}} XHD, \tag{5.4}$$

$$ADH \underset{k_-^{HD}}{\overset{k_+^{HD}}{\rightleftharpoons}} XDH, \tag{5.5}$$

$$ADD \underset{k_-^{DD}}{\overset{k_+^{DD}}{\rightleftharpoons}} XDD, \tag{5.6}$$

where, for example, ALL ≡ ALBLCD and XLL ≡ ABCLDL. There are four reactant species giving contributions to the NMR lineshapes of the L spins. The species AHH, AHD and ADH contribute to the H signals which depend, therefore, on the first order rate constants k_+^{HH}, k_+^{HD} and k_+^{DH} as well as on the corresponding equilibrium constants. k_+^{HH} is most easily determined in a separate ^1H NMR experiment at a deuterium fraction of D = 0, whereas k_+^{HD} and k_+^{DH} have to be determined at higher D values. Similar arguments hold for the ^2H

NMR spectra. Thus, the whole set of kinetic isotope effects can be determined. Since, as mentioned in Sect. 3.1.1.2, liquid state ^2H NMR spectra are sometimes of low kinetic information content, additional experiments on the A/X spins are of help. The latter depend on all quantities k_+^{HH}, k_+^{HD}, k_+^{DH} and k_+^{DD}. In order to check the k_+^{HH} values obtained from the ^1H spectra, and in order to obtain the only lacking quantity k_+^{DD}, A spin NMR experiments are preferentially carried out at $D = 0$ and 1. The determination of k_+^{HD} and of k_+^{DH} at intermediate deuterium fractions may represent problems because of the difficulty to distinguish the different species in the A/X spectra.

5.1.3 Multiple Intramolecular Hydrogen Transfer Reactions

The extension of the arguments given in the two previous sections to cases where more than two protons are transferred along intramolecular pathways is straightforward and will, therefore, not be considered further. In the spectral analysis one only needs to keep in mind that the lineshapes are the sum of contributions from the different isotopic species, which do not interconvert between each other. The larger the number of isotopic rate constants characterizing a given reaction system the more experiments have to be carried out using a certain combination of different multinuclear NMR experiments and deuterium fractions in the mobile proton sites.

5.2 Intermolecular Hydrogen Transfer Reactions

In this section we consider intermolecular multiple hydrogen transfer reactions of proton donors AL containing one labile hydrogen isotope L. By contrast to intramolecular reactions, the kinetic variables which determine the NMR

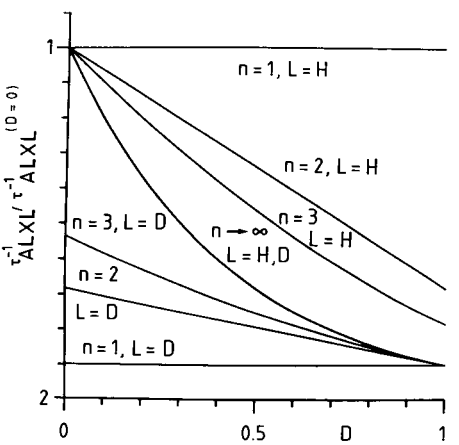

Fig. 5.1. NMR proton inventory plots as a function of the deuterium fraction D for different numbers n of protons transported in the rate limiting step for C_B = constant. L is the nucleus whose NMR spectra are observed. The overall kinetic isotope effect was set arbitrarily to a value of 10. Adapted with permission from Ref. [106]

spectra will depend themselves on the deuterium fractions in the labile proton sites. In the following we will derive appropriate equations for different kinds of hydrogen transfer reactions. Some of these equations are illustrated graphically in Fig. 5.1.

5.2.1 Single Intermolecular Hydrogen Transfer Reactions

Let us first consider the basic single hydrogen transfer reactions

$$AH + X \underset{k_-^H}{\overset{k_+^H}{\rightleftharpoons}} A + XH, \tag{5.7}$$

$$AD + X \underset{k_-^D}{\overset{k_+^D}{\rightleftharpoons}} A + XD, \tag{5.8}$$

where k_+^L is the forward second order rate constant. Equations (5.7) and (5.8) can be decomposed into the following group exchange reaction set

$$AH \xrightarrow{\tau_{\mathbf{AH}\mathbf{XH}}^{-1}} XH, \quad AD \xrightarrow{\tau_{\mathbf{AD}\mathbf{XD}}^{-1}} XD,$$

$$AH \xleftrightarrow{\tau_{\mathbf{AH}\mathbf{A}}^{-1}} A, \quad AD \xleftrightarrow{\tau_{\mathbf{AD}\mathbf{A}}^{-1}} X, \quad X \xleftrightarrow{\tau_{\mathbf{XX}\mathbf{H}}^{-1}} XH, \quad X \xleftrightarrow{\tau_{\mathbf{XX}\mathbf{D}}^{-1}} XD. \tag{5.9}$$

As compared to Sect. 3, we use here a slightly different, for the case of hydrogen transfer reactions, better adapted notation. The exchanging group is marked here in boldface, and the full chemical symbols are used as subscript. Thus, $\tau_{\mathbf{AL}\mathbf{XL}}^{-1}$ represents the average inverse lifetime of L in AL before it is incorporated into XL; $\tau_{\mathbf{AL}\mathbf{A}}^{-1}$ is the lifetime of group A in AL before the change to A. Clearly, $\tau_{\mathbf{AL}\mathbf{XL}}^{-1}$ is obtained by analysis of the L signals and $\tau_{\mathbf{AL}\mathbf{A}}^{-1}$ of the A signals.

From conventional kinetics it follows that

$$\tau_{\mathbf{AL}\mathbf{A}}^{-1} = \tau_{\mathbf{AL}\mathbf{XL}}^{-1} = -(1/C_{AL})\,dC_{AL}/dt = k_+^L\,C_X, \quad L = H, D. \tag{5.10}$$

As a consequence, in a single hydrogen transfer reaction the different inverse lifetimes are independent of the deuterium fraction in the mobile proton sites. E.g. it follows that

$$\tau_{\mathbf{AL}\mathbf{XL}}^{-1}/\tau_{\mathbf{AL}\mathbf{XL}}^{-1}(D = 0) = 1. \tag{5.11}$$

Using an arbitrary kinetic isotope effect of $\tau_{\mathbf{AH}\mathbf{XH}}^{-1}(D = 0)/\tau_{\mathbf{AD}\mathbf{XD}}^{-1}(D = 1) = k_+^H/k_+^D = 10$ one obtains for the quantities $\tau_{\mathbf{AL}\mathbf{XL}}^{-1}/\tau_{\mathbf{AL}\mathbf{XL}}^{-1}(D = 0)$, $L = H, D$ in the graph of Fig. 5.1 two horizontal lines ($n = 1$, $L = H$ and $n = D$).

Note that in the case where the concentrations of A and X become very small, i.e. where only AL and XL can be observed one obtains a formal double proton transfer reaction treated in the following section.

5.2.2 Double Intermolecular Hydrogen Transfer Reactions

Let us consider here the basic hydrogen exchange reaction between two different labile proton sites AH and XH, with an equilibrium constant of K = 1:

$$AH + XH^* \underset{}{\overset{k_+^{HH}}{\rightleftharpoons}} AH^* + XH, \tag{5.12}$$

$$AH + XD \underset{k_-^{HD}}{\overset{k_+^{HD}}{\rightleftharpoons}} AD + XH, \tag{5.13}$$

$$AD + XH \underset{k_-^{DH}}{\overset{k_+^{DH}}{\rightleftharpoons}} AH + XD, \tag{5.14}$$

$$AD + XD^* \underset{}{\overset{k_+^{DD}}{\rightleftharpoons}} AD^* + XD. \tag{5.15}$$

Let k_+^{LL} be the pseudo second order rate constants of the different forward isotopic reactions whose rate constants are to be determined. Note that

$$k_+^{HD} = k_-^{DH} \quad \text{and} \quad k_+^{DH} = k_-^{HD}, \tag{5.16}$$

where k_-^{LL} are again backward pseudo second order rate constants. A star is introduced here to characterize chemically equivalent but physically different groups. The above reaction set can be decomposed into the following set of group exchange reactions:

$$AH \xrightarrow{\tau_{AHAH^*}^{-1}} AH^*, \quad AH \xrightarrow{\tau_{AHAD}^{-1}} AD, \quad AD \xrightarrow{\tau_{ADAH}^{-1}} AH, \quad AD \xrightarrow{\tau_{ADAD^*}^{-1}} AD^*, \tag{5.17}$$

$$XH \xrightarrow{\tau_{XHXH^*}^{-1}} XH^*, \quad XH \xrightarrow{\tau_{XHXD}^{-1}} XD, \quad XD \xrightarrow{\tau_{XDXH}^{-1}} XH, \quad XD \xrightarrow{\tau_{XDXD^*}^{-1}} XD^*, \tag{5.18}$$

$$AH \xrightarrow{\tau_{AHXH}^{-1}} XH, \tag{5.19}$$

$$AD \xrightarrow{\tau_{ADXD}^{-1}} XD \text{ etc.} \tag{5.20}$$

Here $\tau_{ALAL^*}^{-1}$ with LL* = HH*, HD, DH, DD* represents the observable pseudo first order exchange rate constant of group A (marked in boldface) between the environments AL and AL*, or in other words, the inverse correlation time of group A with spin L before the latter is replaced by spin L*. It is evident that $\tau_{ALAL^*}^{-1}$ can be determined only by lineshape analysis of the A-spin spectra when the Hamiltonian of A is modulated by the exchange. By contrast, τ_{ALXL}^{-1}, the inverse lifetime of spin L in the environment AL before the reaction to XL occurs, has to be determined from the NMR spectra of the L spins.

In contrast to single proton transfer reactions, the above inverse group lifetimes depend on the individual deuterium fractions D_A and D_X in the two

mobile proton sites AL and XL. By measuring these lifetimes as a function of the overall deuterium fraction D, the four independent isotopic rate constants k_+^{HH}, k_+^{HD}, k_+^{DH}, and k_+^{DD} can be determined. Relations between these rate constants and the measured inverse lifetimes will be derived in the following.

We first define the inverse equilibrium isotope effect or fractionation factor

$$\Phi^{-1} = k_+^{HD}/k_-^{HD} = k_+^{HD}/k_+^{DH} = C_{AD}C_{XH}/C_{AH}C_{XD}, \tag{5.21}$$

the total concentration,

$$C_A = C_{AH} + C_{AD}, \tag{5.22}$$

the individual deuterium fraction

$$D_A = C_{AD}/C_A, \tag{5.23}$$

and the overall deuterium fraction

$$D = (C_{AD} + C_{XD})/(C_A + C_X). \tag{5.24}$$

By combination of these equations functions of the type $D_A = f(D, \Phi^{-1}, C_A/C_X)$ can be obtained. Φ, i.e. D_A and D_X, can be obtained by lineshape analysis in the slow exchange region. In the absence of equilibrium isotope effects the following relations hold:

$$\Phi = 1, \quad \text{i.e.} \quad k_+^{HD} = k_+^{DH} = k_+^{HD} \quad \text{or} \quad D_A = D_X = D. \tag{5.25}$$

For the observable inverse lifetimes the following relations are easily derived:

$$\tau_{AHAH^*}^{-1} = -(1/C_{AH})\,dC_{AH\to AH^*}/dt = k_+^{HH}C_{XH} = (1 - D_X)\,k_+^{HH}C_X. \tag{5.26}$$

$$\tau_{AHAD}^{-1} = -(1/C_{AH})\,dC_{AH\to AD}/dt = D_X k_+^{HD} C_X. \tag{5.27}$$

$$\tau_{ADAH}^{-1} = -(1/C_{AD})\,dC_{AD\to AH}/dt = (1 - D_X)\,k_+^{DH}C_X. \tag{5.28}$$

$$\tau_{ADAD^*}^{-1} = -(1/C_{AD})\,dC_{AD\to AD^*}/dt = D_X k_+^{DD} C_X \tag{5.29}$$

$$\begin{aligned}\tau_{AHXH}^{-1} &= -(1/C_{AH})\,dC_{AH\to XH}/dt \\ &= k_+^{HH}C_{XH} + k_+^{HD}C_{XD} = ((1 - D_X)k_+^{HH} + D_X k_+^{HD})C_X.\end{aligned} \tag{5.30}$$

$$\begin{aligned}\tau_{ADXD}^{-1} &= -(1/C_{AD})\,dC_{AD\to XD}/dt \\ &= k_+^{DH}C_{XH} + k_+^{DD}C_{XD} = ((1 - D_X)k_+^{DH} + D_X k_+^{DD})C_X.\end{aligned} \tag{5.31}$$

The remaining quantities are obtained by substitution of X by A and of A by X. Equations (5.26) to (5.31) indicate that the different inverse lifetimes depend linearly on the deuterium fraction D_X of the reaction partner XL. When Eq. (5.25) is valid it follows that the inverse lifetimes τ_{AHXH}^{-1} and τ_{ADXD}^{-1} depend linearly on the overall deuterium fraction D. One then obtains from Eqs. (5.26) to (5.31)

$$\tau_{AHXH}^{-1}(D)/\tau_{AHXH}^{-1}(D = 0) = 1 - [1 - k^{HD}/k^{HH}]\cdot D, \tag{5.32}$$

$$\tau_{ADXD}^{-1}(D)/\tau_{ADXD}^{-1}(D = 1) = k^{DH}/k^{DD} - [k^{DH}/k^{DD} - 1]\cdot D \tag{5.33}$$

Note that Eqs. (5.26) to (5.33) also hold for the case of self exchange between

AH molecules, i.e. where $X \equiv A$. In this case one can abbreviate

$$\tau^{-1}_{AHA^*H} \equiv \tau^{-1}_{AH} \tag{5.34}$$

and

$$\tau^{-1}_{ADA^*D} \equiv \tau^{-1}_{AD}. \tag{5.35}$$

Using again an arbitrary kinetic isotope effect of $k^{HH}/k^{DD} = 10$ and the geometric mean values $k^{HH}/k^{HD} = k^{DH}/k^{DD} = 10^{1/2}$ the linear curves n = 2, L = H and n = 2, L = D shown in Fig. 5.1 are obtained. Since equilibrium isotope effects were neglected in Fig. 5.1 it follows from Eqs. (5.30) and (5.31) that $\tau^{-1}_{ADXD}(D = 0) = \tau^{-1}_{AHXH}(D = 1) = k^{HD} = k^{DH}$, which—as an experimental observation—would be a proof for a double proton transfer reaction.

5.2.3 *Triple Intermolecular Hydrogen Transfer Reactions*

Let us consider in this section a triple proton transfer reaction of the kind

$$AH + BH^* + XH' \underset{}{\overset{k_+^{HHH}}{\rightleftharpoons}} AH^* + BH' + XH, \tag{5.36}$$

$$AH + BH^* + XD \overset{k_+^{HHD}}{\rightleftharpoons} AH^* + BD + XH, \tag{5.37}$$

$$AH + BD + XH' \overset{k_+^{HDH}}{\rightleftharpoons} AD + BH' + XH, \tag{5.38}$$

$$AD + BH^* + XH \overset{k_+^{DHH}}{\rightleftharpoons} AH^* + BH + XD, \tag{5.39}$$

$$AD + BD^* + XH \overset{k_+^{DDH}}{\rightleftharpoons} AD^* + BH + XD, \tag{5.40}$$

$$AD + BH^* + XD' \overset{k_+^{DHD}}{\rightleftharpoons} AH^* + BD' + XD, \tag{5.41}$$

$$AH + BD' + XD \overset{k_+^{HDD}}{\rightleftharpoons} AD' + BD + XH, \tag{5.42}$$

$$AD + BD' + XD^* \overset{k_+^{DDD}}{\rightleftharpoons} AD' + BD^* + XD. \tag{5.43}$$

The backward reactions are characterized by the symbols k_-^{LLL}. As in the previous section, let us only consider the inverse average lifetimes of one of the reactants, i.e. here AL. Note that one obtains for AL exactly the same group exchange reaction set as in the case of the double proton transfer reactions in the previous section:

$$AH \xrightarrow{\tau^{-1}_{AHAH^*}} AH^*, \quad AH \xrightarrow{\tau^{-1}_{AHAD}} AD, \quad AD \xrightarrow{\tau^{-1}_{ADAH}} AH,$$

$$AD \xrightarrow{\tau^{-1}_{ADAD}} AD^*, \tag{5.44}$$

$$AH \xrightarrow{\tau^{-1}_{AHXH}} XH, \quad AD \xrightarrow{\tau^{-1}_{ADXD}} XD \text{ etc.} \tag{5.45}$$

In a similar way as in the previous section we then obtain

$$\begin{aligned}\tau^{-1}_{AHAH^*} &= (k_+^{HHH} + k_-^{HHH})C_{BH}C_{XH} + (k_+^{HHD} + k_-^{DHH})C_{BH}C_{XD} \\ &= [(1 - D_B)(1 - D_X)(k_+^{HHH} + k_-^{HHH}) \\ &\quad + (1 - D_B)D_X(k_+^{HHD} + k_-^{DHH})]C_BC_X.\end{aligned} \tag{5.46}$$

$$\begin{aligned}\tau^{-1}_{AHAD} &= (k_+^{HDH} + k_-^{HHD})C_{BD}C_{XH} + (k_+^{HDD} + k_-^{DHD})C_{BD}C_{XD} \\ &= [D_B(1 - D_X)(k_+^{HDH} + k_-^{HHD}) + D_BD_X(k_+^{HDD} + k_-^{DHD})]C_BC_X.\end{aligned} \tag{5.47}$$

$$\begin{aligned}\tau^{-1}_{ADAH} &= (k_+^{DHH} + k_-^{HDH})C_{BH}C_{XH} + (k_+^{DHD} + k_-^{DHD})C_{BH}C_{XD} \\ &= [(1 - D_B)(1 - D_X)(k_+^{DHH} + k_-^{HDH}) \\ &\quad + (1 - D_B)D_X(k_+^{DHD} + k_-^{DDH})]C_BC_X.\end{aligned} \tag{5.48}$$

$$\begin{aligned}\tau^{-1}_{ADAD^*} &= (k_+^{DDH} + k_-^{HDD})C_{BD}C_{XH} + (k_+^{DDD} + k_-^{DDD})C_{BD}C_{XD} \\ &= [D_B(1 - D_X)(k_+^{DDH} + k_-^{HDD}) + D_BD_X(k_+^{DDD} + k_-^{DDD})]C_BC_X.\end{aligned} \tag{5.49}$$

$$\begin{aligned}\tau^{-1}_{AHXH} &= (k_+^{HHH} + k_-^{HHH})C_{BH}C_{XH} + (k_+^{HHD} + k_-^{DHH})C_{BH}C_{XD} \\ &\quad + (k_+^{HDH} + k_-^{HHD})C_{BD}C_{XH} + (k_+^{HDD} + k_-^{DHD})C_{BD}C_{XD} \\ &= [(1 - D_B)(1 - D_X)(k_+^{HHH} + k_-^{HHH}) + (1 - D_B)D_X(k_+^{HHD} + k_-^{DHH}) \\ &\quad + D_B(1 - D_X)(k_+^{HDH} + k_-^{HHD}) + (k_+^{HDD} + k_-^{DHD})D_BD_X]C_BC_X.\end{aligned} \tag{5.50}$$

$$\begin{aligned}\tau^{-1}_{ADXD^*} &= (k_+^{DHH} + k_-^{HDH})C_{BH}C_{XH} + (k_+^{DHD} + k_-^{DDH})C_{BH}C_{XD} \\ &\quad + (k_+^{DDH} + k_-^{HDD})C_{BD}C_{XH} + (k_+^{DDD} + k_-^{DDD})C_{BD}C_{XD} \\ &= [(1 - D_B)(1 - D_X)(k_+^{DHH} + k_-^{HDH}) + D_B(1 - D_X)(k_+^{DHD} + k_-^{DDH}) \\ &\quad + (1 - D_B)D_X(k_+^{DDH} + k_-^{HDD}) + D_BD_X(k_+^{DDD} + k_-^{DDD})]C_BC_X.\end{aligned} \tag{5.51}$$

Note that $k_+^{HHH} = k_-^{HHH}$ and $k_+^{DDD} = k_-^{DDD}$. Now, the inverse average lifetimes depend on products of the individual deuterium fractions. For the case where equilibrium isotope effects are absent, i.e. where

$$k_+^{HHD} = k_+^{HDH} = k_+^{DHH} = k_-^{HHD} = k_-^{HHD} = k_-^{HHD} \text{ etc.}, \tag{5.52}$$

the above equations can be simplified. Setting $k_+^{LLL} + k_-^{LLL} = k^{LLL}$ it follows that

$$\tau^{-1}_{AHAH^*} = [(1 - D)^2k^{HHH} + (1 - D)Dk^{HHD}]C_BC_X, \tag{5.53}$$

$$\tau^{-1}_{AHAD} = [D(1-D)k^{HHD} + D^2k^{HDD}]C_BC_X, \tag{5.54}$$

$$\tau^{-1}_{ADAH} = [(1-D)^2k^{HHD} + (1-D)Dk^{HDD}]C_BC_X, \tag{5.55}$$

$$\tau^{-1}_{ADAD^*} = [D(1-D)k^{HDD} + D^2k^{DDD}]C_BC_X, \tag{5.56}$$

$$\tau^{-1}_{AHXH} = \tau^{-1}_{AH} = [(1-D)^2k^{HHH} + 2(1-D)Dk^{HHD} + D^2k^{HDD}]C_BC_X, \tag{5.57}$$

$$\tau^{-1}_{ADXD} = \tau^{-1}_{AD} = [(1-D)^2k^{HHD} + 2D(1-D)k^{HDD} + D^2k^{DDD}]C_BC_X. \tag{5.58}$$

Note that this set of equations is also valid for the case where $A = B = C$. Using again $k^{HHH}/k^{DDD} = 10$ and $k^{HHD}/k^{HDD} = k^{HDD}/k^{DDD} = 10^{1/3}$ we obtain the non-linear curves in Fig. 5.1 for the case $n = 3$, L = H, D. Note that $\tau^{-1}_{AHXH}(D = 1) = k^{HDD} < \tau^{-1}_{ADXD}(D = 0) = k^{HHD}$.

5.2.4 *Superposed Intermolecular Double and Triple Hydrogen Transfer Reactions*

As one can note by comparison of Eqs. (5.26) to (5.31) with Eqs. (5.53) to (5.58), the inverse lifetimes measured are independent of the particular reaction network. Thus, a superposed double and triple proton transfer reaction can be described just by adding up the corresponding equations. For the case where

$$A = X, \quad \text{i.e.} \quad D_A = D_X = D_B \equiv D, \tag{5.59}$$

we obtain

$$\tau^{-1}_{AHAH^*} = (1-D)\cdot k^{HH}\cdot C_A + [(1-D)^2\cdot k^{HHH} + D\cdot(1-D)\cdot k^{HHD}]\cdot C_A^2, \tag{5.60}$$

$$\tau^{-1}_{AHAD} = D\cdot k^{HD}\cdot C_A + [D\cdot(1-D)\cdot k^{HDH} + D^2\cdot k^{HDD}]\cdot C_A^2, \tag{5.61}$$

$$\tau^{-1}_{ADAH} = (1-D)\cdot k^{DH}\cdot C_A + [(1-D)^2\cdot k^{DHH} + D\cdot(1-D)\cdot k^{DHD}]C_A^2, \tag{5.62}$$

$$\tau^{-1}_{ADAD^*} = D\cdot k^{DD}\cdot C_A + [D\cdot(1-D)\cdot k^{DDH} + D^2\cdot k^{DDD}]\cdot C_A^2, \tag{5.63}$$

and

$$\tau^{-1}_{AHA^*H} = \tau^{-1}_{AH} = [(1-D]\cdot k^{HH} + D\cdot k^{HD}]\cdot C_A + [(1-D)^2\cdot k^{HHH} + 2\cdot D\cdot(1-D)\cdot k^{HHD} + D^2\cdot k^{HDD}]\cdot C_A^2, \tag{5.64}$$

$$\tau^{-1}_{ADA^*D} = \tau^{-1}_{AD} = [(1-D]\cdot k^{DH} + D\cdot k^{DD}]\cdot C_A + [(1-D)^2\cdot k^{DHH} + 2\cdot D\cdot(1-D)\cdot k^{DDH} + D^2\cdot k^{DDD}]\cdot C_A^2. \tag{5.65}$$

The calculated values $\tau^{-1}_{AHA^*H}$ and $\tau^{-1}_{ADA^*D}$ will be located in Fig. 5.1 between those expected for n = 2 and 3.

5.2.5 *Multiple Hydrogen Transfer Reactions*

If more than $n = 3$ protons are transferred in the rate limiting step of the reaction the experimental data generally do not contain enough information in order to determine the different isotopic rate constants, i.e. in order to decide whether the RGM is fulfilled or not. If one assumes the validity of this rule which implies that all single kinetic isotope effects are equal i.e. given for constant total concentrations by

$$\Phi^{\ddagger} = (\tau^{-1}_{AD}(D = 1)/\tau^{-1}_{AH}(D = 0))^{1/n} \tag{5.66}$$

one obtains [106]

$$\tau^{-1}_{AH} = \tau^{-1}_{AH}(D = 0)(1 - D + D\Phi^{\ddagger})^{n-1}, \tag{5.67}$$

$$\tau^{-1}_{AD} = \tau^{-1}_{AH}(D = 0)\Phi(1 - D + D\Phi^{\ddagger})^{n-1}. \tag{5.68}$$

These equations can be easily verified for the case n = 3 by some simple transformations of Eqs. (5.67) and (5.68) using Eq. (5.66). Formally, Eqs. (5.67) and (5.68) resemble the so-called Gross–Butler equation [42–45] with the difference that Eqs. (5.67) and (5.68) have the exponent n − 1 instead of n. Therefore, Eqs. (5.67) and (5.68) contain more information than the Gross–Butler equation. The number of protons involved in the reaction can be obtained using Eqs. (5.67) and (5.68) by measuring the quantities $\tau^{-1}_{AH}(D = 0)$, $\tau^{-1}_{AD}(D = 1)$, and two values of τ^{-1}_{AH} and τ^{-1}_{AD} at the same deuterium fraction, e.g. D = 0.5. When the number of protons transferred becomes effectively infinite, as may be the case in pure protic solvents and when the overall kinetic isotope effect $(\Phi^{\ddagger})^{-n}$ is finite, $\Phi^{\ddagger}$ must be close to one and the lifetimes τ^{-1}_{AH} and τ^{-1}_{AD} measured by ^1H and ^2H NMR spectroscopy become equal, as shown in Fig. 5.1.

5.2.6 *Double Hydrogen Transfer Involving a Preequilibrium*

So far, formally simple first, second, or third order rate laws for the proton transfer processes have been treated. In practice, rate laws of chemical reactions may be more complex when a molecule A can exist in different fast exchanging environments A_i of which only A_r is reactive. The life time of A is then given by

$$\tau_A^{-1} = -\frac{1}{C_A} dc_{A_r}/dt, \quad C_A = \sum_i c_{A_i}. \tag{5.69}$$

C_A is the overall concentration of A, c_{A_i} the concentration of species A_i. In this section it is shown that the relations derived above are still valid even in this more complicated case as long as isotopic fractionation between the different

environments is absent. For this purpose let us consider a double proton transfer involving a fast preequilibrium according to

$$AL + XL^* \underset{\text{fast}}{\overset{K^{LL}}{\rightleftharpoons}} \{AL, XL^*\} \underset{\text{slow}}{\overset{k_{rls}^{LL}}{\rightleftharpoons}} \{AL^*, XL\} \underset{\text{fast}}{\overset{1/K^{LL}}{\rightleftharpoons}} AL^* + XL, \quad (5.70)$$

where

$$K^{LL} = c_{ALXL}/(c_{AL}c_{XL}), \quad LL = HH, HD, DD \quad (5.71)$$

is the preequilibrium constant of the formation of the reaction complex in which the double proton transfer takes place. k_{rls}^{LL} is the rate constant of the rate limiting step of the proton exchange in the reaction complex. With

$$c_A = c_{AH} + c_{AD}, c_{AX} = c_{AHXH} + c_{AHXD} + c_{ADXH} + c_{ADXD} \quad (5.72)$$

it follows that in the absence of isotopic fractionation between AL and ALXL

$$K^{HH} = K^{HD} = K^{DD} = K = c_{AX}/(c_A c_X). \quad (5.73)$$

Taking into account Eq. (5.69) we obtain

$$\tau_{AHXH}^{-1} = -\frac{1}{c_{AH} + c_{AHXH} + c_{AHXD}}[dc_{AHXH}/dt + dc_{AHXD}/dt]. \quad (5.74)$$

With

$$-dc_{ALXL}/dt = k_{rls}^{LL} c_{ALXL} \quad (5.75)$$

it follows that

$$\tau_{AHXH}^{-1} = \frac{1}{c_{AH} + c_{AHXH} + c_{AHXD}}[k_{rls}^{HH} c_{AHXH} + k_{rls}^{HD} c_{AHXD}]. \quad (5.76)$$

Because of Eqs. (5.72) and (5.73) it follows that

$$c_{AH} = (1 - D)c_A, \quad c_{AHXH} = (1 - D)^2 c_{AX}, \quad c_{AHXD} = (1 - D)Dc_{AX}. \quad (5.77)$$

Combining Eq. (5.76) with (5.77) leads to

$$\tau_{AHXH}^{-1} = F[(1 - D)k_{rls}^{HH} + Dk_{rls}^{HD}], \quad F = \frac{c_{AX}}{c_A + c_{AX}}. \quad (5.78)$$

In a similar way it follows that

$$\tau_{ADXD}^{-1} = F[(1 - D)k_{rls}^{HD} + Dk_{rls}^{DD}], \quad F = \frac{c_{AX}}{c_A + c_{AX}}. \quad (5.79)$$

Similar equations can be obtained for τ_{ALXL}^{-1}. Note that these equations are valid not only for the case where $A \neq X$ but also for the self exchange case where $A \equiv X$. Since F is independent of the deuterium fraction D the inverse lifetimes τ_{ALXL}^{-1} depend linearly on D, as was already expressed by Eqs. (5.30) and (5.31). Recalling that the total concentrations

$$C_A = c_A + c_{AX} = c_{AH} + c_{AD} + c_{AHXH} + c_{AHXD} + c_{ADXH} + c_{ADXD} \quad (5.80)$$

$$C_X = c_X + c_{AX} = c_{XH} + c_{XD} + c_{AHXH} + c_{AHXD} + c_{ADXH} + c_{ADXD}, \tag{5.81}$$

it follows from Eqs. (5.71), (5.77) and (5.78) for the case where

$$K \text{ or } C_A \text{ small, i.e. } c_{AX} = Kc_Ac_X \ll C_A$$

that

$$F = KC_X, \quad \text{i.e.} \quad c_A \cong C_A \quad \text{and} \quad c_X \cong C_X. \tag{5.82}$$

The second order rate constants defined in Eqs. (5.26) and (5.27) are then given by

$$k^{LL} = Kk^{LL}_{rls}. \tag{5.83}$$

By contrast, when

$$K \text{ or } C_{XL} \text{ large, i.e. } C_A = c_{AX}, \tag{5.84}$$

it follows that $F = 1$. We can then rewrite Eq. (5.78) and (5.79) in the form

$$\tau^{-1}_{AHXH}/F = \tau^{-1}_{AHXH}(C_{AL} \to \infty) = [(1 - D)k^{HH}_{rls} + Dk^{HD}_{rls}] \tag{5.85}$$

and

$$\tau^{-1}_{ADXD}/F = \tau^{-1}_{ADXD}(C_{AL} \to \infty) = [(1 - D)k^{HD}_{rls} + Dk^{DD}_{rls}] \tag{5.86}$$

Thus, one can obtain k^{HH}_{rls} and k^{HD}_{rls} directly from $\tau^{-1}_{AHXH}(C_A \to \infty)$ and k^{HD}_{rls} and k^{DD}_{rls} from $\tau^{-1}_{ADXD}(C_A \to \infty)$ at $D = 0$ and $D = 1$. Thus,

$$\tau^{-1}_{AHXH}(C_A \to \infty, D)/\tau^{-1}_{AHXH}(C_A \to \infty, D = 0) = 1 - (1 - k^{HH}_{rls}/k^{HD}_{rls})D \tag{5.87}$$

and

$$\tau^{-1}_{ADXD}(C_A \to \infty, D)/\tau^{-1}_{ADXD}(C_A \to \infty, D = 0) = 1 - (1 - k^{HD}_{rls}/k^{DD}_{rls})D. \tag{5.88}$$

At $D = 0.5$ the ^{1}H NMR lineshapes are determined by $\tau^{-1}_{AHXH}(C_A \to \infty) = (k^{HH}_{rls} + k^{HD}_{rls})/2$ and the ^{2}H NMR lineshapes by $\tau^{-1}_{ADXD}(C_A \to \infty) = (k^{HD}_{rls} + k^{DD}_{rls})/2$. Note, however, that this result applies only for a very rapid hydrogen bond preequilibrium as assumed in Eq. (5.70). If these processes were very slow, as for example in intramolecular double proton transfers, one would also obtain k^{HH}_{rls} and k^{DD}_{rls} at $D = 0$ and $D = 1$, but at $D = 0.5$ the ^{1}H NMR lineshape would have to be described by a static superposition of two independent lineshape functions as has been described in Sect. 5.1.

Expressions for F as a function of concentration can easily be derived. This will be done here for the self exchange in dimers $ALAL = A_2$, i.e. the case where $A \equiv X$. Equation (5.80) then becomes

$$C_A = c_A + 2c_{A_2}. \tag{5.89}$$

By simple arithmetics one then obtains

$$F = \frac{c_{A_2}/C_A}{1 - c_{A_2}/C_A}. \tag{5.90}$$

An expression for c_{A_2}/C_A can be obtained by combination of Eqs. (5.71) and (5.80):

$$F = \frac{4KC_A - (8 \cdot KC_A + 1)^{1/2} + 1}{4KC_A + (8 \cdot KC_A + 1)^{1/2} - 1}. \tag{5.91}$$

This equation is used together with Eqs. (5.85)–(5.86). From Eqs. (5.87) and (5.88) it follows then by setting $k_{rls} = k_{A_2}$ that

$$\tau_{AH}^{-1}(C \to \infty, D)/\tau_{AH}^{-1}(C \to \infty, D = 0) = 1 - (1 - k_{A_2}^{HD}/k_{A_2}^{HH})D. \quad (5.91)$$

6 NMR Lineshape Equations of Hydrogen Transfers in the Presence of Kinetic Isotope Effects

All elements are now in place in order to set up specific NMR line shape equations for typical cases of intra- and intermolecular proton exchange reactions in the presence of kinetic hydrogen/deuterium isotope effects. The line shape equations considerably simplify in the absence of strong scalar coupling between the remote and the labile spins. In these cases it is possible to set up two separate NMR lineshape equations for both types of spins. Only when remote and mobile spins are strongly coupled protons with similar chemical shifts it is not possible to separate the two lineshape contributions. An experimental example for this case will be given in Sect. 10.1. The purpose of this section is to demonstrate ways of determining by dynamic NMR spectroscopy the kinetic quantities defined in Sect. 5.

6.1 Intramolecular Hydrogen Transfer Reactions

6.1.1 Remote Spin Studies

Let us consider an intramolecular hydrogen transfer reaction between two states AL and XL according to Eqs. 5.1 and 5.2, characterized by the forward and backward rate constants k_+^H, k_+^D, k_-^D, k_-^D. During the exchange the chemical shift of a remote nucleus is then modulated from the value ν_{AL} to ν_{XL}. The complex matrix $\mathcal{M}$ describing the lineshape of the remote spins is then given by

$\mathcal{M}$ (remote spins) =

$-k_+^H - \pi W_0 + 2\pi i\nu_{AH}$	k_-^H		
k_+^H	$-k_-^H + \pi W_0 - 2\pi i\nu_{XH}$		
		$-k_-^D + \pi W_0 - 2\pi i\nu_{AD}$	k_-^D
		k_+^D	$-k_-^H + \pi W_0 - 2\pi i\nu_{XD}$

,

$$p = [p_{AH}, p_{XH}, p_{AD}, p_{XD}]. \quad (6.1)$$

Because of the absence of scalar coupling all non-diagonal $\mathcal{L}$ elements

connecting $\mathcal{M}$(remote spins) and the counterparts $\mathcal{M}$(mobile spins) vanish. Since in Eq. (6.1) it is assumed that intermolecular exchange processes are absent, $\mathcal{M}$(remote spins) splits into two independent submatrices $\mathcal{M}_{AL}$, L = H, D given by

$$\mathcal{M}_{AL} = \begin{array}{|c|c|} \hline -k_+^L - W_0 + 2\pi i\nu_{AL} & k_-^L \\ \hline k_+^L & -k_-^L - \pi W_0 + 2\pi i\nu_{XL} \\ \hline \end{array},$$

$$p = [p_{AL}, p_{XL}], \quad (6.2)$$

Measurements at deuterium fractions D = 0 and 1 will easily lead to k_+^H and k_+^D; these constants are sufficient to describe the lineshape also at other values of D. If the lineshape at a given D value cannot be simulated one has to take the possibility of intermolecular exchange processes into account, as shown in Sect. 6.3.

Let us consider now the case of a bifunctional molecule subject to an intramolecular double proton transfer between two states ALL and XLL according to Eqs. (5.3) to (5.6). The lineshape equation is obtained by replacing L = H, D in Eq. (6.2) by LL = HH, HD, DD. Thus, because of the absence of intermolecular exchange $\mathcal{M}$(remote spins) splits up into three superposed submatrices:

$$\mathcal{M}_{ALLXLL} = \begin{array}{|c|c|} \hline -k_+^{LL} - \pi W_0 + 2\pi i\nu_{ALL} & k_-^{LL} \\ \hline k_+^{LL} & -k_-^{LL} - \pi W_0 + 2\pi i\nu_{XLL} \\ \hline \end{array},$$

$$LL = HH, HD, DD, \quad p = [p_{ALL}, p_{XLL}]. \quad (6.3)$$

The populations depend on the deuterium fraction D in the mobile proton sites. If the kinetic isotope effects are not very large it will be difficult to obtain k_+^{HH}, k_+^{HD}, and k_+^{DD} by analyzing spectra at intermediate deuterium fractions D. Therefore, one proceeds as follows. From experiments at D = 0 and D = 1, k_+^{HH} and k_+^{DD} can easily be obtained. Using this information one can try to obtain k_+^{DD} at D = 0.5. A better solution is, however, to obtain k_+^{HH} and k_+^{HD} by ^{1}H NMR spectroscopy of the exchanging proton signals as shown in the following.

6.1.2 Mobile Hydrogen Isotope Studies

Let us consider now the lineshape equations of the mobile hydrogen isotopes for the cases presented in the previous section. Again, for simplicity the presence of scalar coupling between the hydrogen isotopes and the remote spins is neglected. For the single proton transfer according to Eqs. (5.1) and (5.2) one

obtains then

$$\mathcal{M}_{ALXL} = \begin{vmatrix} -k_+^L - \pi W_0 + 2\pi i \nu_{AL} & k_-^L \\ k_+^L & -k_-^L - \pi W_0 + 2\pi i \nu_{XL} \end{vmatrix},$$

$$L = H, D, \quad p = [p_{AH}, p_{XH}], \quad (6.4)$$

for the NMR lineshape of the L spins. ν_{AL} is the chemical shift of L in AL.

In the case of intramolecular double proton transfer between ALL and XLL according to Eqs. (5.3) to (5.6) the ^{1}H NMR lineshape is given by

$$\mathcal{M}_{AHHXHH} = \begin{vmatrix} -k_+^{HH} - \pi W_0 + 2\pi i \nu_{AHH} & k_-^{HH} \\ k_+^{HH} & -k_-^{HH} - \pi W_0 + 2\pi i \nu_{XHH} \end{vmatrix},$$

$$p = [p_{AHH}, p_{XHH}], \quad (6.5)$$

$$\mathcal{M}_{AHDXHD} = \begin{vmatrix} -k_+^{HD} - \pi W_0 + 2\pi i \nu_{AHD} & k_-^{HD} \\ k_+^{HD} & -k_-^{HD} - \pi W_0 + 2\pi i \nu_{XHD} \end{vmatrix},$$

$$p = [p_{AHD}, p_{XHD}], \quad (6.6)$$

Similar equations are obtained for the ^{2}H NMR lineshape. Thus, in the case of an intramolecular double proton transfer the ^{1}H NMR lineshape depends on k_+^{HH} and k_-^{HD}, whereas the ^{2}H NMR lineshape depends on k_+^{HD} and k_-^{DD}. k_+^{HH} is best obtained at a deuterium fraction of D = 0. Then Eq. (6.6) can be neglected. k_+^{HD} is to be determined at a value of D close to 1 by ^{1}H NMR in order to minimize the contribution of Eq. (6.5). Because of sensitivity problems one typically chooses D between 0.9 and 0.95. However, at these D values Eq. (6.5) still contributes in a non-negligible way to the lineshapes and has to be taken into account. Similar arguments hold for the determination of k_+^{HD} by ^{2}H NMR at low D-values.

Let us consider now a case of an intramolecular single proton transfer reaction between two states r = 1, 2 in the presence of scalar coupling between the mobile proton and remote spins according to the modified Eqs. (5.1) and (5.2):

$$1 \equiv AL \cdots B \underset{k_-^L}{\overset{k_+^L}{\rightleftharpoons}} 2 \equiv A \cdots LB. \quad (6.7)$$

Let A and B have a spin 1/2 as is the case for proton transfer in ^{15}NH$\cdots{}^{15}$N hydrogen bonds. Because of the intramolecular character of the process the following independent reactions take place:

$$A(\alpha) - L \cdots B(\alpha) \rightleftharpoons A(\alpha) \cdots L - B(\alpha), \quad (6.8)$$

$$A(\alpha) - L \cdots B(\beta) \rightleftharpoons A(\alpha) \cdots L - B(\beta), \tag{6.9}$$

$$A(\beta) - L \cdots B(\alpha) \rightleftharpoons A(\beta) \cdots L - B(\alpha), \tag{6.10}$$

$$A(\beta) - L \cdots B(\beta) \rightleftharpoons A(\beta) \cdots L - B(\beta). \tag{6.11}$$

The fact that the reaction is intramolecular leads to a splitting of $\mathcal{M}$(mobile spins) into four independent superposed submatrices, one for each reaction listed in Eqs. (6.8) to (6.11). Let ν_r be the chemical shift of the mobile hydrogen isotope in r and J_{Xr_Lr}, X = A, B, r = 1, 2 the corresponding coupling constants. Let further be $J_{A^1L^1} = J_{AL} \neq 0$, $J_{B^1L^1} = 0$, $J_{A^2L^2} = 0$, $J_{B^2L^2} = J_{BL} \neq 0$. One then obtains

$$\mathcal{M}^{\alpha\alpha}_{ALBL} = \begin{array}{|c|c|} \hline -k^L_+ - \pi W_0 + 2\pi i(\nu_1 + J_{AL}/2) & k^L_- \\ \hline k^L_+ & -k^L_- - \pi W_0 + 2\pi i(\nu_2 + J_{BL}/2) \\ \hline \end{array},$$

$$p = 0.25[p_1, p_2], \tag{6.12}$$

$$\mathcal{M}^{\alpha\beta}_{ALBL} = \begin{array}{|c|c|} \hline -k^L_+ - \pi W_0 + 2\pi i(\nu_2 + J_{AL}/2) & k^L_- \\ \hline k^L_+ & -k_- - \pi W_0 + 2\pi i(\nu_2 - J_{BL}/2) \\ \hline \end{array},$$

$$p = 0.5[p_1, p_2], \tag{6.13}$$

$$\mathcal{M}^{\beta\beta}_{ALBL} = \begin{array}{|c|c|} \hline -k^L_+ - \pi W_0 + 2\pi i(\nu_1 + J_{AL}/2) & k^L_- \\ \hline k^L_+ & -k^L_- - \pi W_0 + 2\pi i(\nu_2 - J_{BL}/2) \\ \hline \end{array},$$

$$p = 0.25[p_1, p_2]. \tag{6.14}$$

In the slow exchange region the L signal consists of two doublets at the frequencies $\nu_1 \pm J_{AL}/2$ and $\nu_2 \pm J_{BL}/2$. In the fast exchange range the signal consists of a multiplet at the frequency $p_1\nu_1 + p_2\nu_2$ characterized by the effective coupling constants $p_1 J_{AL}$ and $p_2 J_{BL}$.

A special situation arises in a symmetric exchange case where A = B in Eq. (6.7), $p_1 = p_2 = 0.5$, $k^L_+ = k^L_- = k^L$, $\nu_1 = \nu_2 = \nu$. Then $J_{AL} = J_{BL}$ and Eqs. (6.12) to (6.14) reduce to $\mathcal{M}^{\alpha\alpha}_{AL} = -\pi W_0 + 2\pi i(\nu + J_{AL}/2)$, $\mathcal{M}^{\beta\beta}_{AL} = -\pi W_0 + 2\pi i(\nu - J_{AL}/2)$,

$$\mathcal{M}^{\alpha\beta}_{AL} = \begin{array}{|c|c|} \hline -k^L - \pi W_0 + 2\pi i(\nu + J_{AL}/2) & k^L \\ \hline k^L & -k^L - \pi W_0 + 2\pi i(\nu - J_{AL}/2) \\ \hline \end{array} \tag{6.15}$$

with $p_{\alpha\alpha} = p_{\beta\beta} = 0.25$, $p_{\alpha\beta} = 0.5$. Then, in the slow exchange region there is only one doublet at $\nu \pm J_{AL}/2$. Hydrogen isotopes reacting according to Eqs. (6.8) and (6.11) do not change their transition frequencies and, therefore, contribute sharp line components at $\nu \pm J_{AL}/2$. By contrast, the lineshape contributions of protons reacting according to Eqs. (6.9) and (6.10) correspond only in the slow exchange region to a doublet at $\nu \pm J_{AL}/2$; when the exchange becomes faster these line components broaden, coalesce, and eventually give rise to one sharp line in the center of the resonance, i.e. a triplet appears. The ratio of the integrated intensities of the inner exchange broadened line component to each of the outer lines is always 2:1; however, the peak heights behave in this way only at very high temperatures, where the inner line no longer shows line broadening; i.e. peak height ratio of less then 2:1 is, therefore, indicative that the extremely fast exchange has not yet been reached. Note that for the study of kinetic isotope effects one has to perform ^1H and ^2H NMR experiments.

In the case of a double proton transfer according to

$$(AL\cdots B)_2 \underset{k_{-1}^{LL}}{\overset{k_1^{LL}}{\rightleftharpoons}} (AL\cdots B)_2 \tag{6.16}$$

the same lineshape theory applies. One only replaces L in Eqs. (6.12) to (6.15) by LL = HH, HD, DD and takes into account that the ^1H NMR lineshape depends on the sum

$$\mathcal{M}(\text{mobile spins}) = \mathcal{M}_{LL}^{\alpha\alpha} + \mathcal{M}_{LL}^{\alpha\beta} + \mathcal{M}_{LL}^{\beta\beta}, \quad LL = HH, HD, \tag{6.17}$$

i.e. on both k_+^{HH} and k_+^{HD} as well as on the corresponding backward rate constants.

Finally, let us consider a hydrogen isotope jumping between four heavy atoms A to D with spin 1/2, i.e. exchanging between the states r = 1 to 4 as shown in Eq. (6.18):

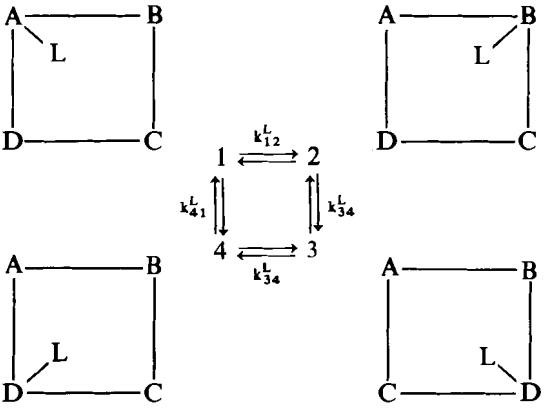

(6.18)

Let the chemical shift of the proton in state r be characterized by ν_r. Let, furthermore, the proton only be coupled to the heavy atom to which it is attached, characterized by the coupling constant J_{XH}. $\mathcal{M}$(mobile spins) is then

the sum of submatrices, each given by [113, 115],

$\mathcal{M}_L(e_1, e_2, e_3, e_4) =$

$-k_{12}^L - k_{14}^L - \pi W_0 + 2\pi i(\nu_1 + e_1 J_{AL}/2)$	k_{21}^L		k_{41}^L
k_{12}^L	$-k_{21}^L - k_{23}^L - \pi W_0 + 2\pi i(\nu_2 + e_2 J_{BL}/2)$	k_{32}^L	
	k_{23}^L	$-k_{32}^L - k_{34}^L - \pi W_0 + 2\pi i(\nu_3 + e_3 J_{CL}/2)$	k_{43}^L
k_{14}^L		k_{34}^L	$-k_{41}^L - k_{43}^L - \pi W_0 + 2\pi i(\nu_4 + e_4 J_{DL}/2)$

,

$$e_r = \pm 1, \quad p = (p_1 = p_{AL}, p_2 = p_{BL}, p_3 = p_{CL}, p_4 = p_{DL}). \quad (6.19)$$

In the slow exchange region the signal consists of four doublets with the chemical shifts ν_r, r = 1, 4. In the fast exchange region Eq. (6.19) predicts a coalesced line split by coupling to all spins A to D, with the effective coupling constants given by

$$J_{XL}^{eff} = p_X J_{XL}. \quad (6.20)$$

In the simplest case where all chemical shifts, coupling constants, and populations are equal Eq. (6.19) predicts in the slow exchange region a splitting of the L signal into a doublet by coupling with the spin to which L is bound; in the fast exchange region a pentet splitting is predicted.

If there are two protons jumping between the four atoms A to D in Eq. (6.18) the superscript L in Eqs. (6.18) and (6.19) has to be replaced by LL = HH, HD, DD. Furthermore, if ^{1}H measurements are performed $\mathcal{M}$(mobile spins) is the sum of the two contributions

$$\mathcal{M}(\text{mobile spins}) = \mathcal{M}^{HH} + \mathcal{M}^{HD}. \quad (6.21)$$

6.2 *Intermolecular Hydrogen Exchange Reactions*

In the case of proton exchange according to Eqs. (5.7) and (5.8) the chemical shifts of both the remote as well as of the mobile spins are modulated. Therefore, both remote as well as mobile spin studies can be performed even in the absence of scalar spin–spin coupling between both types of spins. A scalar interaction is, however, required in the case of Eqs. (5.12) to (5.15) and (5.36) to (5.43) when performing remote spin studies. Therefore, mobile spin studies are indicated in this case because the chemical shifts of the latter are modulated by the exchange. Thus, in the case of intermolecular proton exchange between different species one does not need the scalar spin–spin interaction, and it is straightforward to set up the NMR line shape equations. A special case arises, however, when

A = X in Eqs. (5.12) to (5.15) and A = B = X in Eqs. (5.36) to (5.43). Then, the hydrogen exchange processes do not lead to a modulation of chemical shifts of either remote or of mobile spins. There are, however, often cases where the proton transfer is accompanied by a rearrangement of the group A to A′ in such a way that a remote spin in A exhibits a different chemical shift ν_{AL} before and $\nu_{A,L}$ after the exchange. Then, self exchange rates can be studied by remote spin studies. If this modulation does not occur one needs a strong scalar spin–spin coupling between remote and mobile spins. We will treat both cases in the remainder of this section.

6.2.1 Remote Spin Studies in the Presence of Hydrogen Self Exchange

Let us first consider the NMR line shape problem of remote spins A of monofunctional molecules AL, L = H, D as a function of the deuterium fraction D subject to intermolecular proton self exchange. Here, both species AH and AD contribute to the line shape of A. Naturally, the NMR line shape of A is only sensitive to the proton exchange when the chemical shift of A is modulated by the exchange. Let ν_{AL} be the chemical shift of A before and $\nu_{A'L}$ the chemical shift after the exchange. Using the dynamic quantities defined in Sect. 5 it follows that [108]

$\mathcal{M}$(remote spins) =

$-\tau^{-1}_{AHAH^*} - \tau^{-1}_{AHAD} - \pi W_0 + 2\pi i\nu_{AH}$	$\tau^{-1}_{AHAH^*}$		τ^{-1}_{ADAH}
$\tau^{-1}_{AHAH^*}$	$-\tau^{-1}_{AHAH^*} - \tau^{-1}_{AHAD} - \pi W_0 + 2\pi i\nu_{A'H}$	τ^{-1}_{ADAH}	
	τ^{-1}_{AHAD}	$-\tau^{-1}_{ADAH} - \tau^{-}_{ADAD^*} - \pi W_0 + 2\pi i\nu_{AD}$	$\tau^{-1}_{ADAD^*}$
τ^{-1}_{AHAD}		$\tau^{-1}_{ADAD^*}$	$\tau^{-1}_{ADAH} - \tau^{-1}_{ADAD^*} - \pi W_0 + 2\pi i\nu_{A'D}$

,

$$p = [p_{AH}, p_{AH}, p_{AD}, p_{AD}], \quad \tau^{-1}_{AHAD}/\tau^{-1}_{ADAH} = p_{AD}/p_{AH} \tag{6.22}$$

and

$$p_{AH} = (1 - D) \quad \text{and} \quad p_{AD} = D. \tag{6.23}$$

Note that as compared to the intramolecular case treated in Eq. (6.1) $\mathcal{M}$ does not split any more into two submatrices because of exchange between AH and AD, besides the trivial cases at D = 0 and 1. Thus, at D = 0.5 intra- and intermolecular exchange processes can easily be distinguished. Some spectral features which follow from Eq. (6.22) will be discussed in Sect. 10.2.3

6.2.2 *Mobile Hydrogen Isotope Studies in the Presence of Hydrogen Self Exchange*

As an example relevant in the context of this study let us consider a spin system AL where A represents a spin 1/2 nucleus in the presence of intermolecular proton self exchange. Let the Larmor frequency ν_{AL} of A be so different from the Larmor frequency $\nu_{AL} = \nu$ of the exchanging L isotope that AL constitutes a first order spin system. Let us further analyze only the lineshape of the exchanging L isotope which is affected according to the previous section by the inverse life time $\tau^{-1}_{ALA^*L} \equiv \tau^{-1}_{AL}$. $\mathcal{M}$(mobile spins) and the population vector are then given by

$$\mathcal{M}(\text{mobile spins}) = \begin{array}{|c|c|} \hline -\tau_{AL}^{-1}/2 - \pi W_0 + 2\pi i(\nu + J_{AL}/2) & \tau_{AL}^{-1}/2 \\ \hline \tau_{AL}^{-1}/2 & -\tau_{AL}^{-1}/2 - \pi W_0 + 2\pi i(\nu - J_{AL}/2) \\ \hline \end{array}, \quad p = \begin{bmatrix} 1/2 \\ 1/2 \end{bmatrix}. \tag{6.24}$$

In the slow exchange range the signal of the exchanging proton consists of a doublet at the frequency ν with a splitting corresponding to the coupling constant J_{AH}. The two line components refer to the protons attached to nuclei A in the spin states α(A) and β(A). When the proton exchanges, its Larmor frequency is modulated from $\nu + J_{AH}$ to $\nu - J_{AH}$. This switch occurs, however, only every other exchange process. Thus, the inverse life times are divided by 2 in Eq. (6.24). As the proton transfer becomes faster the two lines broaden and coalesce into one single line at ν. Note that in Eq. (6.24) no assumptions concerning the proton exchange mechanism have been made. Information on the latter can be obtained by performing experiments at different deuterium fractions D as described in Sect. 5.

6.3 *Superposed Intra- and Intermolecular Hydrogen Exchange Reactions*

There may be cases where both intra- and intermolecular hydrogen exchange reactions are present. In this case one has to add up the corresponding lineshape equations. As example let us consider the degenerate superposed intramolecular and intermolecular exchange reactions

$$AH\cdots A^* \overset{k}{\rightleftharpoons} A\cdots HA^*, \tag{6.25}$$

$$AH\cdots A + A^*H^*\cdots A^* \overset{\tau^{-1}}{\rightleftharpoons} AH^*\cdots A + A^*H\cdots A^*, \tag{6.26}$$

where A has a spin 1/2. k is the intramolecular first order rate constant, τ^{-1} the inverse lifetime characterising the intermolecular proton exchange. In both

a separate subroutine has to be written in which $\mathscr{M}$ is calculated. The program runs on the main computer of the University of Freiburg. In a smaller version, it can also be run on a PC.

Generally, the experimental spectra are transferred from the NMR-minicomputer to a PC linked to the main computer.

8 The Preparation of NMR Samples for the Study of Kinetic Hydrogen/Deuterium Isotope Effects

When studying the kinetics of proton and deuteron transfer reactions it is of prime importance to prepare well defined NMR samples which are free from impurities which catalyze or inhibit the exchange reactions to be studied. Solute concentrations must be adjustable. The deuterium fraction in the mobile proton sites must be controlled. The latter requirement is quite easily achieved when protic solvents are employed. In this case it is only necessary to mix the non-deuterated and the deuterated liquids in the desired amounts. However, it is much more difficult to control the deuterium fraction in the mobile proton sites when aprotic media are used as solvents because of slow proton exchange with OH groups of the glass walls of the NMR tubes. Furthermore, the NMR glass tubes have to be sealed in order to prevent contamination by the environment. Sample sealing is especially important because there will always be a substantial time interval between the sample preparation and the NMR measurements. In this section, therefore, some useful sample preparation techniques which have been developed over the past years in our laboratory are described.

8.1 General Techniques for the Preparation of Sealed NMR Samples

A glass apparatus for the preparation of sealed NMR samples used in our laboratory is shown in Fig. 8.1. The apparatus is attached to a vacuum line (1); a turbomolecular pump is used because of its ease of operation and of its capability to quickly provide a vacuum of the order of 10^{-5} to 10^{-6} bar. Greaseless Teflon needle valves (2) are employed to separate the different devices from the vacuum line. Solvents are stored in solvent containers (3) over an appropriate drying agent introduced via a tube (4) sealed before condensing the solvent into (3) from another flask. The apparatus contains a system of high precision glass tubes (5) of different diameters, e.g. 0.2 mm and 2 mm, for volume measurements of liquids. The glass tubes are calibrated by filling with mercury and weighing prior to their attachment to the vacuum line. All liquid components of the NMR sample are condensed into the NMR tube (6) after volume

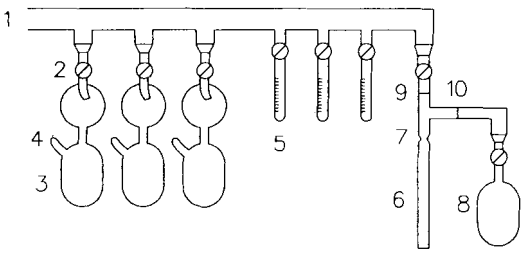

Fig. 8.1. Vacuum apparatus for the preparation of NMR samples. (1) vacuum line; (2) teflon needle valve; (3) solvent flask with drying agent; (4) sealed tube for insertion of the drying agent; (5) graduated capillary tubes; (6) NMR tube; (7) NMR tube sealing place;(8) optional flask, (9), (10) optional glass frits

measurement. Solid components are introduced directly into the NMR tube before it is attached to the vacuum line. An optional glass frit (9) prevents boiling in the tube when evaporating liquids from the NMR tube. Sometimes it is useful to attach to the NMR tube a small solvent flask (8) where solid components of low solubility can be introduced and deuterated; (10) is an optional glass frit.

For the preparation of samples one proceeds as follows. At the first stage all liquids are degassed three times by successive freezing with liquid nitrogen, evacuation of the gas phase, and warm up (freeze pump technique). Then, solvent is condensed on all inner glass surfaces which come into contact with the sample liquid in order to dissolve residual water. For this purpose a piece of cotton—held with a pair of tweezers—is dipped into liquid nitrogen and subsequently brought in contact with the outer glass surfaces. After this procedure the solvent is condensed back into the solvent container or another appropriate trap.

In order to bring a certain quantity of a liquid, solute or solvent, into the NMR tube one proceeds as follows. The liquid is first condensed into a graduated capillary tube by opening the appropriate valves and cooling the tube. Then, the desired part of the liquid is condensed into the NMR tube. For the measurement of the initial and the final volumes of the liquids in the graduated tubes the temperature of the graduated tube has to be controlled.

As mentioned above, solid compounds are placed into the flask (8) or directly into the NMR tube and dried in vacuo. For further drying solvent is condensed on the solid. After dissolution the solvent is again evaporated into a trap. This procedure might be repeated several times. Then, the desired amount of the final solvent is condensed on the compound. The device with the NMR tube is then separated from the vacuum line and the solution is poured through the frit into the NMR tube by cooling the latter. The inner surface at the seal (7) is carefully washed by solvent reflux achieved by cooling the outer glass surface. Finally, the NMR tube is sealed off; during this procedure the tube is cooled to 77 K.

The sample concentrations can be calculated from the known amount of solutes and solvents. Relative concentrations of different samples can be further checked by taking NMR spectra of these samples under identical conditions and comparing the integral intensities of appropriate solute signals.

8.2 *Sample Preparation Techniques for Variable Deuterium Fraction in Mobile Proton Sites*

The preparation of NMR samples with a particular deuterium fraction D in the mobile proton sites demands some further experimental procedures. First, as a source of deuterons an appropriate deuterated protic solvent mixture, generally CH_3OH/CH_3OD or C_2H_5OH/C_2H_5OD is used containing the desired deuterium fraction D. These mixtures are dried over molecular sieve 3 Å. Since the latter contains many OH groups it must, however, first be immersed with a corresponding H_2O/D_2O mixture and regenerated in vacuo at 360 K. For this purpose an electric oven is very useful.

The dried ROH/ROD mixture is then condensed on the glass walls of the NMR tube and evaporated. Then the glass surface is further dried with solvent as described above. Solid compounds are deuterated with the ROH/ROD mixture in the solvent container (8). If the compound does not dissolve in the ROH/ROD mixture a cosolvent is added. Another possibility is to employ a biphasic mixture of an organic solvent and a H_2O/D_2O mixture [127]. In this case great care has to be taken in order to remove excess water from the sample.

8.3 *The Choice of an Appropriate NMR Tube*

The choice of an appropriate NMR tube is very important in dynamic NMR experiments. Generally, for low temperature measurements usual 5 or 10 mm tubes may be sufficient. Note, however, that in sealed samples it is not possible to add a stopper to prevent a vortex during sample spinning. In order to avoid catalysis at the glass surface the ratio volume/inner glass surface should be as large as possible. This may be achieved by using short (~ 3 cm) sealed sample glass tubes placed in an outer NMR tube.

Note that there are solvents which have a non-negligible vapor pressure even at 77 K and which decompose at the hot glass surface during flame sealing of the NMR tube, giving rise to acid impurities in the samples. Such solvents are halogenated hydrocarbons such as CH_2Cl_2, $CHFCl_2$ etc. In order to properly prepare such samples it is mandatory to use NMR tubes with a teflon needle valve at the top (NORMAG, Otto Fritz GmbH, Hofheim, West Germany or Wilmad, New Jersey, USA). These tubes have the advantage that they can still rotate in the NMR probe.

The last problem which has to be addressed is temperature control in the sample tubes. A problem arises when high temperature experiments are to be performed. In ordinary NMR tubes where the upper gasphase remains at room temperature reflux and enrichment of liquid sample components in the gasphase can not be avoided. This problem is solved by using a short inner tube as proposed above. Also, NMR tubes with a needle valve are of help if the valve is pushed into the rotor as far as possible. Using the latter technique NMR

spectra of pure CD_2Cl_2 solutions have been measured at temperatures up to 110 °C, the boiling point of this solvent being 40 °C [122, 126].

9 Kinetic Hydrogen/Deuterium Isotope Effects of Intramolecular Double Hydrogen Transfer in the Liquid State

In this section we will give some examples of the determination of kinetic hydrogen/deuterium isotope effects of intramolecular double proton transfer reactions by dynamic liquid state NMR spectroscopy. Note that the capacity of molecules to bind a proton at different acceptor atoms has often been called proton tautomerism or just tautomerism, a term which will be used throughout this paper.

9.1 The Azophenine Tautomerism

The degenerate tautomerism of azophenine (AP, Fig. 9.1), whose systematic name is *N,N'*-diphenyl-3,6-bis-(phenylimino)-1,4-cyclohexadiene-1,4-diamine, was discovered some years ago [105]. The reaction has also been studied theoretically [131, 132]. A recent study [127] sought to determine the rate constants k^{HH}, k^{HD}, and k^{DD} of this process in order to obtain information on the reaction mechanism. In this section it is shown how this task was accomplished by performing various NMR experiments.

9.1.1 ^1H and ^{13}C NMR Lineshape Analysis of ^{15}N and ^{13}C Labeled Azophenine in $C_2D_2Cl_4$

Let us first discuss ^1H NMR experiments performed on the mobile protons in AP. Whereas the chemical shift of the latter is not modified when the jump process occurs, the scalar spin–spin interaction with the nitrogen atoms is

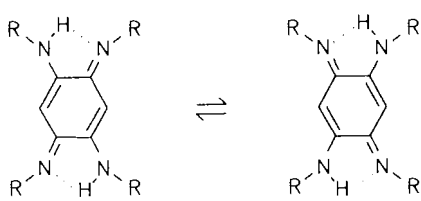

Fig. 9.1. The tautomerism of azophenine (AP)

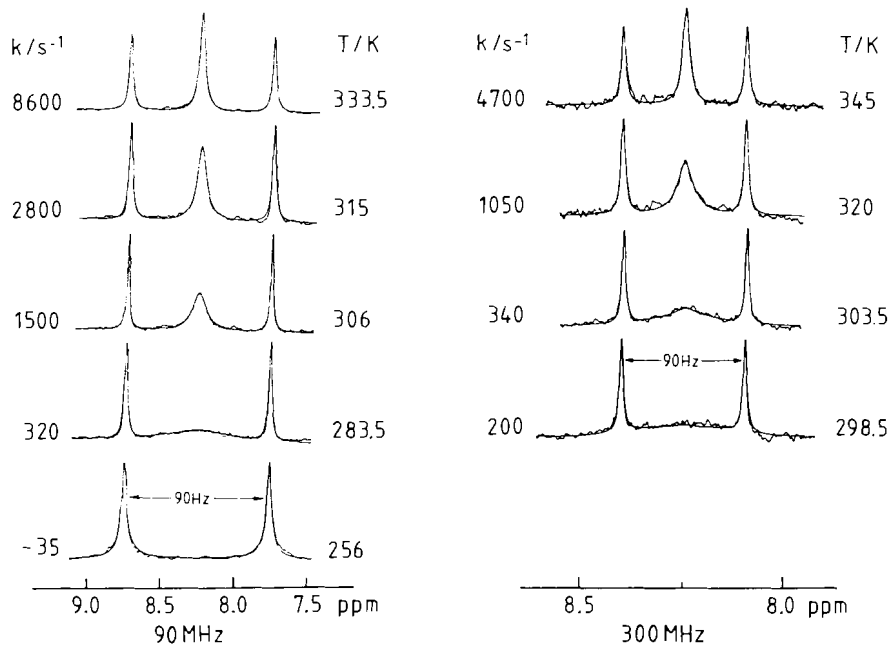

Fig. 9.2. Left: Superposed experimental and calculated 90.02 MHz ^1H NMR signals of the ^1H–^{15}N units of azophenine dissolved in $C_2D_2Cl_4$ at a deuterium fraction D = 0 in the NH sites as a function of temperature. The calculations were done using Eqs. (6.15) and (6.17). 200–500 scans, 60° pulses, 3 s repetition time. $k \equiv k^{HH}$ is the rate constant of the HH transfer. **Right**: Superposed experimental and calculated 300.13 MHz ^1H NMR signals of the ^1H–^{15}N units of azophenine dissolved in $C_2D_2Cl_4$. Deuterium fraction in the NH sites: D = 0.92. 1000–5000 scans, 90° pulses, 4 s repetition time. Reproduced with permission from Ref. [127]. $k \equiv k^{HD}$ is the rate constant of the HD transfer

modulated by the exchange. Unfortunately, the abundant ^{14}N spin has an electric quadrupole moment which leads to short ^{14}N longitudinal relaxation times, and as a consequence to a breakdown of the scalar ^1H–^{14}N coupling. Therefore, AP was labeled with the ^{15}N nucleus which has a spin 1/2.

Figure 9.2 shows the superposed experimental and calculated ^1H NMR signals of the ^1H–^{15}N units of AP dissolved in $C_2D_2Cl_4$ as a function of temperature. At low temperatures the proton signal consists of a doublet with the frequencies $\nu + J_{^1H^{15}N}/2$ and $\nu - J_{^1H^{15}N}/2$, because of coupling of the hydrogen bonded proton to one ^{15}N atom. At high temperatures the signal has a triplet structure. This observation means that the NH proton is now equally coupled to two ^{15}N atoms within the NMR time scale. The doublet–triplet transition can be understood in terms of Eq. (6.15). At low temperature the Larmor frequency ν of a mobile proton depends only on whether the ^{15}N atom to which it is bound is in the spin state α or β. As the proton transfer takes place the Larmor frequency of protons exchanging between two ^{15}N atoms in the spin states $\alpha\alpha$ or $\beta\beta$ is not altered. These protons, therefore, always contribute

sharp lines to the signal at $\nu \pm J_{^1H^{15}N}/2$. However, the Larmor frequency of protons exchanging between two ^{15}N atoms in the spin states $\alpha\beta$ and $\beta\alpha$ is modulated between $\nu + J_{^1H^{15}N}/2$ and $\nu - J_{^1H^{15}N}/2$ which leads to a coalescence of the corresponding line contributions. The coalesced line then constitutes the central line of the triplet in the fast exchange regime. Note that in this regime the lineshapes can be simulated without assumptions. The line width in the absence of exchange and $J_{^1H^{15}N}$ are obtained by simulation of the outer line components, the rate constants by simulation of the inner lines. Note that within the margin of error there are no lineshape contributions due to intermolecular proton exchange as predicted by Eq. (6.26); such contributions would lead to a breakdown of the triplet into a singlet. Thus, it can be concluded that the rate constants obtained by the lineshape analysis in Fig. 9.2 do not contain terms due to intermolecular proton exchange but do arise exclusively from an intramolecular double proton transfer according to Fig. 9.1.

At a deuterium fraction of $D = 0$ in the mobile proton sites the rate constant obtained at 90 MHz by simulation correspond to k^{HH}. However, when AP is deuterated the residual $^1H-^{15}N$ signal dominantly stems from AP–HD and only to a minor extent from AP–HH. Thus, the rate constants obtained in this case by ^1H NMR lineshape correspond to k^{HD}. On the right side of Fig. 9.2 the superposed experimental and calculated spectra of AP in $C_2D_2Cl_4$ at a deuterium fraction of $D = 0.92$ in the NH sites are shown. Naturally, it was much more difficult to obtain these spectra because of the low concentration of the residual $^1H-^{15}N$ units, and the experiments had, therefore, to be carried out at 300.13 MHz. Note that this does not change the signal lineshape because the scalar $^1H-^{15}N$ interaction is independent of the strength of the magnetic field. A comparison of both sets of spectra in Fig. 9.2 shows that the exchange in AP–HD is slower than in AP–H_2. For example, the temperature where the peak height of the inner line component is approximately equal to the peak height of the outer line components is approximately 330 K on the left but 340 K on the right side of Fig. 9.2. At 298 K a kinetic HH/HD isotope effect of 4 was found. Note that in the spectra at D 0.92 the presence of a small amount of AP–H_2 had to be considered in the calculations. Because of the slow intermolecular proton exchange the known contributions of this species were simply added to the lineshape equation according to Eq. (6.17).

Since it was not possible to determine k^{DD} by ^2H NMR spectroscopy because of the smallness of the coupling constant $J_{^2H^{15}N}$ and because of fast deuteron quadrupole relaxation, k^{DD} had to be determined by NMR spectroscopy of a remote spin. Since the chemical shifts of the phenyl protons were not altered enough by the proton transfer, and since the longitudinal relaxation times of the ^{15}N atoms of AP–DD were too long, k^{DD} was determined by dynamic ^{13}C NMR spectroscopy. For this purpose AP was labeled with ^{13}C in the p-position of the phenyl groups [127]. Figure 9.3 shows the superposed experimental and calculated NMR signals of the p-^{13}C atoms of AP dissolved in $C_2D_2Cl_4$ as a function of temperature at a deuterium fraction of $D = 0$ and $D = 1$ in the NH sites. At low temperatures the slow exchange regime is reached, with two sharp

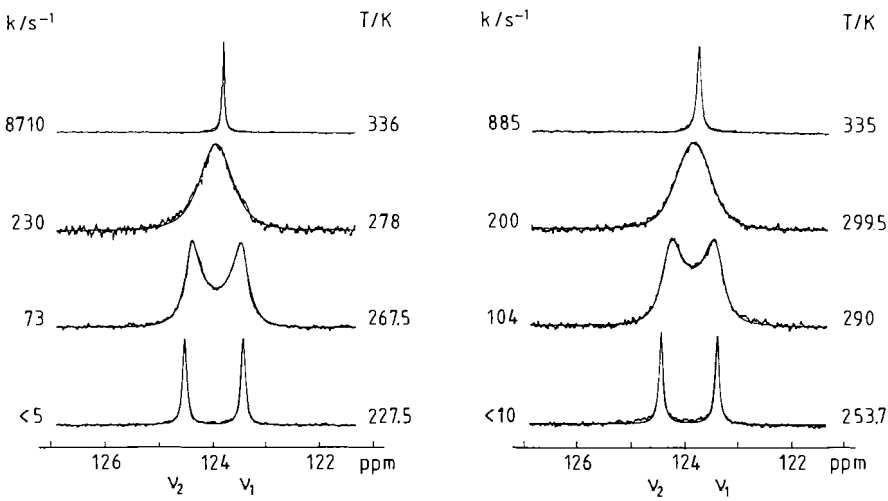

Fig. 9.3. Superposed experimental and calculated 75.47 MHz ^{13}C NMR signals of the isotopically enriched (90%) p-^{13}C atoms of AP dissolved in $C_2D_2Cl_4$ as a function of temperature. **Left**: deuterium fraction in the NH sites $D = 0$, $k \equiv k^{HH}$; **right**: $D = 0.99$, $k \equiv k^{DD}$. The calculations were done using Eq. (2.18). Reproduced with permission from Ref. [127]

signals of equal intensities. As the temperature is raised the lines broaden and finally coalesce into one sharp line, indicating a fast proton exchange. This spectral pattern indicates a symmetric exchange process with an equilibrium constant of $K_{12} = 1$. Figure 9.3 also shows that the exchange becomes much slower as the molecule is deuterated in the NH sites; the coalescence point is raised by about 20 K. The lineshape calculations were performed using Eq. (2.18). The values of $\Delta\nu = \nu_1 - \nu_2$, where ν_1 and ν_2 are the chemical shifts of the exchanging spins, could be obtained by lineshape analysis in the slow exchange regime for both AP–H_2 and AP–D_2 as a function of temperature. Note that for lineshape analyses small differences of the chemical shifts of the two isotopic species can be neglected within the margin of error. Neglecting possible kinetic $^{12}C/^{13}C$ and $^{14}N/^{15}N$ isotope effects, the ^{13}C NMR spectra at $D = 0$ were calculated using the rate constants k^{HH} of AP–H_2 obtained by ^1H NMR spectroscopy. Therefore the only adjustable parameter for the calculation of the ^{13}C NMR spectra of AP–H_2 was W_0. It was assumed that W_0 is the same for AP–HH and AP–DD. Thus, the rate constants k^{DD} could be determined without major assumptions for AP–D_2 at $D = 0.99$.

9.1.2 Polarization Transfer Experiments in the Rotating Frame

As discussed in Sect. 2.3 in the slow exchange regime lineshape analysis is not accurate. In order to overcome this difficulty, we performed low temperature

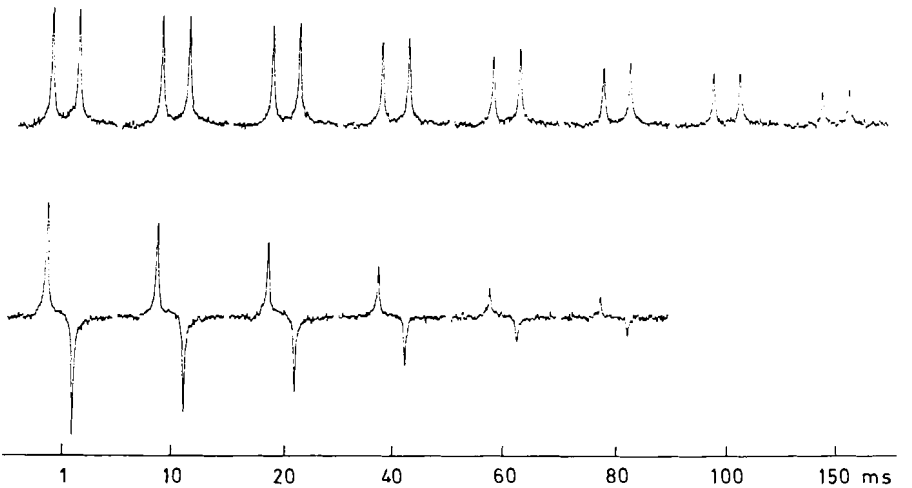

Fig. 9.4. 75.47 MHz ^{13}C NMR magnetization transfer experiment according to Fig. 2.4 in the rotating frame on AP-D_2 in $C_2D_2Cl_4$ at 265 K and a deuterium fraction in the NH sites of D = 0.99. Upper spectral set: experiment I; lower spectral set: experiment II. Reproduced with permission from Ref. [127]

^{13}C NMR polarization transfer experiments on AP–H_2 and AP–D_2 in the rotating frame. A typical experiment is shown in Fig. 9.4. From such measurements accurate kinetic HH/DD isotope effects could be obtained in the slow exchange regime. Similar experiments were performed on the ^1H–^{15}N signal of AP–H_2 [127]. However, both ^1H–^{15}N cross relaxation as well as the circumstance that only half of the exchanging doublet components exchange via proton transfer had to be taken into account.

9.1.3 Kinetic HH/HD/DD Isotope Effects of the Azophenine Tautomerism

The result of the measurements can be expressed in form of the following Arrhenius equations:

$$k^{HH} = 10^{11.6 \pm 0.14} \exp(-49.4 \pm 0.8\,\text{kJ mol}^{-1}/RT), \quad 249 \leqslant T \leqslant 343\text{K}, \quad (9.1)$$

$$k^{HD} = 10^{11.9 \pm 0.74} \exp(-54.7 \pm 0.9\,\text{kJ mol}^{-1}/RT), \quad 299 \leqslant T \ll 352\text{K}, \quad (9.2)$$

$$k^{DD} = 10^{12.1 \pm 0.25} \exp(-56.2 \pm 1.4\,\text{kJ mol}^{-1}/RT), \quad 263 \leqslant T \leqslant 334\text{K}, \quad (9.3)$$

with the kinetic isotope effects

$$k^{HH}/k^{HD} = 4.1, \quad k^{HD}/k^{DD} = 1.4, \quad \text{i.e.} \quad k^{HH}/k^{DD} = 5.6 \quad (9.4)$$

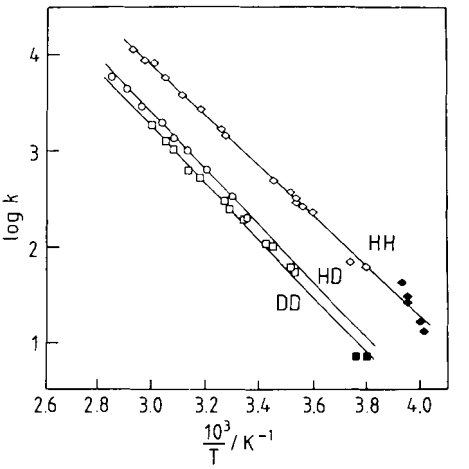

Fig. 9.5. Arrhenius curves of the azophenine tautomerism. *Open symbols*: ^{1}H and ^{13}C NMR line shape analysis; *filled symbols*: magnetization transfer in the rotating frame. Reproduced with permission from Ref. [127]

at 298 K. The corresponding Arrhenius curves are shown in Fig. 9.5. Whereas the substitution of the first mobile hydrogen by deuterium leads to a substantial primary KIE, replacement of the second H by D has only a small effect. These results constitute a considerable deviation from the rule of the geometric mean (RGM). They were taken as evidence for a stepwise proton transfer [127] between forms A and D via the intermediates B, C and the transition states J, G and K, H as shown in Fig. 9.6. This mechanism had been postulated theoretically [131, 132]. For a concerted double proton transfer via transition state E or for a pathway where B and C are transition states the RGM should have been valid in good approximation [127]. A problem with this interpretation remained in the sense that for the formation of a zwitterionic intermediate B, C = ZI in Fig. 9.6 kinetic solvent effects on the rates of proton transfer in AP should have been expected, by contrast to the experimental findings [127]. Therefore, either an unpolar singlet biradical (BR) must be formed as intermediate of the reaction or the phenyl groups in AP effectively minimize interactions between ZI and the solvent.

9.2 *The Oxalamidine Tautomerism*

The oxalamidine tautomerism (Fig. 9.7) was discovered some time ago by dynamic ^{1}H NMR spectroscopy of tetraphenyloxalamidine-$^{15}N_4$ (TPOA) in CD_2Cl_2 [120]. As shown in Fig. 9.8, the $^{1}H-^{15}N$ signal of TPOA consists of a doublet at low and of a triplet at room temperature which proves an intramolecular double proton transfer in this molecule, as in the case of azophenine. Figure 9.8 also indicates lineshape changes of the $^{1}H-^{15}N$ signal arising from a kinetic HH/HD isotope effect on the tautomerism. At higher temperatures the triplet is affected by an extra line broadening due to interconversion with

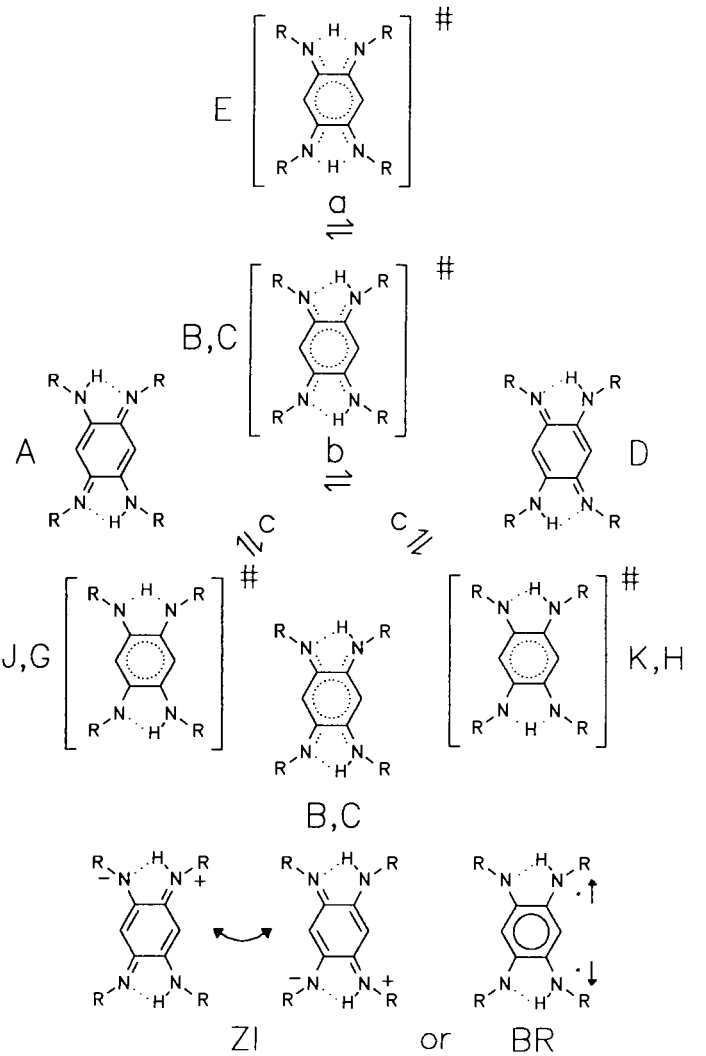

Fig. 9.6. Pathways of the azophenine (AP) tautomerism. ZI ≡ zwitterion, BR ≡ singlet biradical. Reproduced with permission from Ref. [127]

other conformers which are subject to rapid intermolecular proton exchange [120]. These spectra can be described in terms of Eq. (6.27). Unfortunately, the intermolecular exchange terms prevent the determination of the intramolecular exchange rates, especially of the k^{HD} at higher temperatures.

In order to obtain the kinetic isotope effects of the oxalamidine tautomerism ^{1}H NMR experiments were, therefore, performed on the bicyclic compound B7OA (Fig. 9.7), where the molecular structure prevents conformational

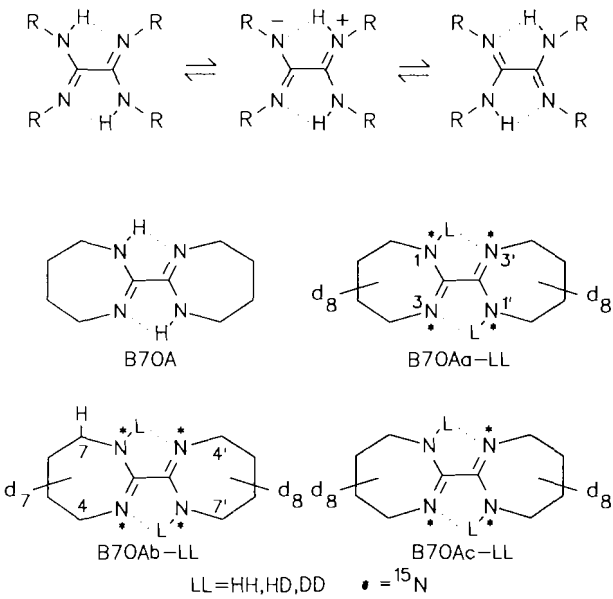

Fig. 9.7. The tautomerism of oxalamidine (OA, R = H), tetraphenyloxalamidine (TPOA, R = Ph) and B7OA, R, R = —$(CH_2)_4$—. Reproduced with permission from Ref. [129]

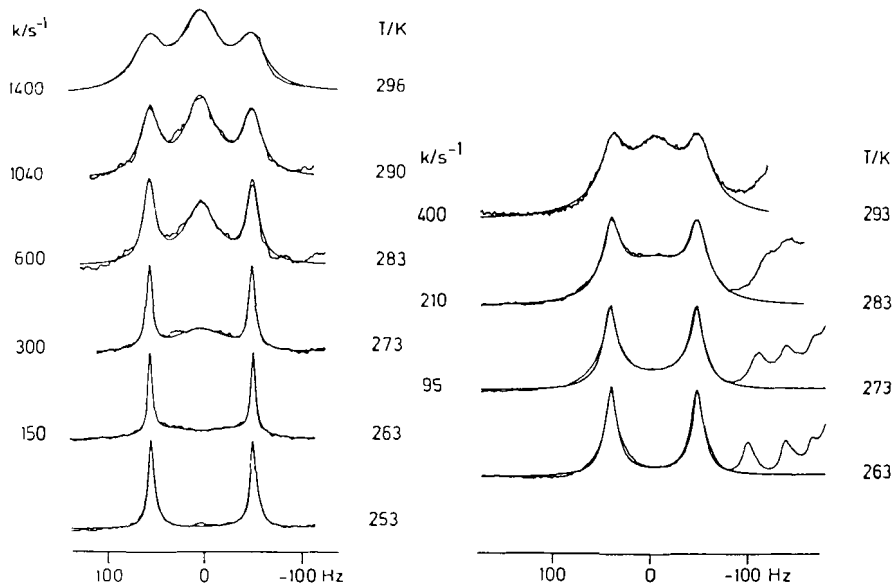

Fig. 9.8. Left: Superposed experimental and calculated 90:02 MHz ^1H NMR signals of the ^1H–^{15}N units of TPOA dissolved in CD_2Cl_2 at a deuterium fraction D = 0 in the NH sites as a function of temperature. k is the rate constant of the intramolecular HH transfer according to Fig. 9.7. The spectra were calculated using Eq. (6.27). Due to intermolecular proton exchange the average inverse lifetimes τ^{-1} are non-zero, although $\ll$ k. The spectrum at 296 K was recorded at 250 MHz. **Right**: As left, but D $\simeq$ 0.9. k corresponds to the rate constants of the intramolecular HD-transfer. Reproduced with permission from Ref. [120]

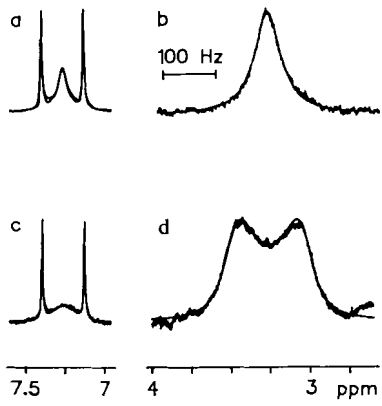

Fig. 9.9 a-d. Superposed experimental and calculated 300.13 MHz ^{1}H NMR spectra of a 0.2 molar solution of B7OA in methylcyclohexane-d_{14} (MCY) at 362 K. (**a**) ^{15}N–^{1}H···^{15}N signal of B7OAa–HH and (**b**) 4,4′ and 7,7′ proton signal of B7OAb–HH at a deuterium fraction D = 0 in the mobile proton sites; (**c**) ^{15}N–^{1}H···^{15}N signal of B7OHa–HD and (**d**) 4,4′ and 7,7′ proton signal of B7OAb–DD at a deuterium fraction D = 0.94 in the mobile proton sites. The presence of a small amount of BCOAc was taken into account in the simulations; in addition, at D = 0.94 also the presence of B7OAa–HH, B7OAa–HH, and B7OAa– HD was taken into account. Further simulation parameters: $\nu_{^1H-^{15}N} = 7.26$ ppm, $^1J_{^1H-^{15}N} = 80.3$ Hz, $W_0 = 3.7$ Hz, and chemical shifts $\nu_4 = \nu_7$, = 3.505 ppm and $\nu_7 = \nu_4$, = 3.03 ppm. Reproduced with permission from Ref. [129]

isomerism [129]. The molecule was enriched with ^{15}N and deuterated on the carbon atoms. A set of experiments was performed at 362 K as shown in Figs. 9.9 and 9.10, using methylcyclohexane-d_{14} (MCY) and acetonitrile-d_3 (AN) as solvents.

The kinetic HH/HD isotope effects could be determined by ^{1}H NMR line shape analysis of the ^{15}N–^{1}H···^{15}N signals of B7OAa–HH and B7OAa–HD as shown in Figs. 9.9a, 9.9c, 9.10a and 9.10c. Although the temperature is elevated, no contributions from intermolecular proton exchange and conformational isomerism could be detected. The signals constitute triplets with two sharp outer line components as expected for a moderately fast degenerate intramolecular proton transfer between two ^{15}N atoms. By line shape analysis of the ^{15}N–^{1}H···^{15}N signals using Eq. (6.15) the rate constants k^{HH} of the HH reaction in B7OA could be obtained for both solvents at D = 0 (Figs. 9.9a and 9.10a). At deuterium fractions close to unity (Fig. 9.9c and 9.10c) the residual ^{15}H–^{1}H···^{15}N proton signal stems from the species B7OAa–HD, i.e. its lineshape depends on the rate constant k^{HD} of the HD process. The

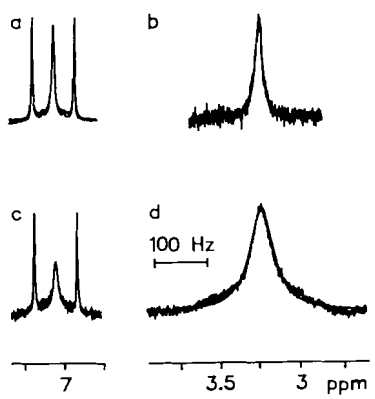

Fig. 9.10 a-d. Superposed experimental and calculated 300.13 MHz ^{1}H NMR spectra of a 0.2 molar solution of B7OA in acetonitrile-d_3 (AN) at 362 K. (**a**) ^{15}N–^{1}H···^{15}N signal of B7OAa–HH and (**b**) 4,4′ and 7.7′ proton signal of B7OAb–HH at a deuterium fraction D = 0 in the mobile proton sites; (**c**) ^{15}N–^{1}H···^{15}N signal of B7OAa–HD and (**d**) 4,4′ and 7,7′ proton signal of B7OAb–DD at a deuterium fraction D = 0.94 in the mobile proton sites. Further simulation parameters: $\nu_{^1H-^{15}N} = 7.05$ ppm, $^1J_{^1H-^{15}N} = 80.3$ Hz, $W_0 = 3$ Hz, and chemical shifts $\nu_4 = \nu_4 = 3.492$ ppm and $\nu_7 = \nu_7$, = 2.965 ppm. For further description see text. Reproduced with permission from Ref. [129]

finding that the center lines of the $^{15}N-^{1}H\cdots{}^{15}N$ signals are larger for MCY as solvent than for AN and larger at D = 0.94 than at D = 0 directly indicates substantial kinetic solvent and HH/HD isotope effects on the reaction rates. Actually, it was found that $k^{HH}(AN)/k^{HH}(MCY) = 4.5$, $k^{HH}(MCY)/k^{HD}(MCY) = 2.44$, and $k^{HH}(AN)/k^{HD}(AN) = 2.63$ at 362 K.

The kinetic HH/DD isotope effects were determined by analysis of the signals of the remote 4,4′ and 7,7′ protons in B7OAb which interconvert by the double proton transfer. Because of the absence of homonuclear couplings the lineshape of these signals can be described in terms of Eq. (2.18). At D = 0 the signals constitute exchange broadened singlets (Figs. 9.9b and 9.10b); since they stem from the species B7OAb–H_2 their lineshape depends again on k^{HH}; however, this quantity as well as W_0 is already known from the simulations in Figs. 9.9a and 9.10a. Therefore, we obtain by lineshape analysis the unknown chemical shifts of the 4,4′ and of the 7,7′ protons. The result agrees very well with the values measured in the slow exchange region at low temperatures. By contrast, at D = 0.94 the signal dominantly stems from the species B7OAb–D_2 and contains information about k^{DD}. A comparison of Fig. 9.9b with 9.9d and of Fig. 9.10b with 9.10d shows then substantial kinetic HH/DD isotope effects. In the case of Fig. 9.9d even the case of slow exchange was reached where the chemical shifts could directly be obtained by lineshape analysis. The following kinetic isotope effects $k^{HD}(MCY)/k^{DD}(MCY) = 1.2$, $k^{HH}(MCY)/k^{DD}(MCY) = 3$, $k^{HD}(AN)/k^{DD}(AN) = 1.3$ and $k^{HH}(AN)/k^{DD}(AN) = 3.5$ were obtained. It was further established that the results found for both solvents were independent of the concentration of B7OA.

The observed kinetic HH/HD/DD isotope effects are similar, as in the case of AP, and can be explained with a stepwise proton transfer mechanism according to Fig. 9.7. By contrast to AP, the observed increase of the rate constants in B7OA with the increase of the dielectric constant—2 for MCY and 37.5 for AN at 298 K—establishes, however, a polar transition state of the reaction as expected for the stepwise double proton transfer via the zwitterion intermediate as shown in Fig. 9.7.

Note that in the experiments of Figs. 9.9 and 9.10 no assumptions concerning chemical shift differences, coupling constants, or line widths in the absence of exchange were necessary. Moreover, the isotopic reaction rate constants of the HD and the DD reactions could be determined by analysis of different parts of the same spectrum. Therefore, there are no temperature errors on the kinetic HD/DD isotope effects which could be introduced when the latter are derived from measurements of different samples.

9.3 The Porphyrin Tautomerism

The tautomerism of porphyrines (Fig. 2.2) was discovered in 1972 by Storm and Teklu via ^{1}H NMR spectroscopy [109]. These authors showed in a qualitative way the existence of kinetic HH/DD isotope effects on this reaction by

observing different ^{1}H NMR lineshapes of the β-pyrrole protons (see Fig. 2.2) in the presence and absence of deuteriomethanol in the NMR samples. Rate constants [80, 105, 110–116, 119, 124] and kinetic HH/DD isotope effects [111, 115] have since been studied quantitatively by dynamic NMR spectroscopy. The possibility of obtaining rate constants of the tautomerism by analysis of the ^{1}H NMR lineshape of the inner proton signal of ^{15}N labeled porphyrines [112–115] also opened the possibility of studying the kinetic HH/HD isotope of the reaction. This was accomplished in 1982 [105], when complete kinetic HH/HD/DD isotope effects were reported for the first time. Since then these effects have been studied in more detail [124–126]. Recently, it has been shown by NMR that the porphyrin tautomerism can also take place in the solid state [167–177]. Note that kinetic HH/DD isotope effects were also obtained by optical methods on porphyrin embedded in solid hexane [141]. The mechanism of the porphyrin tautomerism has been subject to intense theoretical studies [133–142]. The phenomenon of solid state tautomerism of porphyrines will be dealt with in Section 11. Here, we will discuss liquid state NMR experiments devoted to the determination of the kinetic HH/HD/DD isotope effects of the porphyrin tautomerism.

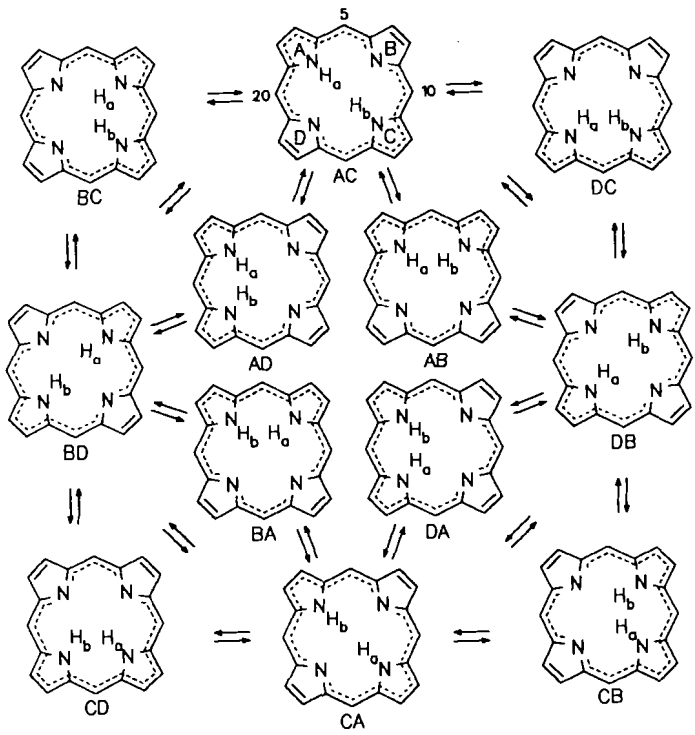

Fig. 9.11. Proton transfer pathways in porphyrins according to Ref. [123]

9.3.1 *Symmetrically Substituted Porphyrines*

The complete reaction pathways of symmetrically substituted porphyrines are shown in Fig. 9.11 [123]. The different tautomers are labeled according to the pyrrole rings to which the mobile protons are attached. The rate constant of the reaction of tautomer MX to NY is then written as $k_{MX \to NY}$. Observable species are the degenerate *trans*-tautomers AC, BD, DB, and CA. The remaining *cis*-tautomers are postulated intermediates of a stepwise reaction pathway. Note that in the case of porphyrins the NMR lineshapes of the mobile protons bound to ^{15}N spins and of the remote spins depend on slightly different quantities. Thus, all published rate constants k, including those given in Sects. 2.2 and 2.3, correspond to the values $2k_{AC \to DB}$. By contrast, the constants $k_{AC \to DB}$ are

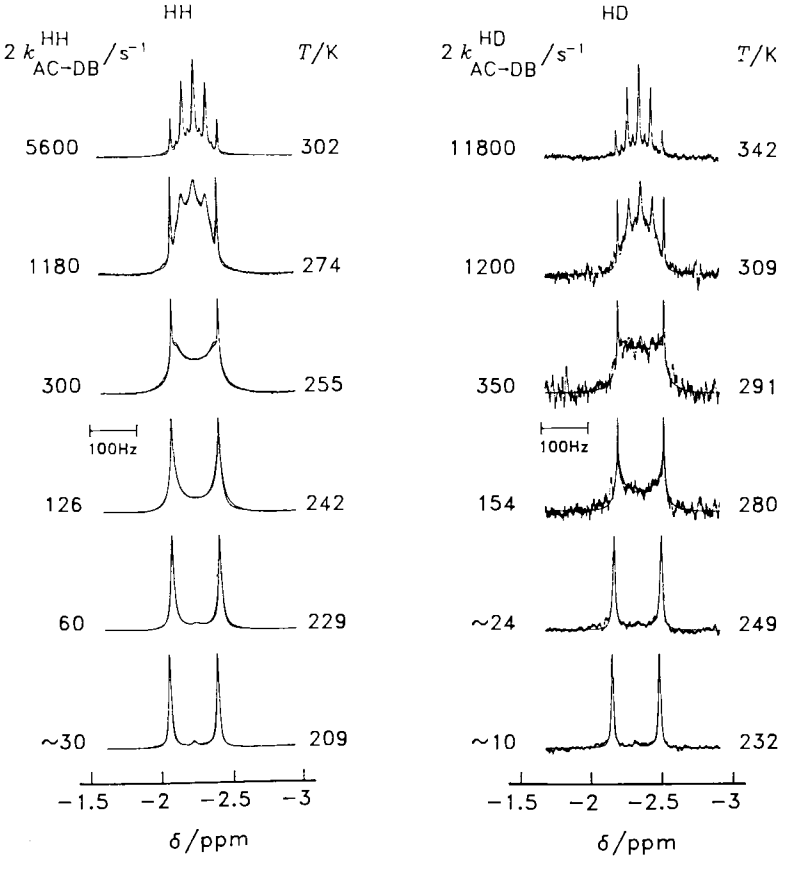

Fig. 9.12. Superposed experimental and calculated 300.13 MHz ^1H NMR spectra of the inner hydrogen atoms of *meso*-tetraphenylporphyrin-$^{15}N_4$ dissolved in toluene-d_8. **Left**: D = 0, **right**, D = 0.85. The spectra were calculated using Eqs. (6.19) and (6.20). Reproduced from Ref. [124]

obtained from the lineshape analysis of the inner proton signals. The lineshape equations of the mobile proton signals migrating between four ^{15}N atoms are set up as indicated in Sect. 6.1.2.

Since the error limits of the early $2k^{HD}_{AC\rightarrow DB}$ determination [105] were large because of experimental limitations in the signal to noise ratio, these measurements have been repeated recently [124]. The results of the 300 MHz ^1H NMR experiments on the inner proton signals of TTP at deuterium fractions of D = 0 and 0.9 in the mobile proton sites are shown in Fig. 9.12. The spectra were calculated using Eq. (6.19). As observed previously [112, 115], the intramolecular proton transfer gives rise to a doublet–pentet transition when going from the slow to the fast exchange regime. As in the case of azophenine, the coupling constant $J_{^1H-^{15}H}$ and W_0 could be obtained by simulation of the outer line components. At D = 0 the lineshapes depend on $2k^{HH}_{AC\rightarrow DB}$, at D = 0.85 mostly on $2k^{HD}_{AC\rightarrow DB}$. Naturally, the signal to noise ratio is not as good at D = 0.85 at to D = 0. In calculating the spectra the 15% of TPP–HH was taken into account.

Figure 9.13 contains the results of ^{13}C NMR experiments performed on TPP with a natural abundant ^{13}C content, dissolved in tetrahydrofuran. The o-, m-, and p-phenyl carbon signals are not affected by the exchange. At

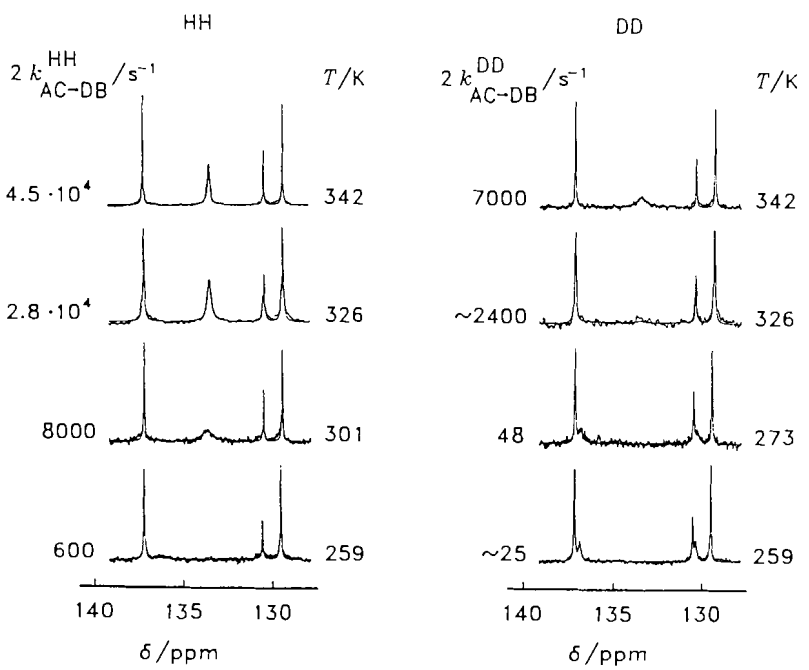

Fig. 9.13. Superposed experimental and calculated 75 MHz ^{13}C NMR spectra of TPP dissolved in tetrahydrofuran-d_8. **Left**: deuterium fraction in the mobile proton sites D = 0, **right**: D = 0.85. Reproduced from Ref. [124]

D = 0.85 and 259 K the deuteron transfer is so slow that the splitting of the two inequivalent β-pyrrole carbons 2,3 and 7,8 can easily be observed. In the intermediate temperature range, i.e. the coalescence region it is very difficult to detect the very broad signal hidden in the noise. The kinetic HH/DD isotope effect is clearly demonstrated in the two sets of spectra, which were calculated using Eq. (2.18).

The Arrhenius diagram of the TPP migration shows similar features to the diagram of azophenine (Fig. 9.5): a large kinetic HH/HD isotope effect is observed and only a very small kinetic HH/HD isotope effect. These results can again most easily be interpreted in terms of a stepwise proton motion via *cis*-intermediates, as predicted theoretically [133, 134, 140–142]. At low temperatures the reaction proceeds by tunneling, which has definitively been established recently using a laser temperature jump method [125, 141]. This idea was proposed a long time ago [105, 115].

9.3.2 *Chemically Perturbed Porphyrines*

So far, we have focused in this review on symmetric exchange reactions with equilibrium constants of unity. However, dynamic NMR spectroscopy can also follow asymmetric exchange reactions with equilibrium constants $\neq 1$ within certain limits. E.g., NMR measurements on asymmetric porphyrines and chlorins have been performed [121–123, 126] which open the possibility of studying kinetic hydrogen/deuterium isotope effects of asymmetric exchange reactions in this class of compounds. As an example, let us consider the tautomerism of a mono-substituted acetylporphyrin (ACP). For this purpose ACP was once triply labeled with ^{15}N (ACP–$^{15}N_3$) and once mono labeled with ^{13}C (ACP–^{13}C) as shown in Fig. 9.14. The full proton transfer pathways

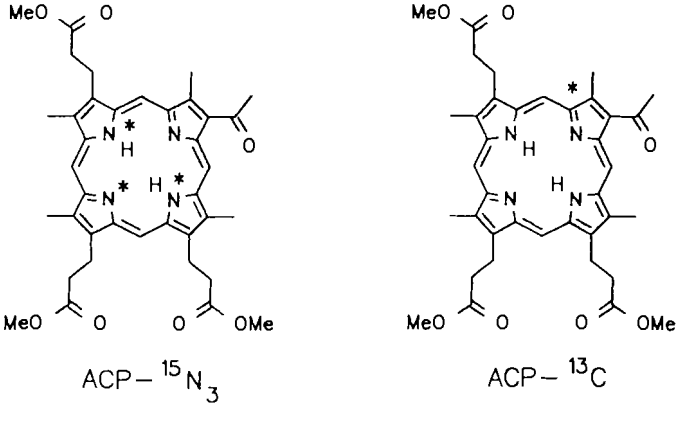

Fig. 9.14. The structure of the triply labeled ACP-$^{15}N_3$ and the ^{13}C labeled ACP-^{13}C

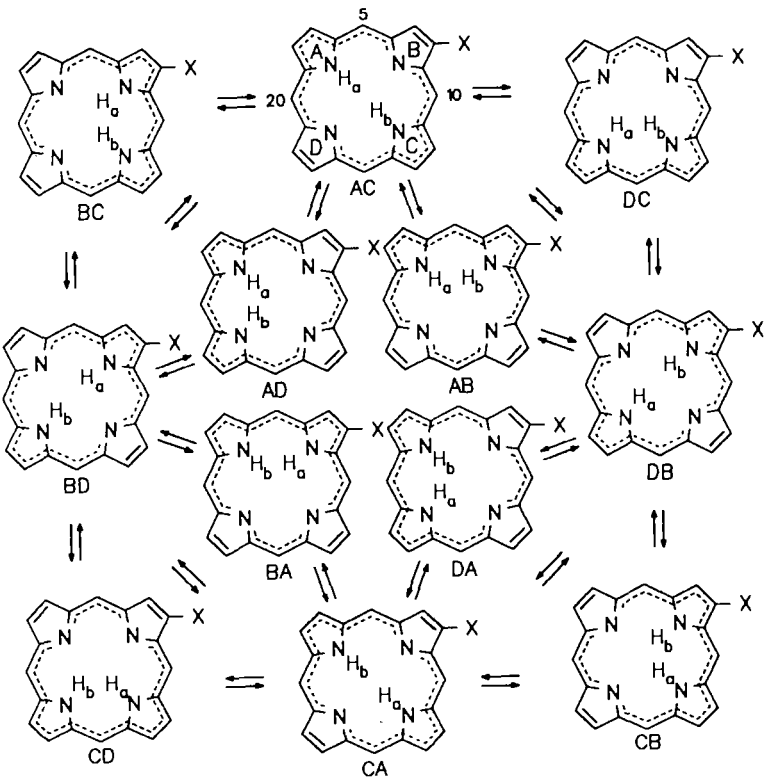

Fig. 9.15. Proton transfer pathways in ACP. Reproduced from Ref. [126]

of ACP are shown in Fig. 9.15. Preliminary HH/HD isotope effects for this compound were reported in Ref. [122]. The full isotope effects could be obtained only recently [126].

The results of the ^{13}C NMR experiments [126] on ACP–^{13}C–HH and ACP–^{13}C–DD are shown in Fig. 9.16. The spectra were calculated using Eq. (2.18). At low temperatures the labeled ^{13}C atom exhibits a strong line at 148 ppm. This line was assigned to the tautomers AC and CA. A second very weak line at $\sim$132 ppm was attributed to the tautomers BD and DB (arrows in Fig. 9.16). The weak line is sharp only in the case of ACP–^{13}C–DD, but exchange broadened in the case of ACP–^{13}C–HH. As temperature is raised both lines broaden and coalesce into one sharp line. The coalescence temperature is higher for the deuterated compound as compared to the protonated compound due to a kinetic HH/DD isotope effect. The analysis of the spectra in Fig. 9.16 is complicated by a temperature dependence of the ^{13}C chemical shifts due to aggregation of ACP. However, it was found by analysis of the spectra of ACP–^{13}C–DD that the difference $\Delta\nu$ of the chemical shifts of the exchanging carbon atoms is almost independent of temperature. Thus, the chemical shifts

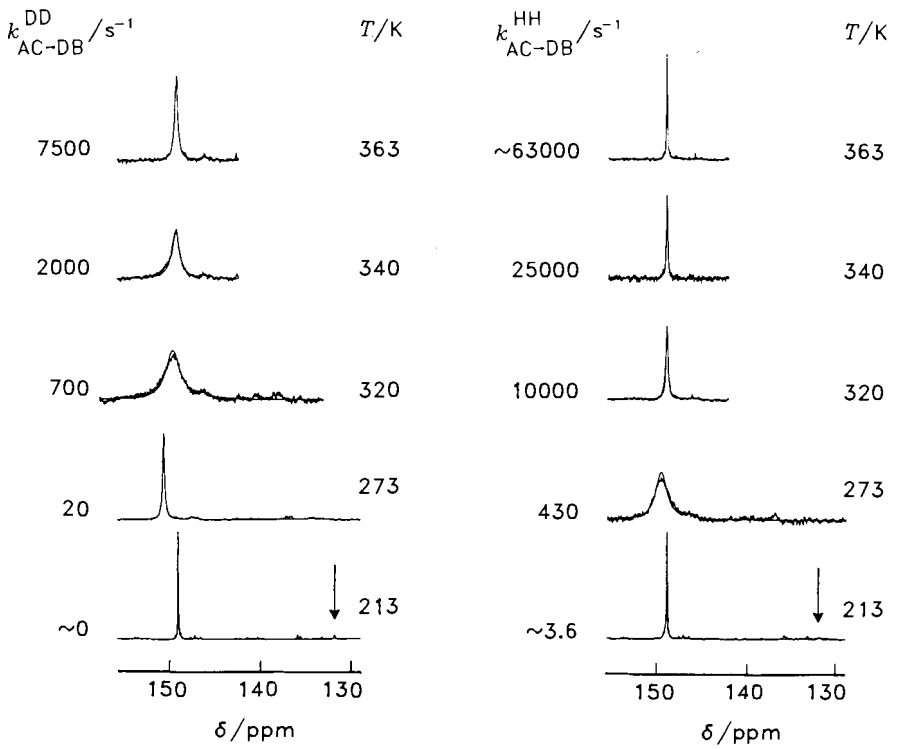

Fig. 9.16. Superposed experimental and calculated 75 MHz ^{13}C NMR signals of the C-6 carbon atom of the monoacetylporphyrin derivative ACP dissolved in highly purified CD_2Cl_2 as a function of temperature. **Left**: D = 0, **right**: D = 0.95. The *arrows* indicate the signals of tautomers DB and BD in the slow exchange limit. The spectra were calculated using Eq. (2.18). Reproduced from Ref. [126]

needed to simulate the exchange broadened spectra of ACP-^{13}C-HH could be obtained from the spectra of ACP-^{13}C-DD at a given temperature. Note that the line shapes depend here on the rate constants $2k^{LL}_{AC\rightarrow DB}$, LL = HH, DD. For comparison with the rates obtained by ^{1}H NMR, however, only the constants $k^{LL}_{AC\rightarrow DB}$ are listed in Fig. 9.16. The ratio of the two tautomers, also needed to calculate the spectra, could be obtained at low temperature directly by simulation. At higher temperatures this ratio was obtained from ^{1}H NMR experiments as shown in the following.

The latter were performed on the inner proton signals of ACP-$^{15}N_3$ as shown in Fig. 9.17 at D = 0 and D = 0.95 [126]. The spectra were simulated using Eqs. (6.19) and (6.21). The two inner protons have different isotropic chemical shifts giving rise to two inequivalent ^{1}H-^{15}N doublets with equal splittings $J_{^1H-^{15}N}$ in the slow exchange range. Unfortunately, the signals of the second tautomer could not be identified. Since ring B was not labeled with ^{15}N the observation of two ^{1}H-^{15}N doublets indicates that the protons are located

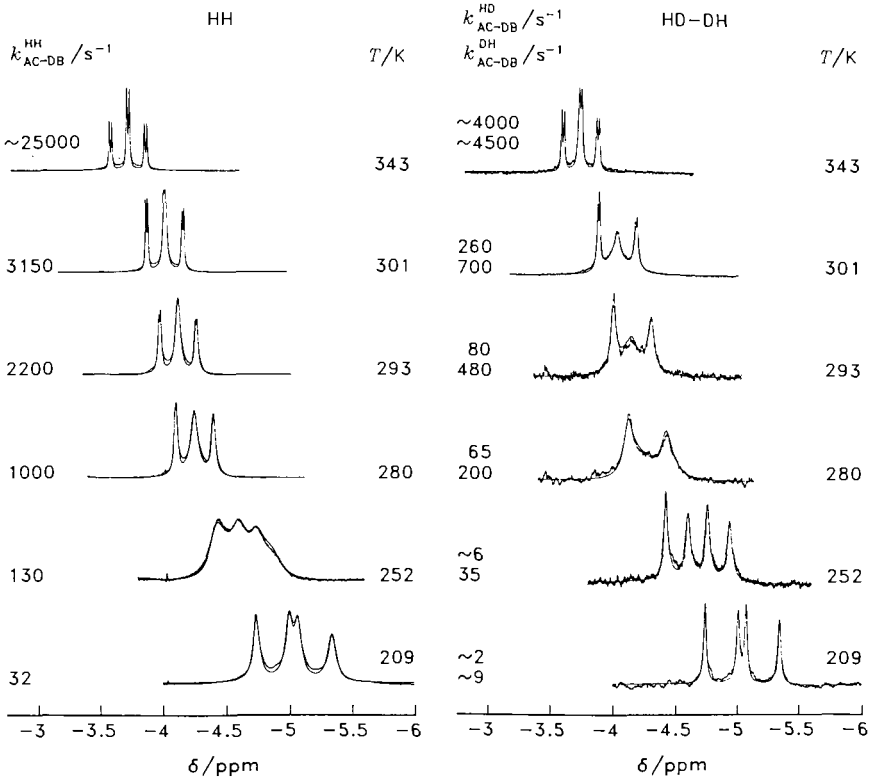

Fig. 9.17. Superposed experimental and calculated 300.13 MHz ^{1}H NMR signals of the inner hydrogen atoms of ACP dissolved at a concentration of 20 mmol l^{-1} in highly purified CD_2Cl_2 as a function of temperature. The spectra were calculated using Eqs. (6.19) and (6.21). According to Eq. (6.20), the temperature dependent ratio of the effective triplet and doublet splittings in the fast exchange region is equal to the tautomer ratio AC vs. BD. $k_{r\to s}$ is the rate constant of the interconversion r → s. **Left**: D = 0, **right**: D = 0.95. Reproduced from Ref. [126]

on the rings A and C and not on B and D in the dominant tautomers, i.e. AC and CA. At high temperatures a coalesced ^{1}H–^{15}N triplet is observed where each line component is further split into a doublet. This result indicates that AC and CA exchange rapidly via the tautomers DB and BD. The doublet splitting arises by coupling of the inner protons with the ^{15}N atom on ring D in the minor tautomers BD and DB. According to Eq. (6.20), the population of all tautomers can be obtained exactly from the effective splittings given by $J_X^{eff} = p_X J_{^1H-^{15}N}$, where p_X is the population of each of the inner protons on ring X [122]. Extrapolation of the data to low temperature showed a good agreement with the value obtained by ^{13}C NMR. A comparison of both sets of spectra in Fig. 9.17 shows significant kinetic isotope effects. Note that in the case of ACP–$^{15}N_3$–HH, i.e. at D = 0, AC and CA are degenerate. In principle, AC and

CA are not degenerate in the case of ACP–$^{15}N_3$–HD; however, they are quasi degenerate when equilibrium isotope effects can be neglected. This is indeed the case: at D = 0.95 where the second set of experiments was performed the lineshape almost exclusively stems from the species ACP–$^{15}N_3$–HD, i.e. of species AC and CA. In the presence of an equilibrium isotope effect the two doublets should be of unequal intensity, which is not the case. Of special importance is that the spectra of ACP–$^{15}N_3$–HD are characterized by two different rate constants, $k^{HD}_{AC\rightarrow DB} \neq k^{DH}_{AC\rightarrow DB}$. Thus, the full kinetic HH/HD/DH/DD isotope effects could be obtained for ACP, further evidence for a stepwise proton transfer pathway in this molecule [126].

Note also that recently the tautomerism of hydroporphyrins has been studied by mobile and remote spin studies [123]. In this class of compounds it was possible to significantly perturb the reaction barrier by specific hydrogenation of the pyrrole rings, which leads to the biologically important hydroporphyrins chlorin, bacteriochlorin and isobacteriochlorin. The increase or decrease of the reaction energy barrier could be explained with an increased or decreased energy of the intermediates along the reaction pathways. In future studies it will be very interesting to know how the kinetic isotope effects vary when the barrier height is altered.

10 Kinetic Hydrogen/Deuterium Isotope Effects of Intermolecular Proton Exchange Reactions in Liquids

Compared to intramolecular rearrangements, the study of intermolecular proton exchange reactions is more tedious. As in ordinary kinetics, one has to perform kinetic runs as a function of the concentration of the reactants in order to establish the rate law of the exchange. Such rate laws can be complicated in the presence of a complex reaction network. Often, it will not even be possible to obtain rate laws when the concentrations of the reacting species cannot be varied as desired because of solubility problems, or because the solvent participates in the exchange either as inhibitor or as catalyst. This is often the case in biochemical reactions. In this situation one can obtain information on the number m of protons transferred in the rate limiting step as well as on kinetic isotope effects by performing a so-called "proton inventory" [41–48]. In a proton inventory kinetic measurements are performed as a function of the deuterium fraction D in the mobile proton sites. This technique has been adapted to dynamic NMR spectroscopy [106–108] and is treated theoretically in Sect. 5 of this review. Here, we will give examples for the application of this technique both in the cases of proton self exchange as well of proton exchange between different molecules.

10.1 *Intermolecular Self Exchange: Pure CH_3OH and CH_3OH/CH_3OD*

As a first example, let us discuss the problem of proton and deuteron exchange in pure methanol. This problem has been studied in Ref. [89]. Fig. 10.1 shows the superposed experimental and calculated ^1H NMR spectra of pure CH_3OH (left) and of 1% CH_3OH dissolved in CH_3OD (right) as a function of temperature. CH_3OH leads to an AB_3 spin system with a doublet splitting of the CH_3 signal and a quartet splitting of the OH signal at low temperatures. Because of hydrogen bond association the OH signal shifts to low field when the temperature is lowered, a phenomenon which has been used for temperature calibration in ^1H NMR spectroscopy [199]. As the temperature is raised the spin–spin splitting pattern collapses into a singlet for the CH_3 and the OH signal, respectively indicating that even in pure CH_3OH a proton exchange takes place which can formally be described by

$$AL + A^*L^* \rightleftharpoons AL^* + A^*L, \tag{10.1}$$

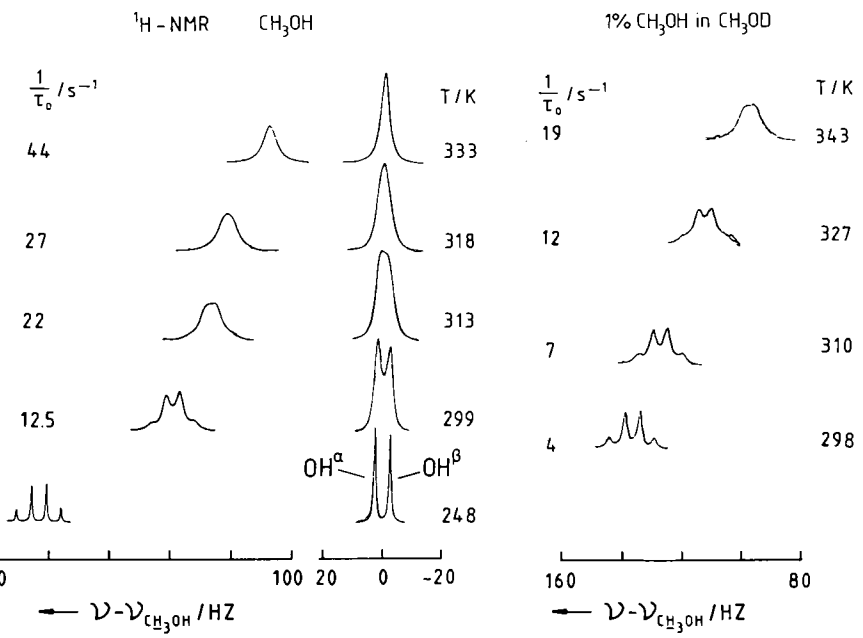

Fig. 10.1. Left: Superposed experimental and calculated ^1H 90.02 MHz NMR signals of pure methanol as a function of temperature. The CH_3OH signal appears at low, the CH_3OH signal at high field. The intensities of the two signals are not normalized to the corresponding number of protons (100 scans, 90° pulses, repetition time 10 s). Reproduced with permission from Ref. [89]. **Right:** Superposed experimental and calculated ^1H 90.02 MHz NMR signals of the residual CH_3OH protons (1 vol-%) in CH_3OD as a function of temperature (1000 scans, 90° pulses, repetition time 10 s). Reproduced with permission from Ref. [89]

with A = CH_3O and L = H. This phenomenon has also been known for a long time and has been used to study proton exchange rates in solutions of acids in methanol [85]. The spectra in Fig. 10.1 were calculated in terms of the exchange operator given in Eq. (3.15), taking into account the magnetic equivalence of the CH_3 spins. Thus, the dimension of $\mathcal{M}$ could be reduced to a 16 × 16 matrix [94]. From the line shape analysis the proton lifetimes $\tau_{AHA^*H}^{-1} \equiv \tau_{AH}^{-1}(\tau_0^{-1}$ in Fig. 10.1) could be obtained as a function of temperature. Note that the coupling constant J_{CH_3OH} is only 5 Hz, which strongly limits the dynamic range in which inverse life times can be obtained. Furthermore, it was not possible to measure the deuteron exchange rates τ_{AD}^{-1} by ^2H NMR spectroscopy of CD_3OD, because the coupling constant $J_{CD_3OD} = 0.9$ Hz is too small to resolve a spin–spin splitting pattern, giving rise to dynamic line shape effects. The only way to obtain information on possible kinetic isotope effects was, therefore, to perform ^1H NMR measurements on mixtures of CH_3OH/CH_3OD, looking selectively at the OH proton signals. The results are shown for a deuterium fraction of D = 0.99 in Fig. 10.1 on the right side. From a comparison of both sets of spectra it immediately becomes evident that the OH-proton lifetime of an individual CH_3OH molecule is longer if it is surrounded by CH_3OD molecules. It follows from the experiments in Fig. 10.1 that $\tau_{AH}^{-1}(D = 0)/\tau_{AH}^{-1}(D = 0.99) \cong 3$ at 298 K. Arguments could be given [89] in favor of an ionic exchange mechanism, in which the proton exchange is catalyzed by the ions AL_2^+ and A^-, L = H, D:

$$A^*L + A^- \rightleftharpoons A^{*-} + AL, \quad A^*L + AL_2^+ \rightleftharpoons A^*L_2^+ + AL \tag{10.4}$$

generated via autoprotolysis

$$AL + AL \rightleftharpoons AL_2^+ + A^-. \tag{10.5}$$

The observed kinetic isotope effect was then attributed to a large extent to an equilibrium isotope effect of the autoprotolysis leading to a smaller concentration of ions At D = 0.99 as compared to D = 0. Unfortunately, the small dynamic range of this system did not allow to obtain more detailed information on the kinetic isotope effects of the different isotopic exchange reactions taking place in this reaction system.

Note that the presence of equilibrium isotope effects between a protic solvent like methanol and reacting acids and bases leads to complicated kinetic expressions [90].

10.2 Intermolecular Self Exchange: The System Diarylformamidine-$^{15}N_2$/Tetrahydrofuran

Much simpler self exchange reactions were found in the systems diphenylformamidine-$^{15}N_2$ (DPFA) [107] and di-*p*-flurophenylformamidine-$^{15}N_2$ (DFFA) [108] dissolved in tetrahydrofuran (THF). The structure of these compound, which can exist in an *s*-trans form A (or AL, L = H, D) and an *s-cis* form B (or BL), is shown in Fig. 10.2. Both conformers represent four-spin-1/2-

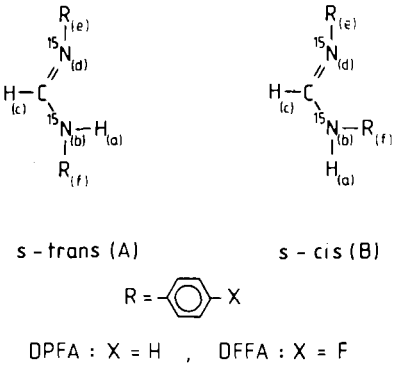

Fig. 10.2. Atom numbering of ^{15}N labeled diarylformamidines in the *s-cis* and the *s-trans* form. Reproduced with permission from Ref. [108]

systems because of the ^{15}N labeling in the nitrogen atom sites. The tautomerism of these compounds was first described by Borisov et al. [96]. In recent kinetic and thermodynamic NMR studies the complex reaction network shown in Fig. 10.3 has been elucidated [107, 108]. Both conformers form at low concentrations solvated monomers A_{1s} and B_{1s} which interconvert slowly on the NMR

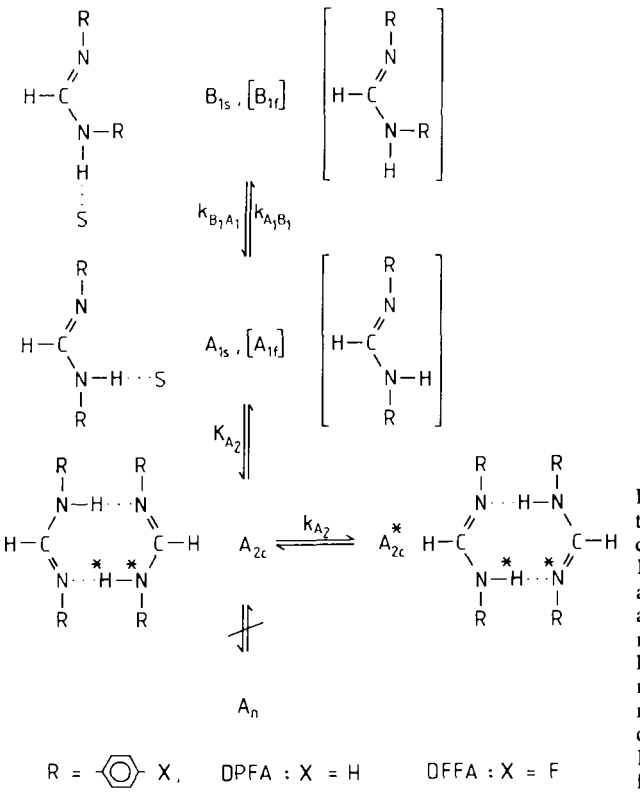

Fig. 10.3. The formamidine tautomerism. Exchange processes of DPFA and of DFFA dissolved in THF as identified by NMR. K_i and k_i are equilibrium and rate constant obtained by lineshape analysis. Brackets represent possible intermediates present in minor concentrations. S ≡ solvent. Reproduced with permission from Ref. [107]

timescale. The free monomers A_{1f} and B_{1f} which are believed to be intermediates of the conformational exchange are present only in very low concentrations. At high concentrations only the *s-trans* conformer AL is able to form cyclic dimers A_{2c} in which a double proton transfer takes place. Higher associates are formed by neither A nor B in detectable concentrations. The following will describe how this information as well as the kinetic HH/HD/DD isotope effects of the double proton transfer were obtained.

10.2.1 Dynamic ^1H NMR Spectroscopy of DPFA in Tetrahydrofuran

Figure 10.4 shows a superposition of experimental and calculated ^1H NMR spectra of DPFA in THF at a very low concentration. At room temperature only one $^1H-^{15}N$ singlet A_a, B_a and one CH-proton signal A_c, B_c are found. By contrast, at low temperatures two CH multiples A_c and B_c as well as two $^1H-^{15}N$ signals A_a and B_a are observed, indicating the presence of two conformers A and B which interconvert at high temperature. Both $^1H-^{15}N$ signals are split into doublets by scalar coupling with the ^{15}N spin b; each component is further split by coupling with c. For B_a an additional long range coupling to d is resolved, leading to an apparent subtriplet structure. As temperature is raised first signal A_a is broadened; at higher temperatures all signals are affected by the rotational isomerism.

The concentration dependent superposed experimental and calculated ^1H NMR spectra of DPFA in THF at 179 K (Fig. 10.5) give further insights

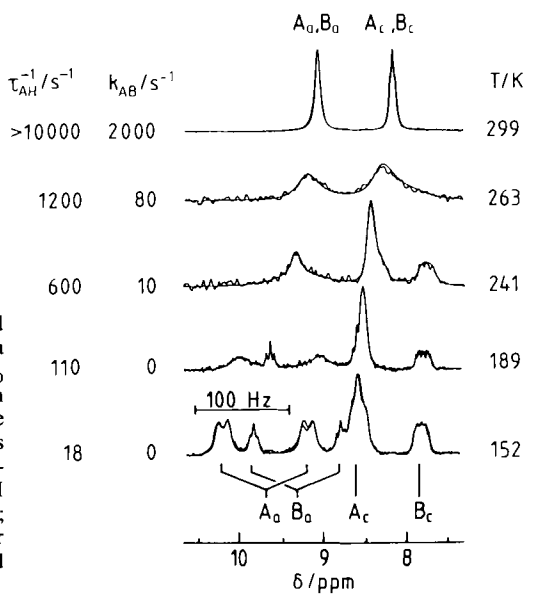

Fig. 10.4. Superposed experimental and calculated ^1H NMR 90.02 MHz spectra of ^{15}N, $^{15}N'$-diphenylformamidine-d_{10} (DPFA) in THF-d_8 for a concentration of 0.004 M as a function of the temperature. k_{AB}: forward rate constants of the hindered rotation between monomeric conformers A and B; A_a, B_a: ^1H NMR signals of the mobile $^1H-^{15}N$ sites; A_c, B_c: ^1H signals of the CH sites. For further description see text. Reproduced with permission from Ref. [107]

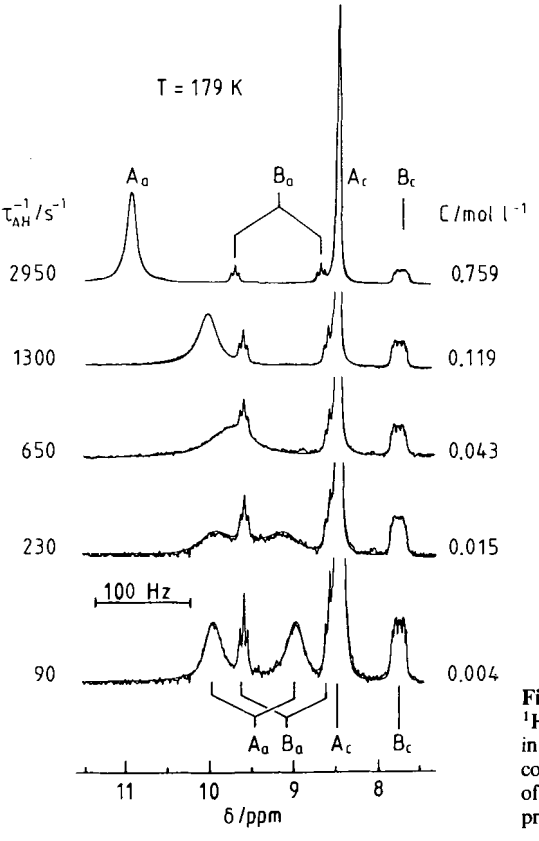

Fig. 10.5. Experimental and simulated ^1H NMR 90.02 MHz spectra of DPFA in THF-d_8 at 179 K as a function of the concentration. τ_{AH}^{-1} is the inverse lifetime of the mobile proton in AH. Reproduced with permission from Ref. [107]

into the reaction network of this molecule. The spectra were calculated using a combination of Eqs. (2.12) and (4.15) according to Ref. [107]. Neither the position nor the shape of the B_a signal changes with concentration, indicating absence of self association and proton exchange of B. By contrast, the $^1H-^{15}N$ proton signal A_a of the *s-trans* from A (i) strongly shifts to lower field and (ii) collapses from a doublet into a singlet as concentration is raised because of (i) self association and (ii) proton self exchange. This is because fast intermolecular proton exchange modulates the Larmor frequency of the mobile proton every other exchange process (see Eq. (6.24)). Because of the self association the AH/BH ratio increases with concentration. When the chemical shifts of A_a are plotted as a function of concentration a non-linear behavior is observed (Fig. 10.6, top); the dependence could be fitted assuming only the formation of dimers, with the monomer and the dimer chemical shifts and the equilibrium constant K_{A_2} (Fig. 9.3) of the dimerization as a parameter. Thus, at low concentration the solvated monomer dominates, at higher concentration the dimer. Note that the dynamic range in which proton exchange rates can be measured is much greater than

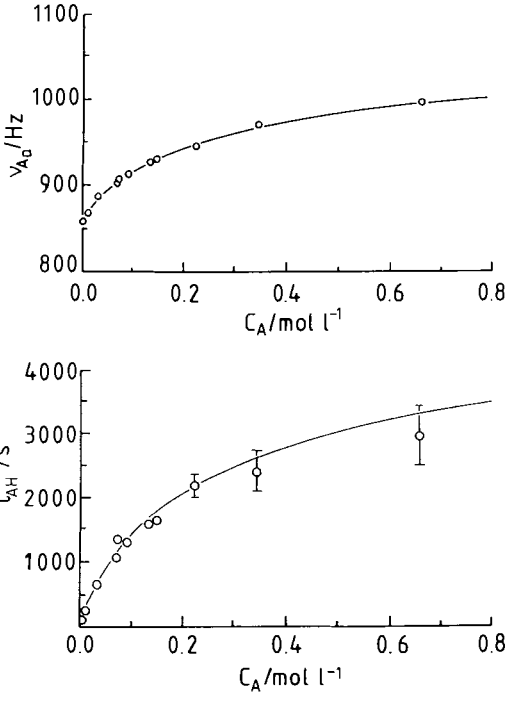

Fig. 10.6. Top: Experimental and calculated chemical shifts ν_{A_a} of the $^1H-^{15}N$ signal A_a of DPFA in THF as a function of the concentration C_A of the conformer A at 179 K. **Bottom**: Experimental and calculated inverse $^1H-^{15}N$ proton lifetimes τ_{AH}^{-1} in conformer A as a function of the concentration C_A of conformer A at 179 K. The *solid line* was calculated using Eqs. (5.85) and (5.91) from the known values of the constants $K \equiv K_{A_2}$ and $k_{A_2} = k_{rls}$. Reproduced with permission from Ref. [107]

in to the case of methanol because the coupling constant $J_{^1H-^{15}N} \approx 92$ Hz. From the calculations the average inverse life times $\tau_{AHAH}^{-1} \equiv \tau_{AH}^{-1}$ are obtained. If the τ_{AH}^{-1} are plotted vs. the concentration C_A also a non-linear dependence is also observed (Fig. 10.6, bottom). Using the known value of K_{A_2} the data could be fitted to Eqs. (5.85) and (5.91) by adapting the exchange rate constant $\tau_{rls}^{-1} = k_{A_2}$ in the cyclic dimer and setting $D = 0$ in Eq. (5.85). At low concentrations τ_{AH}^{-1} is proportional to the concentration C_A of the *s-trans* form A as expected for a second order rate law; at higher concentrations the reaction becomes independent of C_A. This is because A then dominantly forms dimers in which the proton exchange takes place. The ^1H NMR spectra of DFFA in THF exhibit similar characteristics [107].

10.2.2 ^1H NMR Proton Inventory of the System DFFA/Tetrahydrofuran

Having established the reaction rate law the problem arose how to count the number of protons transferred and how to determine the kinetic isotope effects of the double proton transfer. For this purpose, ^1H NMR proton inventories of DPFA and DFFA were performed, i.e. proton exchange rates were measured as a function of the deuterium fraction D in the NH sites. An example is shown in Fig. 10.7 for DFFA/THF. Only the superposed experimental and calculated

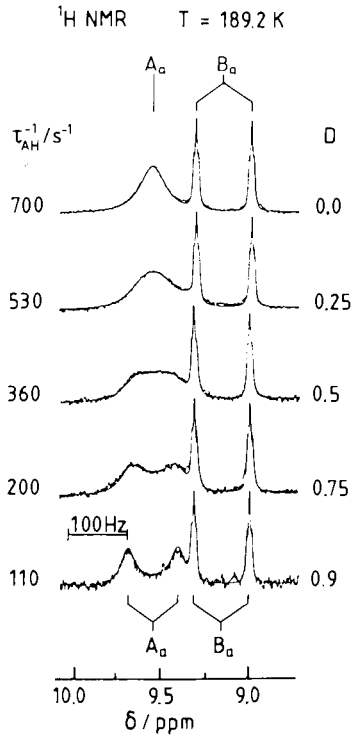

Fig. 10.7. Superposed experimental and calculated 300.13 MHz $^1H-^{15}N$ NMR signals of a 0.02 molar solution of DFFA at 189.2 K as a function of the deuterium fraction *D* in the $^1H-^{15}N$ position. The $^1H-^{15}N$ signals of the *s-trans* form A are labeled as A_a and of the *s-cis* form B as B_a according to Fig. 10.2. The inverse proton lifetimes in X = A, B are labeled as τ_{XH}^{-1}. τ_{BH}^{-1} was set to zero. Reproduced with permission from Ref. [108]

$^1H-^{15}N$ signals A_a and B_a of DFFA are shown as a function of the deuterium fraction D in the mobile proton sites. Whereas the lineshape of signal B_a is not affected by deuteration the exchange broadened singlet A_a splits up into an exchange broadened doublet when D is increased. Thus, the proton life times τ_{AH}^{-1} decrease with increasing D, which is proof of a multiple proton transfer process.

In Fig. 10.8 the ratio of the inverse proton lifetimes in $A \equiv AH$, $\tau_{AHA^*H}^{-1}(D)/\tau_{AHA^*H}^{-1}(D=0) = \tau_{AH}^{-1}(D)/\tau_{AH}^{-1}(D=0)$ is plotted as a function of D. A

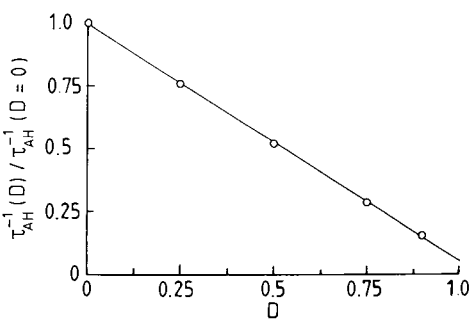

Fig. 10.8. ^{1}H NMR proton inventory plot of the data in Fig. 10.7. According to Eq. (5.32) a linear dependence $\tau_{AH}^{-1} = f(D)$ is expected for a double proton transfer process. The ratio $\tau_{AH}^{-1}(D=0)/\tau_{AH}^{-1}(D=1)$ represents the kinetic HH/HD isotope effect of the exchange. Reproduced with permission from Ref. [108]

linear decrease as predicted by Eq. (5.32) for a double proton transfer process is observed. The inverse lifetimes $\tau_{AH}^{-1}(D=0)$ and $\tau_{AH}^{-1}(D=1)$ can then be identified as the pseudo first order rate constants k^{HH} and k^{HD} of the processes

$$AH + A^*H^* \xrightarrow{k^{HH}} AH^* + A^*H,$$

$$AH + A^*D \xrightarrow{k^{HD}} AD + A^*H.$$

By linear regression analysis we obtain $k^{HH} = 700 \pm 20\,s^{-1}$ and $k^{HD} = 37 \pm 5\,s^{-1}$, i.e. a kinetic HH/HD isotope effect of $k^{HH}/k^{HD} = 19 \pm 3$. Assuming that equilibrium isotope effects on the dimerization are small this value is equal to the intrinsic isotope effect $k_{A_2}^{HH}/k_{A_2}^{HD}$ of the exchange in the cyclic dimer.

Thus, the ^1H proton inventory supports the interpretation of the rate law in terms of the reaction network of Fig. 10.3. These results show the power of the proton inventory technique for the analysis of dynamic processes in the liquid state; this technique is especially important when the concentrations of the reactants cannot be varied.

10.2.3 ^{19}F NMR Proton Inventory of the System DFFA/Tetrahydrofuran

Unfortunately, although the experiments in Fig. 10.8 revealed the kinetic HH/HD isotope effects, the kinetic HD/DD isotope effects could not be determined by ^2H NMR spectroscopy. This is because of the smallness of the scalar coupling constant $J_{^2H-^{15}N} = \gamma_{^2H}/\gamma_{^{15}H-^{15}N} \approx 14$ Hz. In view of the much larger natural ^2H line width arising from quadrupole relaxation at low temperatures this value did not provide a sufficient dynamic range. Using the information that $m = 2$ protons are transferred during the exchange the full kinetic HH/HD/DD isotope effects of the exchange could, however, be determined for the system DFFA/THF by ^{19}F NMR spectroscopy [108] as shown in the following.

Figure 10.9 shows the superposed experimental and calculated ^{19}F NMR spectra of DFFA at 189.2 K and a concentration of $C_{298K} = 0.02\,mol\,l^{-1}$ as a function of the deuterium fraction D. In fact, the spectra in Fig. 10.9 stem from the same samples whose ^1H NMR signals were shown in Fig. 10.7, with exception of the highest deuterated sample where $D = 0.99$. All samples were taken under exactly the same experimental conditions, each with a total number of 1500 scans.

One main difference between the spectra in Figs. 10.7 and 10.9 is that in Fig. 10.7 only the protonated molecules AH and BH are observed, whereas in Fig. 10.9 both $A = \{AH, AD\}$ and $B = \{BH, BD\}$ contribute to the spectra. Two singlets $B_e = \{BH_e, BD_e\}$ and $B_f = \{BH_e, BD_e\}$ (see atom numbering in Fig. 10.3) are observed for the *s-cis* form B, indicating two inequivalent fluorine atom positions in this species, which is conform with the molecular structure. Again, the signals B_e and B_f do not depend on D. By contrast, the lineshape of the

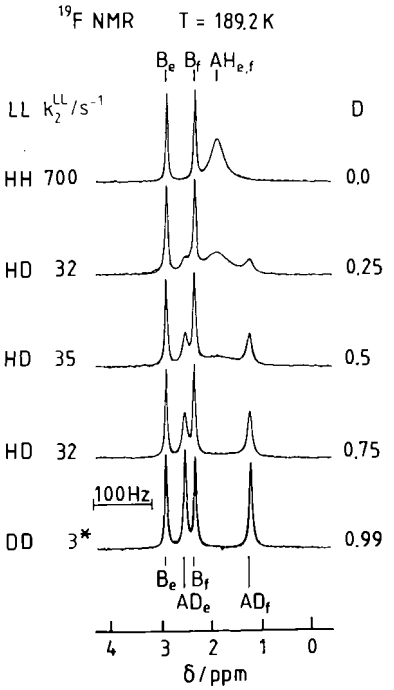

Fig. 10.9. Superposed experimental and calculated ^{19}F–{^{1}H}–NMR-spectra of 0.02 molar solutions of DFFA in THF as a function of the deuterium fraction D. For the explanation of the atom numbering see Fig. 10.2. The pseudo first order rate constants of the proton exchange are labeled as k_2^{LL}, LL = HH, HD, DD. In the fitting procedure k_2^{DD} was set constant to a value of $3\,s^{-1}$ (see Figs. 10.10 and 10.11); by non-linear regression analysis of all spectra the values $k_2^{HH} = 700\,s^{-1}$ and $k_2^{HD} = 33\,s^{-1}$ were obtained. The line width in absence of exchange $W_0 \approx 5$ Hz was obtained from the B_e and B_f signals. Reproduced with permission from Ref. [108]

fluorine signals of A depends strongly on the deuterium fraction D. Let us first take a look at the spectrum with D = 0.99. Two sharp signals AD_e and AD_f are observed which indicate two inequivalent fluorine positions in the AD molecule, as expected for a slow deuterium exchange. Now, at D = 0 one broadened coalesced fluorine signal AH_e, AH_f is observed, indicating that a fast process takes place between protonated AH molecules which renders the two inequivalent AH_e and AH_f fluorine atoms equivalent. In view of the molecular structure of DFFA and the dependence of this process on the deuterium fraction it must correspond to the intermolecular double proton transfer involving two AH molecules as observed in the previous section by ^{1}H, of the type shown in Fig. 10.3, where the proton exchange is associated to an intramolecular exchange of ^{19}F atoms.

Now, a very interesting phenomenon is observed at intermediate deuterium fractions: the fluorine atoms of the protonated AH and the deuterated AD molecules can be separated; they give rise to a **trio**: Whereas the outer two singlets of the **trio** stem from the AD_e and AD_f, the inner broad coalesced line stems from the AH_e, AH_f fluorine atoms. As D increases the latter signal becomes broader, indicating longer lifetimes of the mobile proton in AH. By contrast, the lifetime of the mobile deuteron in AD shortens as D increases, leading to a broadening of the outer two singlets. Note that the line intensities AH_e and

AH_f are determined by the concentration $C_A(1-D)/2$, whereas the line intensities AD_e and AD_f are given by $C_AD/2$.

The lineshape analysis of the spectra in Fig. 10.9 was performed using Eq. (6.22). Unfortunately, not all kinetic quantities $\tau^{-1}_{AHAH^*}(D)$, $\tau^{-1}_{AHAD}(D)$, $\tau^{-1}_{AHAD}(D)$, and $\tau^{-1}_{ADAD^*}(D)$ can be obtained at all values of D. This is clear because AD does not contribute to the line shape at $D=0$. The same is true for AH at $D=1$. Therefore, it was a great help to know from the ^1H spectra that $m=2$, i.e. that Eqs. (5.26)–(5.31) apply. In other words, the deuterium fraction dependent inverse life times in Eq. (6.22) could be replaced by the three pseudo first order rate constants k^{HH}, k^{HD}, and k^{DD} in the following way:

$$\tau^{-1}_{AHAH^*} = (1-D)\cdot k^{HH}, \quad \tau^{-1}_{AHAD} = D\cdot k^{HD}, \tag{10.2}$$

$$\tau^{-1}_{ADAH} = (1-D)\cdot k^{DH}, \quad \tau^{-1}_{ADAD^*} = D\cdot k^{DD}. \tag{10.3}$$

The value of $k^{HH} = 700\,s^{-1}$ was determined from the spectrum at $D=0$; this value concides well with the value obtained by ^1H NMR line shape analysis. Unfortunately, the value of $k^{DD} = 3\,s^{-1}$ was too small to induce a measurable line broadening. The latter value was, therefore, determined by the method of magnetization transfer in the rotating frame (see Sect. 2.4) between the lines AD_e and AD_f at $D=0.99$ as shown below. From the spectra in the intermediate D range we obtained then values of $k^{HD} = 33\,s^{-1}$ by non-linear least squares fit of the simulated to the experimental spectra. Again, W_0 was determined by simulation of the signals B_e and B_f.

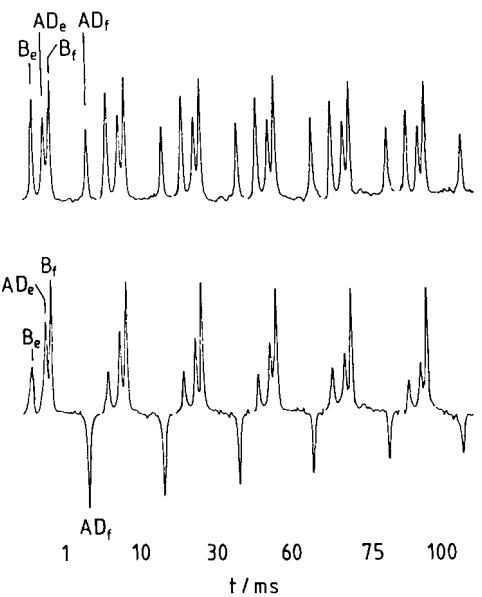

Fig. 10.10. ^{19}F-magnetization transfer experiments in the rotating frame of a 0.02 molar solution of DFFA in THF at a deuterium fraction of $D=0.99$ in the mobile proton sites. The carrier frequency was set to the position of the AD_f line. **Upper curves**: experiment (i) corresponding to a usual $T_{1\rho}$ experiment; **lower curves**: experiment (ii) with a delay $\tau = 1/(2\Delta\nu) =$ 4.2 ms between the first 90° pulse and the spin locking pulse. $\Delta\nu$ is the frequency difference between the signals AD_e and AD_f. B_e, B_f: non-exchanging, AD_e, AD_f: exchanging magnetizations. Repetition time 3.8 s, 4.2 μs 90° pulses, strength of the spin locking field $t_{180} = 165\,\mu s$. Reproduced with permission from Ref. [108]

The results of the magnetization transfer experiments are shown in Fig. 10.10. As described in Sect. 2.3 two sets of experiments were carried out. In the "parallel" experiment (i) the decay of the magnetizations AD_e and AD_f is solely governed by the longitudinal relaxation time in the rotating frame, (Eq. (2.20)):

$$M_{AD_f} = M_{AD_f}(t=0)\exp(-t/T_{1\rho}), \tag{10.4}$$

whereas in the "antiparallel" experiment (ii), (Eq. (2.21))

$$M_{AD_f} = M_{AD_f}(t=0)\exp(-t(2k_2^{DD} + T_{1\rho}^{-1})). \tag{10.5}$$

Since it was difficult to measure the line intensity of AD_e due to signal overlap, only the integrated intensities of AD_f were used to determine k_2^{DD} by non-linear least-squares fit of the data shown in Fig. 10.11.

The following full kinetic isotope effects at 189.2 K and a concentration of 0.02 mol l^{-1} were then obtained:

$$k_2^{HH}/k_2^{dd} = 233 \pm 20,\ k_2^{HH}/k_2^{HD} = 21 \pm 3 \text{ and } k_2^{HD}/k_2^{DD} = 11 \pm 2.$$

The kinetic HH/HD-isotope effect of 21 agrees well within the margin of error with the value of 19 ± 3 determined in the ^1H experiments. Note that the kinetic HH/DD isotope effect is the largest kinetic hydrogen/deuterium isotope effect measured so far by dynamic NMR spectroscopy. Note also that the rule of the geometric mean (RGM) would predict on the basis of the known HH/DD isotope effect for the HH/HD and the HD/DD isotope effects equal values of 15.

It was further shown [200] that the kinetic isotope effects of the proton exchange did not depend in a significant way on concentration, i.e. that equilibrium isotope effects of the dimerization of DFFA are absent. Thus, after determination of the equilibrium constants of dimerization it was possible to obtain the rate constants k_{A_2} of proton exchange in the cyclic dimer as a function of temperature. The Arrhenius diagram is shown in Fig. 10.12. By contrast to the intramolecular proton transfer systems large kinetic HD/DD isotope effects are observed. This has been interpreted with a concerted proton transfer process in the cyclic formamidine dimer [108] which has also been supported theoretically [44]. The deviation from the rule of the geometric mean value was attributed

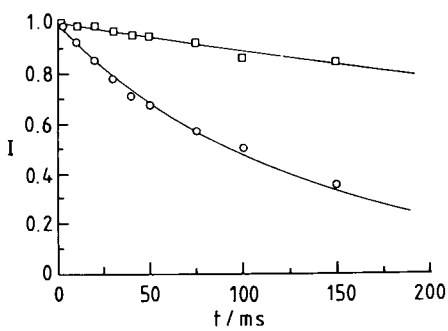

Fig. 10.11. Analysis of the data in Fig. 10.10 in terms of Eqs. (10.4) and (10.5). Parameters of the non-linear regression analysis: $T_{1\rho} = 808$ ms and $k_2^{DD} = 3.05\,s^{-1}$. Reproduced with permission from Ref. [108]

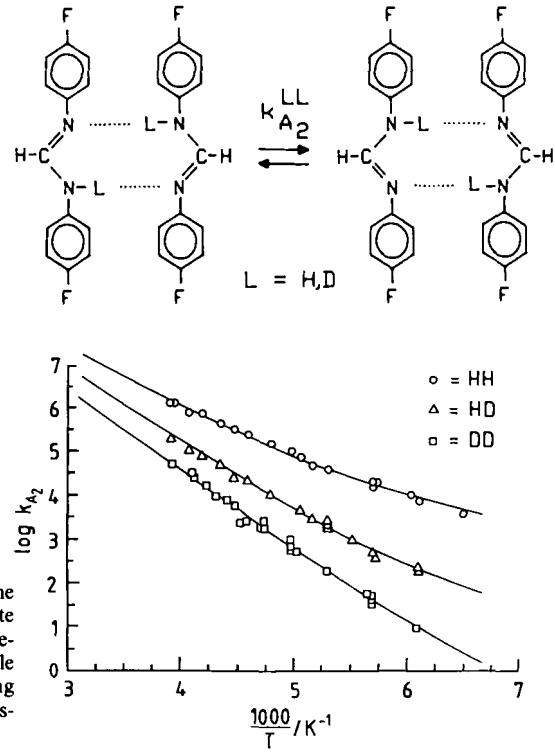

Fig. 10.12. Arrhenius diagram of the DFFA tautomerism in THF. The rate constants correspond to the unimolecular rate constants k_{A_2} of the double proton transfer in the dimer according to Fig. 10.3. Reproduced with permission from Ref. [200]

to tunneling [108]. The calculation of the Arrhenius curves in Fig. 10.12 was performed with a modified Bell model described in Refs. [106] and [200].

10.3 Exchange Between Different Sites: The System Acetic Acid/Methanol/Tetrahydrofuran

In this section an example of an intermolecular proton and deuteron exchange between two proton donors with different spin Hamiltonians is presented: the system acetic acid (AL)/methanol (BL)/tetrahydrofuran (THF). A 1:1 cyclic proton transfer between both molecules in THF shown in Fig. 10.13 was first established by ^{1}H NMR line shape analysis at a deuterium fraction of $D = 0$ in the mobile proton sites [94, 97]. Later, the number of protons transferred as well as the multiple kinetic hydrogen/deuterium isotope effects were studied by a combination of ^{1}H and ^{2}H NMR spectroscopy [102–106] as a function of temperature, concentration, and D; thus, an additional 2:1 proton exchange according to Fig. 10.13 was detected at higher concentrations of acetic acid.

In order to understand how the results of this study were obtained let us first have a look at the superposed experimental and calculated ^{1}H NMR spectra

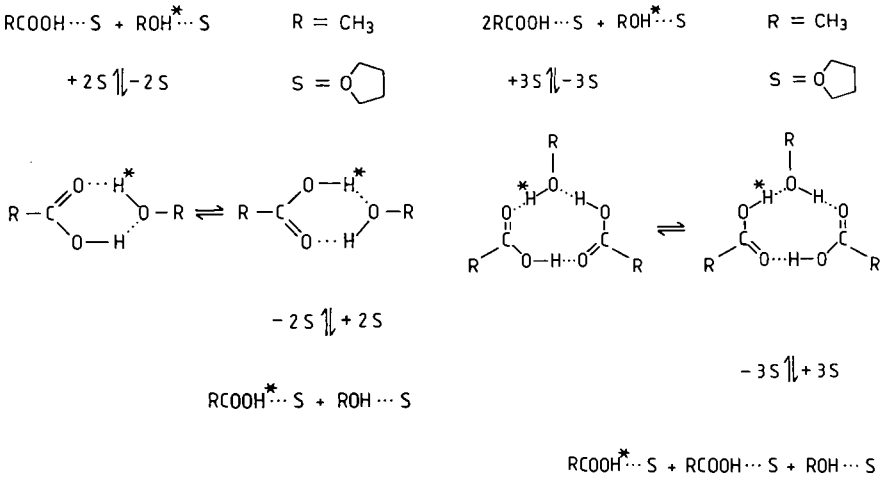

Fig. 10.13. Cyclic 1:1 (**left**) and 2:1 (**right**) proton transfer between acetic acid and methanol in THF; S ≡ THF. Reproduced with permission from Ref. [106]

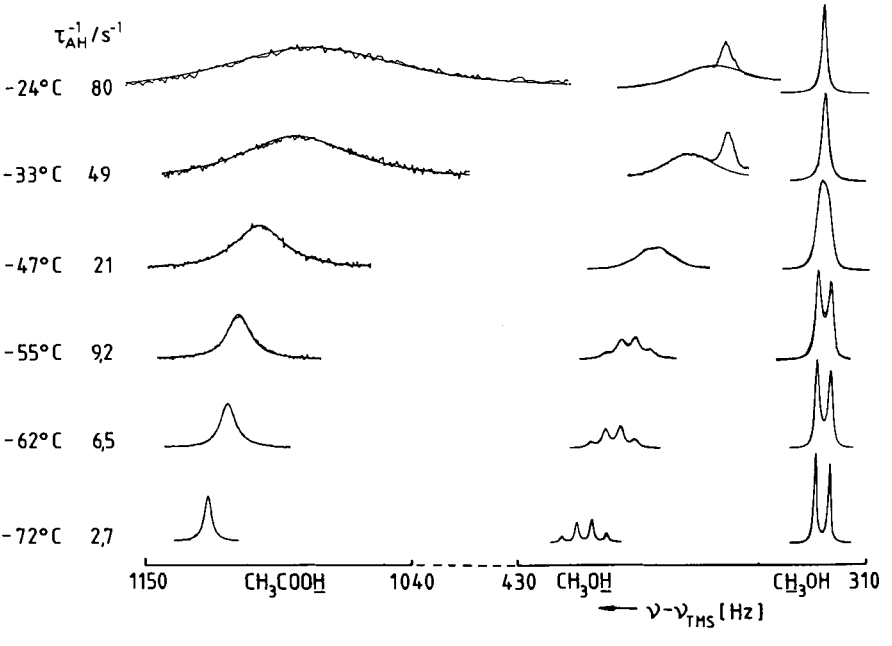

Fig. 10.14. Superposed experimental and calculated 100 MHz ^{1}H CW NMR spectra of a solution of 0.29 mol l^{-1} CH_3COOH(AH) and 0.8 mol L^{-1} CH_3OH(BH) in THF-d_8 as a function of temperature. The peak at 370 Hz arises from residual solvent protons. $\tau_{AH}^{-1} \equiv \tau_{AHBH}^{-1}$. The τ_{BHBH}^{-1} values were found to be zero. Reproduced with permission from Ref. [97]

of a solution of 0.19 mol l^{-1} CH_3COOH(AH) and of 0.8 mol l^{-1} CH_3(BH) in THF-d_8 shown in Fig. 10.14 as a function of temperature. At low temperatures the slow exchange range is reached where the COOH signal represents an exchange broadened singlet; the two signals of CH_3OH are those expected for an AB_3 spin system as found for pure methanol, i.e. a quartet for the OH and a doublet for the CH_3 group. From the simulation of these spectra using the exchange operator of Eq. (4.15) [94, 97] the inverse lifetimes $\tau_{AH}^{-1} = \tau_{AHBH}^{-1} = \tau_{BHAH}^{-1} C_B/C_A$, and τ_{BHBH}^{-1} could be obtained. C_A and C_B are the concentrations of the reactants. The values of τ_{AHAH}^{-1} characterizing the inverse lifetime of a carboxylic proton before the exchange with another carboxyl group occurs could not be obtained because this process does not modulate the spin Hamiltonian of the COOH proton, which is not coupled to a remote spin. It was found that the quantities τ_{BHBH}^{-1} were zero in pure samples [94, 97]; this means that within the errorlimits no proton jumps directly from one methanol molecule to another.

Because of the limited dynamic range of the NMR receiver all methyl groups in this system had to be deuterated in order to obtain exchange broadened NMR spectra in the region of the coalescence of the COOH and the OH signals [106]. The results are shown in Fig. 10.15 which contains on the right side the superposed experimental and calculated FT ^{1}H NMR spectra of a 0.4 molar 1:1 solution of CD_3COOH/CD_3OH/THF-d_8. The residual solvent signals were minimized by subtracting the spectra from those of the pure solvent recorded under the same conditions. Although this procedure leads to some artifacts at high field, they do not hinder the lineshape analysis. Thus, the spectra were easily calculated using Eq. (2.18).

In order to obtain the kinetic isotope effects ^{2}H NMR spectra of a mixture of 0.29 mol l^{-1} CH_3COOD and 0.19 mol l^{-1} CH_3OD in THF were recorded [106]. The superposed experimental and calculated spectra are shown in Fig. 10.15 on the left side. Since isotope effects on chemical shifts, measured in ppm, are small, $\delta_{COOH} - \delta_{OH} \cong \delta_{COOD} - \delta_{OD}$ to a good approximation. However, the frequency differences in Hz are related by $\nu_{COOH} - \nu_{OH} \cong \gamma_{^1H}/\gamma_{^2H}(\nu_{COOD} - \nu_{OD})$, with $\gamma_{^1H}\gamma_{^2H} = 6.51$. This means that the COOD and the OD signals coalesce at much smaller exchange rate constants than the COOH and the OH signals. Thus, the observation that the external aspect of both sets of spectra in Fig. 10.15 is similar signifies a large kinetic hydrogen/deuterium isotope effect.

These spectra and the kinetic isotope effects obtained so far do not yet indicate the rate law of the exchange or the number of protons transferred in the rate limiting step. Before performing experiments in a large concentration range an NMR proton inventory was performed which consisted of ^{1}H and ^{2}H NMR measurements as a function of the deuterium fraction D in the mobile proton sites at fixed concentrations and a fixed temperature of T = 298 K. The ^{2}H NMR results are shown in Fig. 10.16. The slow deuteron exchange range is reached at values of $D \approx 1$. As the deuterium content is lowered, the inverse deuteron life times increase. Coalescence of the signals is reached at about D = 0.2. Since for a single proton transfer reaction the deuterium life times

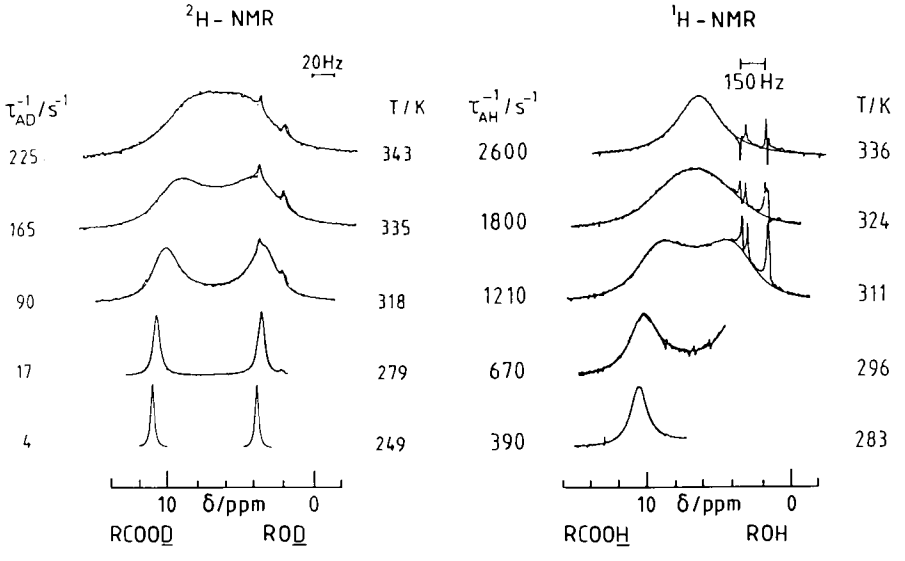

Fig. 10.15. Right: Superposed experimental and calculated ^{1}H 90.02-MHz FT NMR difference spectra of a solution of 0.4 mol L^{-1} CD_3COOH and 0.4 mol L^{-1} CH_3OH in THF-d_8 and of pure THF-d_8 at different temperatures using a 10-mm probe head (1000 scans, 60° pulses, 10-s repetition time, non-spinning sample). The sealed sample tube had a diameter of 8 mm, a height of 40 mm and was placed in a 10 mm NMR tube. The gas phase in the sample was about 20% of the total sample volume. The small sharp peaks arise from the residual aliphatic protons of the solvent and the solutes. The calculations were performed using Eq. (2.18). **Left**: Superposed experimental and calculated ^{2}H 13.82-MHz FT NMR spectra of a solution of 0.29 mol L^{-1} CH_3COOD and 0.29 mol L^{-1} CH_3OD in THF at different temperatures. The deuterium fraction of the exchangeable protons was D = 0.99. The small two sharp lines arise from the natural deuterium content of THF. Reproduced with permission from Ref. [106]

should be independent of D according to Fig. 5.1, this observation is proof of a multiple proton transfer reaction. On the other hand, the proton exchange rates measured by ^{1}H NMR spectroscopy decrease with increasing deuterium fraction. The resulting NMR proton inventory plot is shown in Fig. 10.17. Note that it was possible to obtain both $\tau_{AH}^{-1} = \tau_{AHBH}^{-1}$ (filled circles) and $\tau_{AD}^{-1} = \tau_{ADBD}^{-1}$ (open circles) from successive ^{1}H and ^{2}H NMR measurements on the same samples of CH_3COOL/CH_3OL in THF at D = 0.5 and 0.7. Thus, within a given sample the protons exchange faster than the deuterons! In first order, straight lines for τ_{AH}^{-1} and τ_{AD}^{-1} vs. D in Fig. 10.17 indicate that m = 2 according to Eqs. (5.32) and (5.33). This signifies the presence of the cyclic 1:1 process depicted in Fig. 10.13. Moreover, the intercepts $\tau_{AH}^{-1}(D=0)$ and $\tau_{AD}^{-1}(D=1)$ are approximately equal and can, therefore, be identified with the pseudo first order rate constant of the 1:1 process k^{HD} in Fig. 10.13. A closer look shows that $\tau_{AD}^{-1}(D=0) > \tau_{AH}^{-1}(D=1)$. This result can be explained with superposed double and triple proton transfers according to Fig. 10.13. For this case, the predicted dependence of the proton and deuteron exchange rates as a function of D was derived in Eqs. (5.64) and (5.65). Then, according to Eq. (5.65), $\tau_{AD}^{-1}(D=0)$ is strongly influenced by k^{HHD}, which is larger than k^{HDD}. Since $\tau_{AH}^{-1}(D=1)$ is

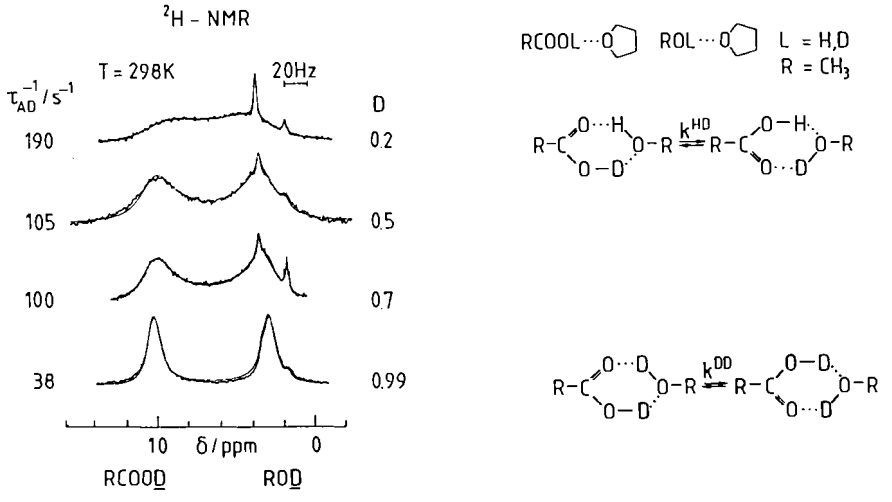

Fig. 10.16. Superposed experimental and calculated ^{2}H 13.82-MHz FT NMR spectra of solutions of 0.3 mol L^{-1} CH_3COOL and 0.3 mol L^{-1} CH_3OL (L = H, D) in THF at 298 K as a function of the deuterium fraction D. The calculations were performed using Eq. (2.18). Reproduced with permission from Ref. [106].

influenced by the latter the result that $\tau_{AD}^{-1}(D=0) > \tau_{AH}^{-1}(D=1)$ is understandable. As a consequence, the solid lines in Fig. 10.17 were calculated using Eqs. (5.64) and (5.65). Further concentration dependent experiments supported this interpretation. Actually, it was found that the pseudo first order rate constants increased linearly with the acetic concentration. This result was consistent with the previous finding of absence of methanol self exchange in acetic

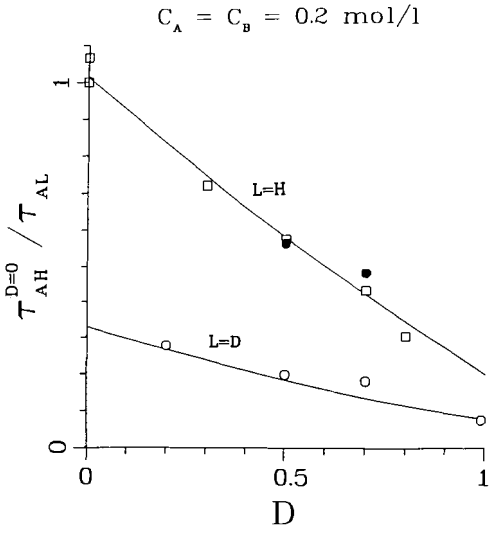

Fig. 10.17. Experimental NMR proton inventory plot at 298 K and a concentration of 0.2 mol L^{-1} for the system acetic acid/methanol/THF. (□): data obtained by ^{1}H NMR of the system $CD_3COOL/CD_3OL/THF\text{-}d_8$; (●): data obtained by ^{1}H NMR of the system $CH_3COOL/CH_3OL/THF$ (selective pulses on the COOH signal); (○): data obtained by ^{2}H NMR of the system $CH_3COOL/CH_3OL/THF$. The curves were calculated according to Eqs. (5.64) and (5.65) using the known rate constants and a value of k^{HDD} = 634 L mol^{-2} s^{-2} calculated from k^{DDD} using the RGM. Reproduced with permission from Ref. [106]

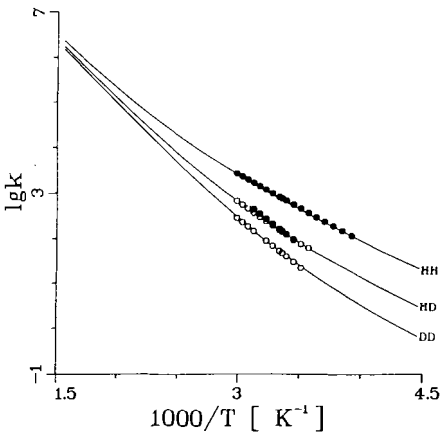

Fig. 10.18. Arrhenius curves of the intermolecular double HH, HD, and DD exchange involving one molecule each of acetic acid and methanol in tetrahydrofuran. The three curves were calculated according to a tunnel model described in Ref. [106] using only four parameters. (●): values obtained by ^{1}H NMR spectroscopy; (○): values obtained by ^{2}H NMR spectroscopy. Reproduced with permission from Ref. [106]

acid/methanol/THF mixtures, i.e. with the exchange mechanism shown in Fig. 10.13.

From the analysis of all kinetic data the following multiple kinetic isotope effects of the processes shown in Fig. 10.13 could be derived:

$$(k^{HH}/k^{DD})_{298K} = 15.5 \pm 4.4,\ (k^{HH}/k^{HD})_{298K} = 5.1 \pm 1.4,$$
$$(k^{HD}/k^{DD})_{298K} = 3.1 \pm 0.9, \tag{10.6}$$

$$(k^{HHH}/k^{DDD})_{298K} = 11.5 \pm 2.7,\ (k^{HHH}/k^{HHD})_{298K} = 2.1 \pm 0.5. \tag{10.7}$$

As in the case of the formamidines these data can not easily be explained with a stepwise exchange mechanism. The deviation from the geometric means values were interpreted in terms of a model described in Ref. [106]. With this model the Arrhenius curves of the 1:1 exchange (Fig. 10.18) and of the 2:1 exchange could well be reproduced [106].

11 NMR Studies of Kinetic Hydrogen/Deuterium Isotope Effects in the Solid State

In the previous sections we have discussed the possibilities of dynamic NMR spectroscopy to elucidate kinetic hydrogen/deuterium isotope effects of reversible chemical reactions in the liquid state. As discussed already in Sects. 1 and 3, dynamic NMR spectroscopy is also able to follow proton and deuteron transfer dynamics in the solid state. The easiest way to do so is to take advantage of a modulation of chemical shifts of remote spin 1/2 nuclei by the processes studied and to perform high resolution solid state CPMAS NMR measurements on microcrystalline powders or amorphous solids. In this method, proposed

by Schaefer and Stejskal [154], all orientation dependent spin interactions are removed by ^1H decoupling and magic angle spinning (MAS) [155–157]. The sensitivity is increased by ^1H–X cross polarization (CP) [152, 153]. Thus, CPMAS NMR spectra of e.g. ^{13}C or ^{15}N spins are comparable to those obtained by liquid state NMR spectroscopy. As a consequence magnetization transfer and exchange broadening phenomena can be observed in the presence of dynamic processes which modulate the isotropic chemical shifts [162–179]. In the nomenclature defined above such experiments correspond to remote spin studies and all possibilities to determine kinetic isotope effects by looking at remote spins apply. Note that other solid state interactions may also be used [158–161, 180–189] in order to follow the dynamics of proton transfers; generally, such studies require, however, single crystals and the determination of kinetic isotope effects is not easy.

In this section we do not intend to give a comprehensive overview of dynamic CPMAS spectroscopy of solid state proton transfers. Instead, we would like to demonstrate how kinetic hydrogen/deuterium isotope effects can be measured using this method. In addition, other solid state NMR techniques will only be discussed briefly.

11.1 ^{15}N CPMAS NMR Studies of Kinetic Isotope Effects of Hydrogen Transfer Between Nitrogen Atoms

Usually, in CPMAS studies of organic compounds natural abundance ^{13}C atoms are monitored [154, 161, 162]. Thus, several solid state hydrogen transfer systems have been studied by natural abundance ^{13}C CPMAS NMR [163, 166, 175–178]. However, with the exception of hydride transfers in carbonium ions [166], carbon atoms are not directly involved in hydrogen transfers and their NMR lines may not always be sensitive to these processes. Therefore, nitrogen NMR is a more suitable method for organic dyes, where nitrogen atoms often act as proton donors or acceptors. Because of the quadrupole moment of the ^{14}N nucleus, it is, at present, necessary to enrich the molecules studied with the less abundant ^{15}N isotope. Using the ^{15}N CPMAS technique of ^{15}N enriched compounds fast proton tautomerism in a number of organic crystalline dyes was detected [164, 167–174]. In this section we show two examples of the determination of kinetic hydrogen/deuterium isotope effects using this method.

11.1.1 Intramolecular Proton and Deuteron Transfer in Solid meso-Tetratolylporphyrin

As an example for an intramolecular proton transfer reaction let us consider the tautomerism of *meso*-tetraarylporphyrins. As already mentioned in Sects 2 and 9.3, porphyrins are subject in the liquid state to a degenerate tautomerism according to Figs. 2.2 and 9.11. This tautomerism also takes place in the solid

state. Generally, the two tautomers are no more degenerate by contrast to the liquid state because of a reduction of the molecular site symmetry [167]. In special cases, e.g. porphyrin [171, 176] and *meso*-tetratolylporphyrin (TTP) [167], it was found, however, that the two tautomers are quasi-degenerate. This is demonstrated in Fig. 11.1 on the left side which shows the variable temperature ^{15}N CPMAS NMR spectra of ^{15}N enriched polycrystalline TTP, at a deuterium fraction of $D = 0$ and $D \cong 1$. As expected from the liquid state studies, two singlets for the protonated and the non-protonated nitrogen atoms are obtained at low temperature which indicates that the proton migration is slow on the NMR time scale. In the fast exchange regime one coalesced line is observed

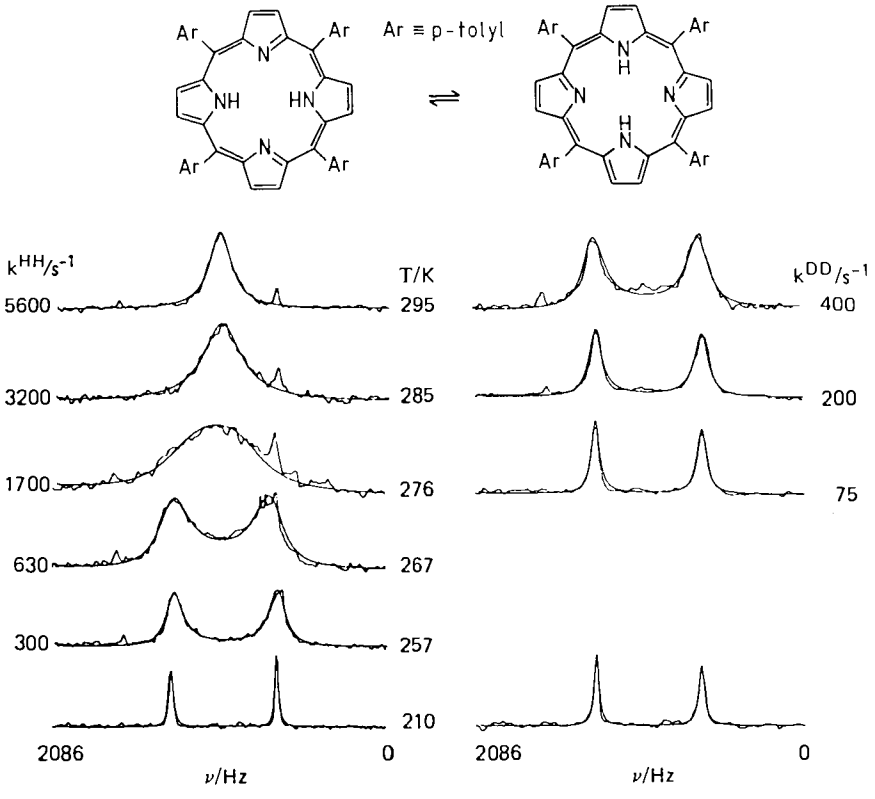

Fig. 11.1. Superposed experimental (6.082 MHz) and calculated ^{15}N CPMAS NMR spectra of 95% ^{15}N-enriched *meso*-tetratolylporphyrin (TTP) as a function of temperature. The calculations were performed using Eq. (2.18). **Left**: deuterium fraction in the mobile proton sites $D = 0$ (reproduced with permission from Ref. [167]); **right**: deuterium fraction in the mobile proton sites $D = 1$ (HH Limbach, CS Yannoni, unpublished). 10 Hz line broadening, 8000 Hz sweep width, 1.2 s repetition time, 9 μs ^1H-$\pi/2$ pulses, quadature detection, 25000 scans on the average; reference, external $^{15}NH_4NO_3$. The line width in the absence of exchange was taken from the spectrum at 210 K. The equilibrium constant of the tautomerism was assumed to be unity. k^{LL} is the LL = HH, DD migration rate constant. The sharp small high-field line stems from the NH signal of a low-level impurity of nonexchanging meso-tetratolylchlorin, a byproduct of the synthesis

indicating equivalent nitrogen atoms with an average proton density 1/2 within the NMR timescale. The lineshape analysis was carried out using Eq. (2.18) with an equilibrium constant of $K = k_{12}/k_{21} = 1$. The rate constants observed are very close to those obtained for the liquid solution [167].

Figure 11.1 shows on the right side what happens when the compound is deuterated in the mobile proton sites. The kinetic HH/DD isotope effect is manifest in view of the observation that at room temperature the slow exchange regime is observed. There is an additional line broadening of the high-field ^{15}N signal for the ^{15}N atom bound to deuterium. This broadening arises both from small non-averaged dipolar coupling with deuterium, which is not averaged by MAS [201–204] because of the quadrupole moment of ^{2}H, and from a nonresolved scalar $^{2}H-^{15}N$ coupling. These effects were taken into account by using a larger value of W_0, the line width in the absence of exchange, for the simulation of this signal. Unfortunately, the rate constants of the HD reaction in the solid state have not yet been determined via ^{15}N CPMAS NMR spectroscopy. One can expect that such measurements will be possible in the future by lowering the deuterium fractions in the mobile proton sites. In such studies one has to take into account that the ^{15}N signal intensities of protonated nitrogen are enhanced as compared to deuterated ^{15}N atoms, due to different $^{1}H-^{15}N$ cross polarization dynamics.

Since lineshape analysis yields unsatisfactory results in the slow exchange regime polarization transfer experiments in the rotating and the laboratory frame were performed in order to obtain kinetic isotope effects at low temperatures [164]. Here, attention had to be paid to the possibility that polarization transfer between dipolar coupled spins can also arise from "spin diffusion".

The kinetic HH/DD isotope effect found here for the solid state is similar to that observed for the tautomerism of TPP in the liquid state [124]. Thus, in the case of TTP liquid/solid state effects on the tautomerism cannot be observed. This result is very important when combining kinetic results obtained by laser methods [141] on porphyrin in solid hexane and data obtained by dynamic liquid state NMR spectroscopy.

11.1.2 Intermolecular Triple Proton and Deuteron Transfer in Solid Dimethylpyrazole

As an example of an intermolecular proton transfer we discuss in this section the ^{15}N CPMAS spectra of ^{15}N enriched solid 3,5-dimethylpyrazole (DMP) which forms in the solid state a cyclic trimer [178,179] (Fig. 11.2). In this trimer a moderately fast proton transfer takes place. A superposition of the experimental and calculated ^{15}N CPMAS NMR spectra of DMP are shown in Fig. 11.3 for deuterium fractions $D = 0$ and 1 in the mobile proton sites. Let us first discuss the spectra at $D = 0$. At 223 K two sharp lines are observed (Fig. 11.3a) indicating the presence of two types of nitrogen atom, one

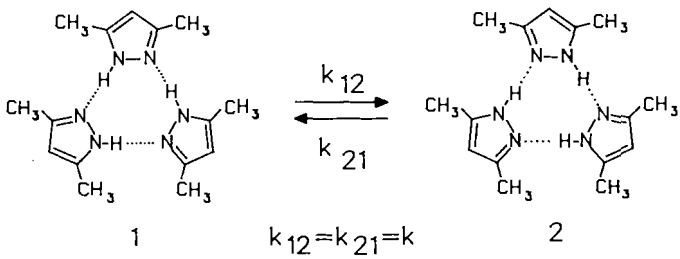

Fig. 11.2. The tautomerism of 3,5-dimethylpyrazole (DMP) in the solid state where the molecule forms cyclic trimers. Reproduced with permission from Ref. [179]

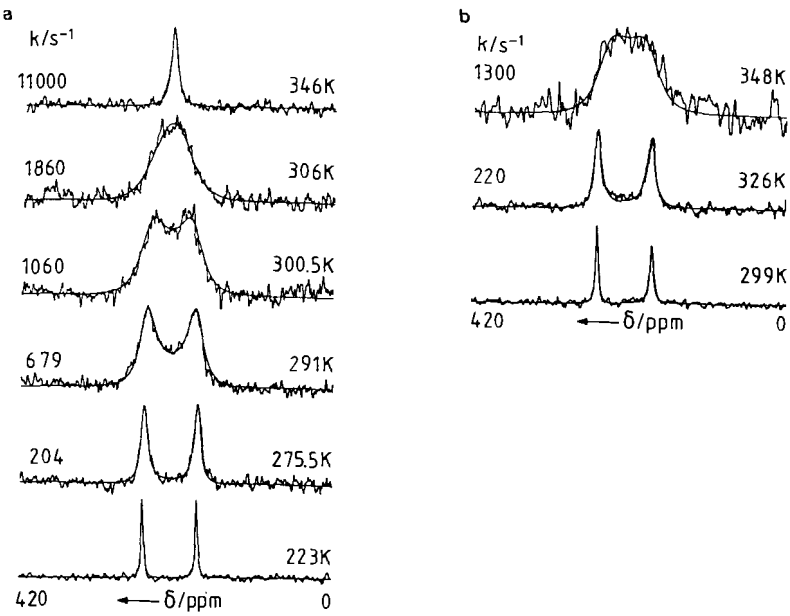

Fig. 11.3a, b. ^{15}NCPMAS NMR spectra of 95% ^{15}N enriched 3,5-dimethylpyrazole (DMP) at 9.12 MHz as a function of temperature. (a) deuterium fraction in the mobile proton sites D = 0; (b) deuterium fraction in the mobile proton sites D = 1. Reference: external $^{15}NH_4Cl$. The spectra were calculated using Eq. (2.18). Parameters of the calculation: $\nu_{NH} = 180$ ppm; $\nu_N = 254$ ppm (at 9.12 MHz), i.e. $\Delta\nu = 544$ Hz; a: $W_0 = 35$ Hz including 15 Hz line broadening; b: $W_{0_{ND}} = 54$ Hz and $W_{0_N} = 55$ Hz. k is the rate constant. Rotation frequencies between 2.6 and 3.5 kHz. Reproduced with permission from Ref. [179]

protonated (N(1)) and one non-protonated (N(2)). As the temperature is raised, the two lines broaden and coalesce into one sharp line at 346 K. The fact that the line appears in the center of the two low temperature singlets indicates again that all nitrogen atoms have an equal proton density of 0.5, i.e. that the equilibrium constant $K_{12} \cong 1$ within the margin of error of ^{15}N CPMAS NMR spectroscopy. The rate constants obtained can be represented by the Arrhenius

equation

$$k_{12}^{H} \approx A_{12} \exp(-E_{a_{12}}/RT), \quad A_{12} \approx 10^{11}, \quad E_{a_{12}} \approx 45.7\,\text{kJ mol}^{-1}. \quad (11.1)$$

Because of the relatively small temperature range covered so far the activation parameters in Eq. (11.1) might be subject to changes when rate constants can be obtained in the future over a larger temperature range.

At $D \approx 1$ the proton transfer rates are drastically reduced as shown in Fig. 11.3b. Thus, at room temperature the slow exchange regime is realized. Whereas the width of the low field line is almost as sharp as in the 223 K spectrum of DMP at $D = 0$, the high field line is again broadened by residual scalar and dipolar coupling with deuterium. By line shape analysis a kinetic hydrogen/deuterium isotope effect of about 8 at 347 K is obtained. One can estimate that at 298 K the rate of deuteron exchange cannot exceed a value of $50\,s^{-1}$. This leads to a kinetic HHH/DDD isotope effect of $\geqslant 20$ at 298 K.

Again, it has not yet been possible to study the mixed rate constants k^{HHD} and k^{HDD} at intermediate D values. Note that hydrogen bond exchange and diffusion is extremely slow in the solid state by contrast to the liquid state. Therefore, the ^{15}N CPMAS NMR lineshape of DMP at intermediate D values is a static superposition of line shapes arising from the isotopic HHH, HHD, HDD, and DDD species. The mobile protons jump then always between the same nitrogen atoms, a situation which is equal to the one encountered in intramolecular proton transfer systems in liquid solution.

Although the value of $10^{11}\,s^{-1}$ found here for the frequency factor of this process might be subject to changes when kinetic data are obtained over a larger temperature range, one can already say that this value indicates the absence of a large negative activation entropy. This finding is expected for an intramolecular reaction. Future experiments will have to establish the origin of the large kinetic isotope effect on the solid state tautomerism of DMP.

11.2 The Use of Orientation Dependent Nuclear Spin Interactions for the Study of Kinetic Hydrogen/Deuterium Isotope Effects

There are a number of fast proton transfer processes which do not lead to a modulation of isotropic chemical shifts in the solid state. In these cases, it is not possible to obtain proton transfer rates by the CPMAS technique. As an example, consider the tautomerism of carboxylic acid dimers shown in Fig. 11.4. However, as discussed in Sect. 3, in the solid state there are orientation dependent interactions which are modulated in the presence of molecular motion. Among these are dipolar coupling, the nuclear quadrupole interaction and the chemical shift anisotropy. The first two interactions have been used in order to study the dynamics of proton and deuterium transfer in single crystals of carboxylic acids [180–189] because both the dipolar interaction between the

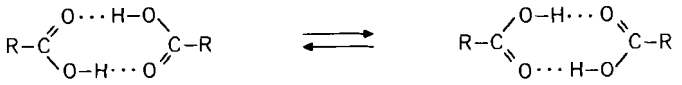

Fig. 11.4. Double proton transfer in carboxylic acid dimers

two mobile protons as well as the quadrupole interaction of the mobile deuterons are modulated when the jump processes occur.

Unfortunately, because of a reduction of the molecular site symmetry in the solid state the two tautomers in Fig. 11.4 have slightly different energies. Therefore, at low temperatures where one could hope to "freeze out" the exchange process on the NMR timescale only the energetically favored tautomer is populated and dynamic line broadening does not occur. Therefore, rate constants could not directly be obtained by lineshape analysis. However, as has been shown by Graf et al. [180], the double proton transfer provides an efficient longitudinal relaxation mechanism for the mobile protons in carboxylic acids. Thus, by measuring T_1 of the mobile protons of benzoic acid single crystals it has been possible to determine rate constants k^{HH} of the carboxylic acid tautomerism as a function of temperature. In a similar way, rate constants k^{DD} of the deuteron tautomerism of carboxylic acid dimers have been measured where advantage of the quadrupole interaction of the ^2H isotope was taken into account [180–186]. One can show that these different methods can be combined in order to obtain the full kinetic HH/HD/DD isotope effects of the carboxylic acid tautomerism [206].

12 Discussion of Kinetic Isotope Effects

We have described strategies to measure kinetic hydrogen/deuterium isotope effects of multiple intra- and intermolecular proton transfer reactions by dynamic NMR spectroscopy, including lineshape analysis and polarization transfer experiments in the liquid and the solid state. In such studies either mobile protons or deuterons or remote spins such as immobile protons or heavy atoms are monitored whose spin Hamiltonians are modulated by the exchange. In order to detect the kinetic isotope effects as well as the number of protons in flight in the rate limiting step of the processes studied dynamic NMR experiments are performed as a function of the deuterium fraction in the mobile proton sites. Such experiments are called "proton inventories". The theory of exchange broadened NMR lineshapes in connection with the proton inventory technique has been described in Sects. 2–6. Examples for this technique coming from the field of intra- and intermolecular proton transfer reactions in the liquid and the solid state were given in Sects. 9–11, after the experimental Sects. 7 and 8.

In the case of pure CH_3OH and CH_3OD evidence for an ionic proton exchange mechanism was obtained where the ionic catalysts $CH_3OH_2^+$ and CH_3O^- are created by autoprotolysis of the solvent. The apparent kinetic

isotope effect is then also influenced by the equilibrium isotope effect of the autoprotolysis [89]. Such ionic proton transfer processes can be suppressed when proton donors are studied in organic solvents. Thus, for proton exchange between acetic acid and methanol in tetrahydrofuran [105, 106] the number of protons transported was measured and multiple kinetic HH/HD/DD isotope effects were obtained for these reactions. This was possible because the chemical shifts of the exchanging protons in the two environments are different. By contrast, the determination of kinetic isotope effects of proton self exchange reactions where the chemical shifts of the exchanging protons is not modulated is more difficult. Here, one has to take advantage of the modulation of the scalar spin–spin coupling of the mobile hydrogen isotopes to remote spins, e.g. scalar $^{1}H-^{15}N$ coupling and/or the modulation of chemical shifts of remote spins by the exchange. An example where this concept was successfully applied is the double proton transfer between formamidine molecules (Fig. 10.3) dissolved in tetrahydrofuran (Sect. 10.2 and Refs. [107, 108]). Concentration dependent studies even allowed the determination of rate constants of exchange in the cyclic dimer which are no more affected by the equilibrium constants of the preequilibrium. In addition, kinetic HH/HD/DD isotope effects were obtained for several intramolecular double proton transfer reactions in azophenine [127], oxalamidine [120, 129] and porphyrines [105, 124–126] which were labeled with ^{15}N for this purpose.

Although the number of systems where multiple kinetic isotope effects have been studied so far is not yet very large, in the following the question will be discussed what the observed kinetic isotope effects determined can tell us about the reaction mechanisms, without going into different theories of multiple kinetic isotope effects.

The kinetic HH/HD/DD isotope effects of symmetric intramolecular double proton transfer reactions determined so far heavily violate the so called "rule of the geometric mean" [43] which states that there are two primary kinetic isotope effects P_1 and P_2 of similar size:

$$P_1 = k^{HH}/k^{HD} \cong P_2 = k^{HD}/k^{DD}. \tag{12.1}$$

In fact, for the azophenine, oxalamidine, and the porphyrin tautomerism (Sect. 9) it is found that the rate constants of the different isotopic reactions are related by

$$k^{HH} \gg k^{HD} \cong k^{DD}. \tag{12.2}$$

Furthermore, in the case of the oxalamidine tautomerism a strong solvent dependence of the rate constants was observed [129] indicating a highly polar transition state, as expected for a stepwise proton transfer via a zwitterionic intermediate and transition states where one proton is bound and the other in flight as indicated Fig. 9.7. Thus, it is clear that these reactions can not be characterized by two but only by one primary kinetic isotope effect. The substitution of the bound proton by deuterium contributes then only a small secondary isotope effect S to the reaction rates. Actually, for degenerate double

hydrogen transfer reactions the following equations have been derived without making any assumptions concerning an over barrier or a tunneling pathway [127]:

$$\frac{k^{HD}}{k^{DD}} = \frac{2}{S^{-1} + P^{-1}} \quad \text{and} \quad \frac{k^{HH}}{k^{DD}} = PS. \tag{12.3}$$

Since S is of the order of 1 and $P \gg 1$ Eq. (12.3) represents a very large deviation from the RGM since in this case $k^{HH}/k^{HD} \approx P$ and $k^{HD}/k^{DD} \approx 2$. The Arrhenius curves of the intramolecular HH reactions (e.g. Fig. 9.5) can easily be calculated in terms of Eq. (12.3). These findings give experimental evidence for stepwise reaction pathways in the case of the azophenine and the oxalamidine tautomerism. In the azophenine case the kinetic data were consistent with a reaction over the barrier and the kinetic isotope effects were interpreted in terms of Eq. (12.3) with values of $P = 7.2$, $S = 0.78$ at 298 K [127]. Novel independent theoretical [140–142] and experimental [123–125, 141] studies favor also a stepwise mechanism for the tautomerism of porphyrines, i.e. an interpretation of the kinetic HH/HD/DD isotope effects in terms of Eq. (12.3). Further information on the mechanism of the porphyrin tautomerism comes from a comparison of the rates of the porphyrin tautomerism in a very wide temperature range. Deviations from a non-Arrhenius behavior at low temperatures [125, 141] give then evidence for a thermally activated single proton tunneling mechanism in this temperature range.

The kinetic isotope effects of intermolecular symmetric double proton transfers differ in a significant way from the intramolecular proton transfers. In the intermolecular case the rule of the geometric mean (Eq. (12.1)) is much better fulfilled—although small deviations were still observed—indicating a more or less concerted double proton transfer mechanism. Thus, Eq. (12.3) is not able to accommodate neither the acetic acid/methanol nor the formamidine data. E.g., for the formamidines a kinetic HH/DD isotope effect of 233 is found at 189.2 K and the partial kinetic HH/HD and HD/DD isotope effects are 21 and 11. The rule of the geometric mean (RGM) would predict for both quantities equal values of 15. Note that the value of 233 is the largest kinetic hydrogen/deuterium isotope effect found so far by dynamic NMR spectroscopy, using a combination of lineshape analysis and polarization transfer methods. In the case of the double proton transfer between acetic acid and methanol it was found that $k^{HH}/k^{HD} \approx 5$ and $k^{HD}/k^{DD} \approx 3$ at 298 K [105, 106]. It is clear that these values are not consistent with a stepwise double proton transfer. This means that in the intermolecular case both protons contribute to the kinetic isotope effects. Therefore, it is understandable that the overall kinetic HH/DD isotope effects are larger in intermolecular than in intramolecular double proton transfer reactions. The largest value found at 298 K by NMR is the kinetic HHH/DDD isotope effect of the intermolecular triple proton transfer process in 3,5-dimethylpryazole (Fig. 11.2). For the formamidine reaction evidence for a concerted proton transfer [108] is

supported by ab initio calculations [144]. How can one then rationalize the small deviations from the RGM in the case of intermolecular exchange reactions?

In the case of the systems formamidine/THF and acetic acid/methanol/THF these deviations could be interpreted in terms of thermally activated tunneling assuming a concerted proton motion. Such deviations from the RGM in the presence of tunneling are well understood on theoretical grounds [105, 106]. The deviations may arise because tunneling enhances the reaction rates especially of the light hydrogen isotopes. Tunneling also induces a curvature of the Arrhenius curves in a wide temperature range. This is demonstrated in the calculated Arrhenius curves of the formamidine and the acetic acid/methanol tautomerism shown in Figs. 10.12 and 10.18. These curves were calculated for a modified one-dimensional Bell-tunneling model [106]. Since the concave curvatures of the calculated Arrhenius curves is not easily detected experimentally the deviation of the HH/HD/DD isotope effects from the RGM in the case of concerted double degenerate proton transfer reactions may be taken as an additional criterion for tunneling.

Let us try now to give a qualitative explanation for the reaction pathways of intra- and intermolecular double proton transfer systems. This explanation is based on the observation that intramolecular proton transfer systems such as porphyrin and azophenine lack the usual flexibility of hydrogen bonded systems, i.e. the usual low frequency hydrogen bond stretching vibration [21] which modulates the hydrogen bond distance. Thus, the molecular frame of heavy atoms in these compounds is relatively rigid and a high energy would be required to reduce the hydrogen bond distance in such systems. This feature is expressed at the bottom of Fig. 12.1 by an outer square which schematically represents the molecular frame. It is understandable that it costs too much energy to break the bonds of both protons to their neighboring heavy atoms at the same time, and the proton transfer will be stepwise. Note that proton tunneling in this case will always require a minimum energy of activation corresponding to the energy difference between the intermediate and the initial state.

By contrast, the presence of low frequency hydrogen bond stretching vibrations in the flexible intermolecular proton transfer systems allows a comparatively easy compression of the hydrogen bond as schematically shown in the model of Fig. 12.1 top. This model has been used for the calculation of the Arrhenius curves of the proton transfer between acetic acid and methanol [105, 106]. In this case the hydrogen bond lengths are variable, i.e. the energy of activation of the proton transfer is pooled into the hydrogen bond stretching vibration which shortens the hydrogen bond length. A consequence of the shorter bond length is a smaller barrier for the proton transfer. At extreme short hydrogen bond lengths the barrier for proton transfer vanishes and, therefore, the difference between a stepwise and a concerted proton transfer mechanism. The imaginary frequency required for a transition state corresponds then to the hydrogen bond stretching rather than to the AH-stretching

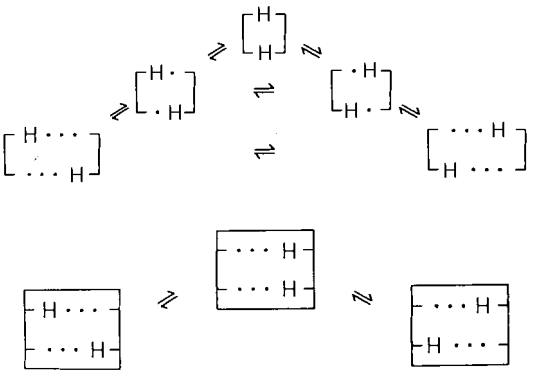

Fig. 12.1. Bottom: Stepwise double proton transfer in the case of a fixed molecular frame of heavy atoms. Top: Double proton transfer in the case of variable hydrogen bond lengths according to a model proposed in Ref. [106]. For further explanation see text. Reproduced with permission from Ref. [108]

vibrations. Now, it is well known that the latter are shifted to lower frequencies when the hydrogen bond distance is shortened [22]. Therefore, there will be a considerable loss of zero point energy of both vibrations in the highly compressed transition state and the RGM will be fulfilled at high temperatures. At lower temperatures the transfer may occur by tunneling leading to a violation of the RGM at low temperatures, as has been proposed previously [105, 106]. Thus, for the intermolecular proton transfer systems a reaction mechanism according to Fig. 12.1 top has been proposed [108]. Note that one might find intermolecular proton transfer systems with rigid hydrogen bond distances and intramolecular proton transfer systems with flexible hydrogen bonds which could lead to an inverse behavior of kinetic isotope effects.

13 Conclusions

In this review it has been shown that kinetic hydrogen/deuterium isotope effects of fast intra- and intermolecular proton transfer reactions in liquids and solids can today be determined using advanced methods of dynamic NMR spectroscopy. Thus, new insights have been obtained which could influence future experimental and theoretical development of the physics and chemistry of isotope effects. A theoretical framework has been given which could guide future research. So far, the method has mostly be applied to small organic molecules dissolved in liquid aprotic solvents where it is very difficult to obtain kinetic isotope effects with other methods.

One might ask now whether there are additional fields where dynamic NMR spectroscopy in the presence of isotope effects might be important. So far, only proton transfer reactions between nitrogen and oxygen atoms have been studied. Recent experiments show that also hydrogen transfers between carbon atoms can also be studied by NMR [207] as well as the corresponding kinetic hydrogen/deuterium isotope effects [208]. Proton, hydrogen and hydride

transfer reactions also play a role in metallorganic chemistry where they are related to the problems of homogeneous catalysis. Such reactions can be followed by dynamic NMR spectroscopy; thus, NMR studies of kinetic hydrogen/deuterium isotope effects might also be useful for a better understanding of inorganic reaction mechanism in the future. NMR spectroscopy in one and two dimensions has also contributed significantly in the past to the study of biologically important molecules, such as nucleic acids, proteins, and enzymes. So far, the scope of these studies was mostly the elucidation of the structure of the biomolecules. Since interesting insights into the mechanisms of enzyme reactions have been obtained from conventional studies of kinetic hydrogen/deuterium isotope effects of enzyme reactions in H_2O/D_2O mixtures [43], one can anticipate that dynamic NMR experiments as a function of the deuterium fractions in the mobile proton sites will also contribute to an understanding of the dynamics of enzyme reactions in the future.

Thirdly, as has been shown in Sect. 11, the whole potential of NMR in the study of kinetic isotope effects of proton transfer reactions in the solid state has not yet been fully developed and future efforts in this direction can be anticipated. Such investigations are especially important because of the possibility of studying solids at low temperatures, i.e. the possibility of obtaining kinetic isotope effects in a very wide temperature range.

14 Acknowledgements

I would like to thank all my collaborators which have contributed to the work described in this review. Dr. J. Hennig was involved with the early work on porphyrines and on polarization transfer. Dr. D. Gerritzen performed the kinetic isotope effect studies on the system methanol and methanol/acetic acid/THF. Dr. H. Rumpel studied the azophenine tautomerism, Dr. L. Meschede the formamidines, Dr. M. Schlabach the hydroporphyrins. Dr. B. Wehrle, F. Aguilar-Parilla and J. Braun were responsible for most of the solid state studies. The initial solid state studies were performed during the year 1983 in the laboratory of Dr. C. S. Yannoni, IBM, San Jose, to whom I am greatly indebted for introducing me into variable temperature high resolution solid state NMR spectroscopy. The acetylporphyrin studies were performed in collaboration with Professor C. Djerassi and his coworkers.

I also would like to thank many friends who have been involved for a long time in problems of proton transfer and isotope research. They have not only encouraged me to pursue the study of proton transfer kinetics by dynamic NMR spectroscopy but have also contributed many ideas to this work. Among these are Prof. H. W. Zimmermann, Prof. R. P. Bell, Prof. E. F. Caldin, Prof. M. M. Kreevoy and Prof. R. L. Schowen.

Finally, I have to thank the Deutsche Forschungsgemeinschaft, Bonn–Bad Godesberg for a Heisenberg grant during the years 1981–1986 as well as for continuous financial support. In addition, I would like to thank the Fonds der Chemischen Industrie, Frankfurt, for a Dozentenstipendium and other financial support.

15 References

1. Urey HC, Brickwedde FG, Murphy GM (1931) Phys Rev [2] 39: 164; (1932) Phys Rev [2] 40: 1
2. Washbourn EW, Urey HC (1932) Proc Natl Acad Sci 18: 4998
3. Melander L, Saunders WH (1980) Reaction rates of isotopic molecules, New York, Toronto: John Wiley & Sons
4. Urey HC (1947) J Chem Soc 569
5. Bigeleisen J, Goeppert Mayer M (1947) J Chem Phys 15: 261; Bigeleisen J (1955) J Chem Phys 23: 2264
6. The May issue of Z Naturfosch 44a, 1989 is devoted to the 70th birthday of Professor J Bigeleisen and contains recent developments in isotope chemistry
7. Glasstone S, Laidler KJ, Eyring H (1941) The theory of rate processes, New York, McGraw-Hill
8. Bigeleisen J (1949) J Chem Phys 17: 675
9. Bell RP (1980) The Proton in Chemistry, 2nd ed, London, Chapman and Hall
10. Bell RP (1980) The tunnel effect in chemistry, London, Chapman and Hall
11. German ED, Kusnetzov AM, Dogonatze RR (1980) J Chem Soc Faraday 2 76: 1128 and references cited herein
12. Bruniche-Olsen N, Ulstrup J (1979) J Chem Soc Faraday 1 75: 205
13. German ED, Kusnetsov AM, Dogonadze RR (1980) J Chem Soc Faraday 2 76: 128 and references cited therein
14. Kuznetsov AM, Ulstrup J (1982) J Chem Soc Far Trans 2 78: 1497
15. Siebrand W, Wildman TA, Zgierski MZ (1984) J Am Chem Soc 106: 4083
16. Siebrand W, Wildman TA, Zgierski MZ (1984) J Am Chem Soc 106: 4089
17. Brickmann J, Zimmermann H (1966) Ber Bunsenges Phys Chem 70: 157
18. Brickmann J, Zimmermann H (1966) Ber Bunsenges Phys Chem 70: 521
19. Brickmann J, Zimmermann H (1967) Ber Bunsenges Phys Chem 71: 160
20. Brickmann J, Zimmermann H (1969) J Chem Phys 50: 1608
21. Schuster P, Zundel G, Sandorfy C (eds) (1976) The hydrogen bond, vols 1–3, Amsterdam, North Holland Publ Comp
22. Novak A (1974) Struct Bond 14: 177
23. Brickmann J (1980) Ber Bunsenges Phys Chem 84: 186
24. Klöffler M, Brickmann J (1982) Ber Bunsenges Phys Chem 86: 203
25. Borgis DC, Lee S, Hynes JT (1989) Chem Phys Lett 162: 19
26. Barbara PF, Trommsdoff (eds) (1989) Chem Phys 136 p 153–360
27. Caldin E, Gold V (1975) Proton Transfer, Chapman and Hall, London
28. Swain CG, Brown JF (1952) J Am Chem Soc 74: 2534
29. Swain CG, Brown JF (1952) J Am Chem Soc 74: 2538
30. Cox MH, Jencks WP (1981) J Am Chem Soc 103: 580
31. Bell RP, Critchlow JE (1971) Proc Roy Soc A 325: 35
32. Ek M, Ahlberg P (1980) Chemica Scripta 16: 62; Ahlberg P, Janne K, Löfas S, Nettelblad F, Swahn L (1989) J Phys Org Chem 2: 429
33. Klaer AM, Nilsen H, Sorensen PE, Ulstrup J (1980) A Chem Scand A34: 281
34. Bensaude O, Chevrier M, Dubois, JE (1979) J Am Chem Soc 101: 2423
35. Bensaude O, Dreyfus H, Dodin G, Dubois JE (1977) J Am Chem Soc 99: 4438
36. Bensaude O, Chevrier M, Dubois JE (1979) J Am Chem Soc 101: 2423
37. Albery WJ (1982) J Chem Soc Far I 78: 1579

38. Albery WJ (1982) Far Disc Chem Soc 74: 245
39. Caldin EF, Mateo S (1975) J Chem Soc Faraday 2 71: 1876
40. Ek M, Ahlberg P (1980) Chemica Scripta 16: 62
41. Engdahl KA, Bivehed H, Ahlberg P, Saunders Jr WH (1982) J Chem Soc Chem Comm 423
42. Elrod JP, Gandour RD, Hogg JL, Kise M, Maggiora GM, Schowen RL, Venkatasubban KS (1975) Faraday Symp Chem Soc 10: 145
43. Gandour RD, Schowen RL (1978) Transition states of biochemical processes, New York, Plenum Press
44. Gross P, Steiner H, Krauss F (1936) Trans Faraday Soc 32: 877
45. Hornell JC, Butler JAV (1936) J Chem Soc 1361
46. Kresge AJ (1964) Pure Appl Chem 8: 243
47. Gold V (1960) Trans Far Soc 56: 255
48. Gold V (1969) Adv Phys Org Chem 7: 259
49. Albery WJ, Limbach HH (1982) J Chem Soc Faraday Disc 24: 291
50. Albery WJ (1986) J Phys Chem 90: 3773
51. Hermes JD, Cleland WW (1984) J Am Chem Soc 106: 7263
52. Hermes JD, Morrical SW, O'Leary MH, Cleland WW (1984) Biochemistry 23: 5479
53. Belasco JG, Albery WJ, Knowles JR (1986) Biochemistry 25: 2529
54. Belasco JG, Albery WJ, Knowles JR (1986) Biochemistry 25: 2552
55. Taylor CA, El Bayoumi MA, Kasha M (1969) Proc Natl Acad Sci USA 63: 253
56. Tokumura K, Watanabe A, Udagawa M, Itoh M (1987) J Am Chem Soc 109: 1346 and references cited therein
57. Moerner WE (1986) J Molecular Electronics 1: 55
58. Völker S, van der Waals JH (1976) Mol Phys 32: 1703
59. Voelker S, Macfarlane R (1979) IBM Res Develop 23: 547
60. Friedrich J, Haarer D (1984) Ang Chem 96, 96; (1984) Ang Chem Int Ed Engl 23: 113
61. Eigen M (1963) Ang Chem 75: 489; (1964) Ang Chem Int Ed Engl 3: 1
62. Eigen M, De Maeyer L (1963) In Friess SL, Lewis ES, Weissberger A (eds) Techniques of organic chemistry, vol 8, Part 2, New York, Interscience
63. Gettins WJ, Wyn-Jones E (eds) (1979) Techniques and applications of fast reactions in fast solution, D Reidel
64. Gutowsky HS, McCall DW, Slichter CP (1953) J Chem Phys 21: 279
65. Kubo R (1957) Nuovo Cimento Suppl 6: 1063
66. Sack RA (1958) Mol Phys 1: 163
67. Abragam A (1961) The principles of nuclear magnetism, Oxford: Clarendon Press
68. Alexander S (1962) J Chem Phys 37: 971
69. Kaplan JI (1958) J Chem Phys 28: 278
70. Kaplan JI, Fraenkel G (1972) J Am Chem Soc 94: 2907
71. Binsch G (1969) J Am Chem Soc 91: 1304
72. Farrar TC, Becker E (1971) Pulse and fourier transform NMR, New York, Academic Press
73. Ernst RR, Bodenhausen G, Wokaun A (1987) Principles of nuclear magnetic resonance in one and two dimensions, Oxford: Clarendon Press
74. Doddrell DM, Bendall MR, Barron PF, Pegg DT (1979) J Chem Soc Chem Comm 2, 77; Doddrell DM, Barron PF (1980) Field J Org Magn Reson 13: 119
75. Forsén S, Hofmann RA (1963) J Chem Phys 39: 2892; Forsen S, Hofmann RA (1964) J Chem Phys 40: 1189
76. Hofmann RA, Forsén S (1966) J Chem Phys 45: 2049
77. Campbell ID, Dobson CM, Ratcliffe RG, Williams RJP (1978) J Magn Reson 29: 397
78. Morris GA, Freeman R (1978) J Magn Reson 29: 433
79. Jeener J, Meier BH, Bachmann P, Ernst RR (1976) J Chem Phys 71: 4546
80. Hennig J, Limbach HH (1982) J Magn Reson 49: 322
81. Bleich H, Wilde J (1984) J Magn Reson 56: 149
82. Martin GJ, Martin ML (1981) Tetrahedron Lett 22: 3525
83. Pascal RA, Jr, Baum MW, Wagner CK, Rodgers LR (1984) J Am Chem Soc 106: 5377; Pascal RA, Jr, Baum MW, Wagner CK, Rodgers LR, Huang DS (1986) J Am Chem Soc 108 6477
84. Martin GJ, Martin ML (1990) In: NMR Basic Principles and Progress, vol 23, Springer, Berlin Heidelberg New York
85. Grunwald E, see Referece 27, p 103
86. Denisov GS, Bureiko SF, Golubev NS, Tokhadse KG (1980) In: Molecular interactions, Ratajczak H, Orville-Thomas WJ (eds) vol 2, Chichester, Wiley, Chap 2, p 107

87. Limbach HH (1983) The use of NMR spectroscopy in the study of hydrogen bonding in solution, in aggregation processes In: Gormally J, Wyn-Jones E (eds) Elsevier Amsterdam, Chap 16
88. Grunwald E, Fong DW (1972) J Am Chem Soc 94: 7371
89. Gerritzen D, Limbach HH (1981) Ber Bunsenges Phys Chem 85: 527
90. Lankhorst D, Schriever J, Leyte JC (1983) Chem Phys 77: 319
91. Limbach HH, Seiffert W (1974) Ber Bunsenges Phys Chem 78: 532
92. Limbach HH, Seiffert W (1974) Ber Bunsenges Phys Chem 78: 641
93. Halliday JD, Symons EA, Bindner PE (1978) Can J Chem 56: 1470
94. Limbach HH (1979) J Magn Reson 36: 287
95. Lunazzi L, Panciera G (1980) J Chem Soc Perkin 2: 52
96. Borisov EV, Kratsov DN, Peregudov AS, Fedin EI (1980) Izv Akad Nauk SSSR, Ser Khim 2151
97. Limbach HH, Seiffert (1980) W J Am Chem Soc 102: 538
98. Litchman WM (1979) J Am Chem Soc 101, 545
99. Chenon MT, Coupry C, Grant DM, Pugmire R (1977) J Org Chem 42: 659
100. Nesmeyanov AN, Zavelovitch EB, Babin VN, Kochetkova NS, Fedin EI (1976) Tetrahedron 31: 1461
101. Nesmeyanov AN, Babin VN, Zavelovitch EB, Kochetkova NS, Fedin EI (1976) Chem Phys Lett 37: 184
102. Bureiko SF, Denisov GS, Golubev NS, Lange IY (1979) React Kinet Cat Lett 11: 35
103. Limbach HH, Gerritzen D, Seiffert W (1980) Bull Magn Reson 2: 315
104. Gerritzen D, Limbach HH (1980) J Phys Chem 84: 799
105. Limbach HH, Hennig J, Gerritzen D, Rumpel H (1982) Far Discuss Chem Soc 74: 822
106. Gerritzen D, Limbach HH (1984) J Am Chem Soc 106: 869
107. Meschede L, Gerritzen D, Limbach HH (1988) Ber Bunsenges Phys Chem 92: 469
108. Limbach HH, Meschede L, Scherer G (1989) Z Naturforsch 44a, 459
109. Storm CB, Teklu Y (1974) J Am Chem Soc 94: 1745; Storm CB, Teklu Y (1973) Ann NY Acad Sci 206: 631
110. Abraham RJ, Hawkes GE, Smith KM (1974) Tetrahedron Lett 1483
111. Eaton SS, Eaton GR (1977) J Am Chem Soc 99: 160
112. Yeh HJC (1977) J Magn Reson 28: 365
113. Irving CS, Lapidot A (1977) J Chem Soc Chem Comm 184
114. Gust D, Roberts JD (1977) J Am Chem Soc 99: 3637
115. Hennig J, Limbach HH (1979) J Chem Soc Faraday 2 75: 752
116. Stilbs P, Moseley ME (1980) J Chem Soc Faraday 2 76: 729; Stilbs P (1984) J Magn Reson 58: 152
117. Graf F (1979) Chem Phys Lett 62: 291
118. Bren VA, Chernoivanov VA, Konstantinovskii, LE, Nivorozhkin LE, Zhdanov YA, Minkin VI (1980) Dokl Akad Nauk SSSR 251: 1129
119. Hennig J, Limbach HH (1984) J Am Chem Soc 106: 292
120. Otting G, Rumpel H, Meschede L, Scherer G, Limbach HH (1986) Ber Bunsenges Phys Chem 90: 1122
121. Crosswell MJ, Field LD, Harding MM, Sternhell S (1987) J Am Chem Soc 109: 2335
122. Schlabach M, Wehrle B, Limbach H, Bunnenberg E, Knierzinger A, Shu AYL, Tolf BR, Djerassi C (1986) J Am Chem Soc 108: 3856
123. Schlabach M, Rumpel H, Limbach HH (1989) Angew Chem 101: 84; (1989) Ang Chem Int Ed Engl 28: 76; Schlabach M, Scherer G, Limbach HH (1990) J Am Chem Soc (submitted for publication)
124. Schlabach M, Wehrle B, Braun J, Scherer G, Limbach HH (manuscript in preparation)
125. Schlabach M, Braun J, Wehrle B, Limbach HH, Köcher M, Vogel E (manuscript in preparation)
126. Schlabach M, Limbach HH, Bunnenberg E, Knierzinger A, Shu AYL, Tolf BR, Djerassi C (1990) J Am Chem Soc (submitted for publication)
127. Rumpel H, Limbach HH (1989) J Am Chem Soc 111: 5429
128. Rumpel H, Limbach HH, Zachmann G (1989) J Phys Chem 93: 1812
129. Scherer G, Limbach HH (1989) J Am Chem Soc 111: 5946
130. Ady E, Brickmann J (1971) Chem Phys Lett 11: 302
131. Dewar MJS, Merz KM (1985) J Mol Struct (Theochem) 124: 183
132. Holloway KM, Reynolds CH, Merz KM (1989) J Am Chem Soc 111: 3466
133. Sarai A (1981) Chem Phys Lett 83: 50
134. Sarai A (1982) J Chem Phys 76: 5554

135. Sarai A (1984) J Chem Phys 80: 5341
136. Bersuker GI, Polinger VZ (1984) Chem Phys 86: 57
137. Limbach HH, Hennig J (1979) J Chem Phys 71: 3120
138. Limbach HH, Hennig J, Stulz J (1983) J Chem Phys 78: 5432
139. Limbach HH (1984) J Chem Phys 80: 5343
140. Merz KM, Reynolds CH (1988) J Chem Soc Chem Comm 90
141. Butenhoff T, Moore CB (1988) J Am Chem Soc 110: 8336
142. Smedarchina Z, Siebrand W, Zerbetto F (1989) Chem Phys 136: 285
143. Yanabe T, Yamashita K, Kaminoyama M, Koizumi M, Tachibana A, Fukui K (1984) J Phys Chem 88: 1459
144. Svensson P, Bergmann NÅ, Ahlberg P (1989) Z Naturf 44a: 473
145. Prokofiev AI, Bubnov NN, Solovnikov SP, Kabachnik HI (1973) Tetrahedron Lett 2479
146. Prokofiev AI, Masalimov AS, Bubnov NN, Solodnikov SP, Kabachnik MI (1978) Izv Akad Nauk SSSR Ser Khim 310
147. Bubnov NN, Solodnikov SP, Prokofiev AI, Kabachnik MI (1978) Russian Chem Rev 47: 1048
148. Loth K, Graf F, Andris H, Gunthardt HsH (1976) Chem Phys Lett 29: 163
149. Loth K, Graf F, Gunthardt HsH (1976) Chem Phys 13: 95
150. Limbach HH, Gerritzen D (1982) J Chem Soc Far Disc 74: 279
151. Beinhölzl R, Grampp G, Jaenicke W (1989) Z Phys Chem NF 160: 169
152. Hartmann SR, Hahn EL (1952) Phys Rev 128: 2042
153. Pines A, Gibby MG, Waugh IS (1973) J Chem Phys 59: 569
154. Schaefer J, Stejskal EO (1976) J Am Chem Soc 98: 1031
155. Andrew ER, Bradbury A, Eades RG (1958) Nature (London) 182: 1659
156. Andrew ER, Bradbury A, Eades RG (1959) Nature (London) 183: 1802
157. Lowe IJ (1959) Phys Rev Lett 2: 285
158. Haeberlen U (1976) Advan Magn Reson supplement, New York, Academic Press
159. Spiess HW (1978) Rotation of molecules and nuclear spin relaxation In: NMR-Basic Principles and Progress, vol 15, p 55 Springer, Berlin Heidelberg New York
160. Mehring M (1978) High resolution NMR in solids, NMR-Basic Principles and Progress, vol 11, 2nd edn, Springer, Berlin Heidelberg New York
161. Fyfe CA (1983) Solid state NMR for Chemists, Guelph: CFC Press
162. Lyerla JR, Yannoni CS, Fyfe CA (1982) Acc Chem Res 15: 208
163. Szeverenyi NM, Sullivan MJ, Maciel GE (1984) J Magn Reson 56: 149
164. Limbach HH, Wehrle B, Schlabach M, Kendrick RD, Yannoni CS (1988) J Magn Reson 77: 84
165. Schmidt A, Vega S (1987) J Chem Phys 87: 6895
166. Myrrhe PC, Kruger JD, Hammond BL, Lok SM, Yannoni CS, Macho V, Limbach HH, Vieth HM (1984) J Am Chem Soc 106: 6079
167. Limbach HH, Hennig J, Kendrick RD, Yannoni CS (1984) J Am Chem Soc 106: 4059
168. Kendrick RD, Friedrich S, Wehrle B, Limbach HH, Yannoni CS (1985) J Magn Reson 65: 159
169. Limbach HH, Gerritzen D, Rumpel H, Wehrle B, Otting G, Zimmermann H, Kendrick RD, Yannoni CS (1985) In: Photoreaktive Festkörper, Sixl H, Friedrich J, Bräuchle C (eds) Karlsruhe, M Wahl, p 19–43
170. Limbach HH, Wehrle B, Zimmermann H, Kendrick RD, Yannoni CS (1987) J Am Chem Soc 109: 929
171. Limbach HH, Wehrle B, Zimmermann H, Kendrick RD, Yannoni CS (1987) Ang Chem 99: 241; (1987) Ang Chem Int Ed Engl 26: 247
172. Wehrle B, Limbach HH, Köcher M, Ermer O, Vogel E (1987) Ang Chem 99: 914; (1987) Ang Chem Int Ed Engl 26: 934
173. Wehrle B, Zimmermann H, Limbach HH (1987) Ber Bunsenges Phys Chem 91: 941
174. Wehrle B, Limbach HH, Zimmermann H (1988) J Am Chem Soc 110: 7014
175. Meier BH, Storm CB, Earl WL (1986) J Am Chem Soc 108: 6072
176. Frydman L, Olivieri AC, Diaz LE, Frydman B, Morin FG, Mayne CL, Grant DM, Adler AD (1988) J Am Chem Soc 110: 8336; Frydman L, Olivieri AC, Diaz LE, Frydman B, Kustanovich I, Vega S (1989) J Am Chem Soc 111: 7001
177. Frydman L, Olivieri AC, Diaz LE, Valasinas A, Frydman B (1988) J Am Chem Soc 110: 5651
178. Baldy A, Elguero J, Faure R, Pierrot M, Vincent EJ (1985) J Am Chem Soc 107: 5290
179. Smith JAS, Wehrle B, Aguilar-Parrilla, Limbach HH, Foces-Foces M, Xano FH, Elguero J, Baldy A, Pierrot M, Khurshid MMT, Larcombe-McDuall JB (1989) J Am Chem Soc 111: 7304
180. Graf F, Meyer R, Ha TK, Ernst RR (1981) J Chem Phys 75: 2914
181. Meier BJ, Graf F, Ernst RR (1982) J Chem Phys 76: 767 (1982)

182. Nagoka S, Terao T, Imashiro F, Saika A, Hirota N, Hayashi S (1981) Chem Phys Lett 80: 580
183. Nagoka S, Terao T, Imashiro F, Saika A, Hirota N, Hayashi S (1983) J Chem Phys 79: 4694
184. Schajor W, Post H, Grosescu R, Haeberlen U (1983) J Magn Reson 53: 213
185. Benz S, Haeberlen U, Tegenfeldt J (1986) J Magn Reson 66: 125
186. Scheubel W, Zimmermann H, Haeberlen U (1988) J Magn Reson 80: 401
187. Idziak S Pislewski N (1987) Chem Phys 111: 439
188. Jarvie TP, Thayer AM, Millar JM, Pines A (1987) J Phys Chem 91: 2240
189. Agaki T, Imashiro F, Terao T, Hirota H, Hayashi S (1987) Chem Phys Lett 139: 331
190. Jonsen P, Luzar M, Pines A, Mehring (1986) MJ Chem Phys 85: 4873
191. Meier P, Kothe G, Jonsen P, Trekoske M, Pines A (1987) J Chem Phys 87: 6867
192. Bothner-By AA, Stephens RL, Lee JM, Jeanloz RW (1984) J Am Chem Soc 106: 811
193. Bax A, Davis DG (1985) J Magn Reson 63: 207
194. Braunschweiler L, Ernst RR (1983) J Magn Reson 53: 521
195. Davis DG, Bax A (1985) J Am Chem Soc 107: 2820
196. Chambers VMA, Evans EA, Elvidge JA, Jones JR (1978) Tritium Nuclear Magnetic Resonance Spectroscopy, The Radiochemical Centre, Amersham, Bucks, England, Review No 19
197. Bloxsidge JP, Elvidge JA (1983) Progr NMR Spect 16: 99
198. Binsch G, Kleier A, Quantum Chem Progr Exchange, Indiana University, program DNMR2, DNMR3, and DNMR5
199. Van Geet AL (1970) Anal Chem 42: 679
200. Meschede L (1989) Dissertation Freiburg; Meschede L, Limbach HH (1990) J Phys Chem (submitted for publication)
201. Hexem JG, Frey MH, Opella SJ (1982) J Chem Phys 77: 3847
202. Olivieri AC, Frydman L, Diaz LE (1987) J Magn Reson 75: 50
203. Olivieri AC, Frydman L, Grasselli M, Diaz LE (1988) Mag Res Chem 26: 615
204. Swanson SD, Ganapathy S, Bryant RG (1987) J Magn Reson 73: 239
205. Martin GJ, Martin ML, Gouesnard JP (1981) ^{15}N-NMR spectroscopy, In: NMR Basic Principles and Progress, vol 18, Springer, Berlin Heidelberg New York
206. Meyer R, Meier BH, Ernst RR (private communication)
207. Ahlberg P, Davidsson Ö (1986) J Chem Soc Chem Comm 623
208. Ahlberg P (private communication)